Sistema de Controlo Inferencial com Dispositivos Sensoriais Direcionados para o Uso Eficiente da Água na Agricultura

JUCILENE DE MEDEIROS SIQUEIRA

ORIENTADORES: Doutor Luís Santos Pereira
Docente Emérito

Doutora Maria Teresa Gomes Afonso do Paço

Doutor José Machado da Silva
Professor Associado
Faculdade de Engenharia
Universidade do Porto

TESE ELABORADA PARA OBTENÇÃO DO GRAU DE DOUTOR EM
ENGENHARIA DOS BIOSSISTEMAS

2019

Sistema de Controlo Inferencial com Dispositivos Sensoriais Direcionados para o Uso Eficiente da Água na Agricultura

JUCILENE DE MEDEIROS SIQUEIRA

ORIENTADORES: Professor Doutor Luís Santos Pereira
                  Professora Doutor Teresa Afonso do Paço
                  Professor Doutor José Machado da Silva

TESE ELABORADA PARA OBTENÇÃO DO GRAU DE DOUTOR EM

ENGENHARIA DOS BIOSSISTEMAS

Presidente: Doutor Ricardo Manuel de Seixas Boavida Ferreira
Professor Catedrático
Instituto Superior de Agronomia
Universidade de Lisboa.

Vogais: Doutora Maria Isabel Freire Ribeiro Ferreira
Professora Catedrática
Instituto Superior de Agronomia
Universidade de Lisboa;

Doutor Nildo da Silva Dias
Professor Associado III
Universidade Federal Rural do Semi-Árido, Brasil;

Doutor Aureliano Natálio Coelho Malheiro
Professor Auxiliar
Escola de Ciências Agrárias e Veterinárias
Universidade de Trás-os-Montes e Alto Douro;

Doutora Maria Teresa Gomes Afonso do Paço
Professora Auxiliar
Instituto Superior de Agronomia
Universidade de Lisboa;

Doutor João Rui Rolim Fernandes Machado Lopes
Professor Auxiliar Convidado
Instituto Superior de Agronomia
Universidade de Lisboa;

Doutor José Manuel Couto Silvestre
Investigador Auxiliar
Instituto Nacional de Investigação Agrária e Veterinária.

2019
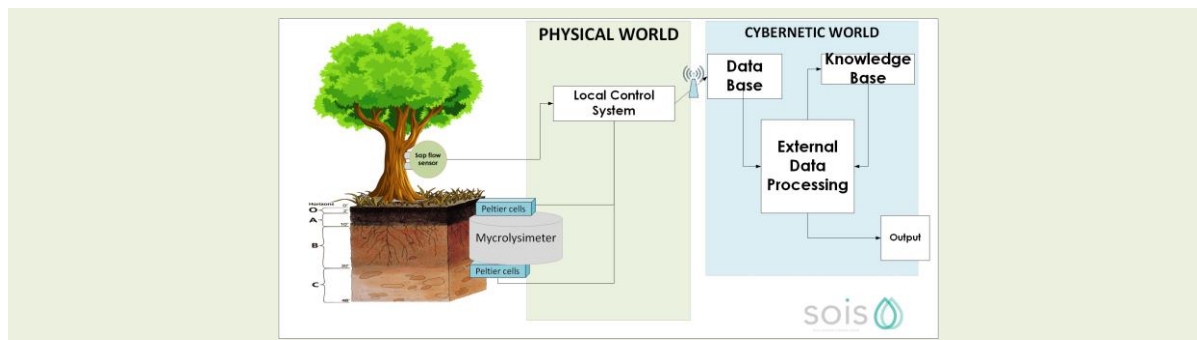
LOW-COST OPEN SYSTEM FOR THE EFFICIENT USE OF WATER IN ORCHARDS AND VINEYARDS

JUCILENE DE MEDEIROS SIQUEIRA

ORIENTADORES: PhD Luís Santos Pereira
PhD Teresa Afonso do Paço
PhD José Machado da Silva

TESE ELABORADA PARA OBTENÇÃO DO GRAU DE DOUTOR EM
ENGENHARIA DOS BIOSSISTEMAS

2019

Este trabalho é para honra e glória do Senhor

Ele fortalece o cansado e dá grande vigor ao que está sem forças. Até os jovens se cansam e ficam exaustos, e os moços tropeçam e caem; mas aqueles que esperam no Senhor renovam as suas forças. Voam alto como águias; correm e não ficam exaustos, andam e não se cansam.

Isaías 40: 29-31

AGRADECIMENTOS

ABSTRACT

The efficient use of water in agriculture is decisive to the issues related to the sustainable exploration of water resources. For this reason, the scientific community has been impelled to develop new technologies for improving the transferability and applicability of irrigation scheduling techniques based on specific crop water requirements and soil characteristics.

The efficient use of water based on the accurate information on orchards and vineyards water requirements at different growth phases and soil water holding capacity and the development of innovative technologies for applications in the agricultural environment should consider the usual constraints, *e.g*., economic, social and technical. For this reason, the present thesis aims to design and implement a low-cost open, interactive and user-friendly irrigation system tool to improve irrigation scheduling in orchards and vineyards aiming the efficient use of water in agriculture, the SOIS - Smart Orchard Irrigation System – defined as a low-cost open system is proposed.

The innovative contributions of the present study reside in the development of hardware and software using low-cost approach to control the use of water in commercial orchards and vineyards, and in the establishment and validating of a fuzzy algorithm system to automate data analyses in real time. Furthermore, the research study improved and validated a modified *Granier* sap flow sensor using thermistors, obtaining success in adopting a new approach to compute the *Granier* sap flow index, it developed an automatable weighing device aiming to assess under-canopy soil evaporation, which is adequate to use continually, and it tested a methodology to use *Peltier* cells to estimate the soil latent heat flux from the story.

Keywords: Water using efficiency; Evapotranspiration measurement; Low-cost sensors, Orchard and vineyard using water.

RESUMO ALARGADO

O uso eficiente da água na agricultura é uma questão prioritária no contexto da exploração sustentável dos recursos hídricos. A escassez de água não ocorre apenas em áreas áridas e propensas a secas, mas também em regiões onde a precipitação é abundante, e diz respeito à quantidade e à qualidade de água disponível. Por essa razão, vários estudos têm sido realizados para suprir a elevada e crescente demanda de água usada na agricultura, propondo soluções para melhorar a sua qualidade e reduzir os desperdícios, sem produzir novos impactos ambientais e minorar a produtividade agrícola. A fruticultura e a vinicultura são entre outras atividades agrícolas, boas soluções para fazer face à escassez hídrica, uma vez que apresentam um elevado retorno económico e são bem-adaptáveis à utilização de sistemas de rega usados em condições de restrições do uso da água. Por esta razão, a comunidade científica tem sido impelida a desenvolver novas tecnologias para o uso eficiente da água com base nas informações precisas das necessidades requeridas pelos plantios em diferentes ciclos de crescimento.

Diante da complexidade imputada para determinar as necessidades de rega em tempo real, têm surgido uma série de ferramentas de tomada de decisão para programas de rega visando otimizar o uso da água e manter níveis suficientes de produtividade da cultura.

O desafio principal no planejamento de regadios com base nas necessidades de água das culturas consiste no desenvolvimento de abordagens específicas de medição do uso da água de acordo com as faixas de produtividade e características do solo nos diferentes ecossistemas e realidades locais. Contudo, os esforços das estratégias de sofisticação associadas à fácil operacionalidade destes dispositivos não melhoraram necessariamente a precisão das metodologias adotadas. Pelo contrário, este facto tem facilitado a realização da quantificação do uso da água por indivíduos com experiência ou compreensão limitada dos processos físicos e metodológicos envolvidos, resultando no uso da água de forma ineficiente.

Várias razões explicam o fracasso dessas abordagens, por exemplo, aspetos económicos, manutenção ineficiente, inexistência de formação e interação precária entre todos os agentes envolvidos, ou seja, investigadores, técnicos, agricultores e agências governamentais. Consequentemente, os esforços de pesquisa e demonstração são por vezes desperdiçados. Assim, recai nos investigadores, o desafio de propor o desenvolvimento de novas alternativas tecnológicas para o uso eficiente da água, que sejam prontamente adaptáveis ao meio agrícola, categorizado pelas suas restrições económicas, sociais e técnicas.

As novas tecnologias direcionadas para o uso sustentável da água a serem implementadas no meio agrícola deveriam ter um custo justificável, bem como, serem de simples instalação e

manutenção. Outrossim, como requisito obrigatório, a sua instalação deveria ser acompanhada por formação específica dos utilizadores finais. Por fim, justifica-se refletir sobre a comunicação interativa entre investigadores, técnicos e agricultores. Um sistema de fácil aquisição e implantação atenderia a essas solicitações, desde que facultasse o acesso aberto e transparente aos projetos de *hardware* e *software*. Isto, seguramente, acompanhado com o uso de novas tecnologias associadas a ferramentas matemáticas eficientes, que permitam construir, replicar, modificar ou reparar transdutores a baixo custo e racionalizar a necessidade de recuso a especialistas ou profissionais.

Considerando o que acima foi dito, é proposto um sistema inteligente para o uso eficiente da água em pomares e vinhas (SOIS - *Smart Orchard Irrigation System*). SOIS é delineado como um sistema de fácil aquisição e implantação, que permitirá melhorar a transferibilidade e aplicabilidade das técnicas de programação de rega com base em requisitos específicos de água para a cultura e as características do solo. Neste contexto, este trabalho aborda a construção e implementação do SOIS como forma de gerir a gestão do uso da água em pomares e vinhas, demonstrando a sua adaptabilidade, vantagens e desafios.

O objetivo geral desta tese é projetar e implementar ferramentas de tomada de decisão para o uso eficiente da água em pomares e vinhas, interativos, de fácil aquisição, implantação e manutenção. Especificamente, os objetivos se desdobram em: a) projetar o sistema de fácil aquisição e implantação, caracterizado por materiais e métodos simples de usar e de baixo custo; b) desenvolver um algoritmo baseado em lógica difusa para a análise automática dos dados originados de um sistema simples de aquisição de dados; c) otimizar os sensores de fluxo de seiva tipo *Granier* recorrendo a termístores como componente do sensor de temperatura, o que permitirá melhorar o cálculo dos parâmetros da equação de *Granier*; d) desenvolver e fabricar material e os métodos para um microlisímetro automático alternativo que se caracteriza por dispensar um contentor de volume, com o objetivo de medir a variação do volume de água do solo em contínuo; e) utilizar as células *Peltier* como sensores alternativos de fluxo de calor do solo em duas profundidades e estimar o fluxo de calor latente do solo.

As contribuições originais são as seguintes:

a) Foram desenvolvidos componentes de hardware e software baseados em materiais e dados de fácil aquisição e implementação;

b) Foi estabelecido e validado um sistema baseado em lógica difusa para análise automática de dados em tempo real.

c) Foi otimizado e validado um novo sensor de fluxo de seiva *Granier* modificado usando termístores, que permitiu o desenvolvimento de uma nova abordagem para o cálculo do coeficiente de fluxo de seiva *Granier*.

d) Foi desenvolvido um novo microlisímetro automatizável para a medição em tempo contínuo da evaporação do solo sob os copados;

e) Estabeleceu-se e testou-se uma metodologia baseado em células de *Peltier*, que permite a estimativa do fluxo de calor latente do solo a partir do subsolo.

Ademais, foram extraídos desta tese dois artigos científicos:

a. Siqueira, J. M., Paço, T. A., Silvestre, J. C., Santos, F. L., Falcão, A. O. & Pereira, L. S. (2014). Generating fuzzy rules by learning from olive tree transpiration measurement – An algorithm to automatize Granier sap flow data analysis. Computers and Electronics in Agriculture, 101, pp. 1–10.

b. Siqueira, J., Silva, J. & Paço, T. (2015). Smart Orchard Irrigation System., November 2015. pp. 1–6. IEEE.

Esta tese está organizada em oito capítulos. O capítulo 1 descreve a leitura do problema, os objetivos necessários para resolver o problema e a estrutura da tese. O capítulo 2 refere-se ao estado da arte. Neste capítulo, as secções primeira e segunda abordam o uso eficiente da água na agricultura oriundos da literatura existente, retratando os modelos e técnicas de medições da transpiração e evaporação do solo comumente utilizados em pomares e vinhas. Além disso, são descritos os procedimentos existentes para a deteção e modelagem da evapotranspiração da cultura em dois componentes, transpiração e evaporação do solo, respetivamente. Finalmente, o último tópico apresenta o conceito dos sistemas de baixo custo aplicado as estimas da evapotranspiração a luz da literatura existente sobre esta matéria. O capítulo 3 descreve o conceito, material e abordagens referentes ao sistema SOIS. Primeiramente, são descritos o conceito SOIS, sua arquitetura e as entradas e saídas necessárias para integrar os dois componentes da evapotranspiração e os princípios físicos que são baseados o sistema SOIS, ou seja, estimativas de transpiração e evaporação do solo. No tópico seguinte do capítulo 3, são descritos o material e os métodos adotados para a construção e implementação do sistema SOIS, como também é referido a ferramenta matemática implementada. Os subsequentes capítulos IV, V, VI e VII descrevem o trabalho experimental usando a abordagem SOIS de modo parcial e global. Finalmente, o capítulo VIII consiste nas conclusões e perspetivas futuras.

Palavras-chave: Uso eficiente da água; Medição da evapotranspiração; Sensores de baixo custo, Uso de água em pomares e vinhas.

INDEX

LIST OF FIGURES

LIST OF TABLES

LIST OF ABBREVIATIONS AND SYMBOLS

Symbol	description
$\bar{\theta}$	Global mean mass moisture [$cm^3\ cm^{-3}$]
$\Delta\theta$	Change of substrate water content [$cm^3\ cm^{-3}$]
a_j, b_j and c_j	Parameters of the triangular membership function for the j_{th} fuzzy set.
A_{mly}	Area of the superior plate of the weighing device [cm^2]
A_{TK}	Area of the conducting xylem section [cm^2]
Biot	Biot number
CV	Coefficient of variation [%]
Cv	Soil volumetric heat capacity [$J\ m^{-3}\ °C^{-1}$]
D	Deep percolation observed [mm]
d	Height displacement of reference plane [m]
DOY	Day of Year
D_Z	Depletion depth [mm]
E	Evaporation [$m\ s^{-1}$]
e	Event.
Es	Soil evaporation rate [$mm\ h^{-1}$]
Es_{mLy}	Soil evaporative rate from weighing device [$mm\ h^{-1}$]
ET	Evapotranspiration rate [$mm\ h^{-1}$]
ETc	Crop Evapotranspiration [$mm\ d^{-1}$]
ET_{EC}	Evapotranspiration rate from Eddy Covariance [$mm\ h^{-1}$]
ETo	Reference evapotranspiration [$mm\ h^{-1}$] and [$mm\ d^{-1}$].
F	Sap flow rate [$m^3\ s^{-1}$]
F_{adj}	Sap flow rate adjusted [$m^3\ s^{-1}$]
FAUSY	Fuzzy Algorithm Automation System
$F_{Biot(mG)}$	Sap flow rate (modified *Granier* sensors (Biot approach)) [$m^3\ s^{-1}$] and [$mm\ h^{-1}$]
$F_{Conv(CO)}$	Sap flow rate from conventional *Granier* sensors [$m^3\ s^{-1}$] and [$mm\ h^{-1}$]
$F_{Conv(mG)}$	Sap flow rate (modified *Granier* sensors (conventional approach))[$m^3\ s^{-1}$] and [$mm\ h^{-1}$]
F_{GY}	Sap flow rate from gravimetry approach [$m^3\ s^{-1}$] and [$mm\ h^{-1}$] and [$mm\ h^{-1}$]
f_{mLy}	Calibration factor of weighing device [$mV\ g^{-1}$]
F_{na}	Sap flow rate not adjusted [$m^3\ s^{-1}$]
F_{pred}	Sap flow rate predicted [$m^3\ s^{-1}$]
FS_j	Fuzzy set j_{th}.
FV	Explicative fuzzy variables.
$f_{\Delta j}$	Triangular membership function.
G_{conv}	Conventional *Granier* sensor
GM	*Granier* heat dissipation method
G_Z	Soil heat flux density on depth z [$W\ m^{-2}$]

h	Height of the cover of soil [cm].
HM	Heat pulse-sap velocity method
I_{100}	Daily irrigation depth 100% ETo [mm]
I_{60}	Daily irrigation depth 60% ETo [mm]
k	Thermal conductivity [W m^{-1} ºC^{-1}]
k_{adj}	Adjusted *Granier* sap flow index (*Granier* coefficient).
k_{Biot}	Adjusted *Granier* sap flow index in analogy at Biot number
k_{Conv}	*Granier* sap flow index (original approach)
k_{Gadj}	Adjusted *Granier* flow index (FAUSY approach)
k_{Gna}	Not adjusted *Granier* sap flow index (FAUSY approach)
k_{Gpred}	Predicted *Granier* sap flow index (FAUSY approach)
L	Latent heat of vaporization and [J m^{-3}]
LE	Latent heat flux [W m^{-2}]
LE^{-}	Latent heat of vaporization [W m^{-2}]
LE^{+}	Latent heat of condensation [W m^{-2}]
LE$_{soil}$	Soil latent heat flux [W m^{-2}]
lrc	Linear regression curve
m a.s.l	Metres above sea level [m]
mG	Modified *Granier* sensor
mLy	Weighing device
MSE	Mean square error
n_{fr}	Number of fuzzy regions.
NTG	Natural temperature gradient [ºC]
NTG$_{obs(t)}$	Observed temperature difference by the *Granier* sensors switched OFF at *t* time [ºC]
NTG$_{pred(t)}$	Predicted NTG via FAUSY at *t* time [ºC].
P	Precipitation [mm]
Pcell	Calibrated *Peltier* cell
PFC	Percentage of FAUSY contribution [%]
P$_{heater}$	Nominal power resistance of heater element [W]
Qc	Cumulative normalised flux
Qf	One-dimensional footprint (or footprint function) [m^{-1}]
RE	Residual error.
RE$_{f}$	Residual error from FAUSY [m^3 s^{-1}]
RE$_{na}$	Residual error from manual computation [m^3 s^{-1}]
RE$_{pred}$	Residual error of sap flow predicted. [m^3 s^{-1}]
RH	Relative humidity [%]
RMSE	Root mean square error
Rs	Solar radiation [W m^{-2}]
S	Soil heat storage [W m^{-2}]
S$_{\Delta t}$	Variation of soil heat storage per time *t* on Δz soil layer [W m^{-2}]
SBT	Steps backwards over time
SOH	SOIS hardware

SOIS	Smart Orchard Irrigation System
SOS	SOIS software
s_t^{mLy}	Signal of mLy device in t time [mV]
t	Variable time [s]
T_{no_heat}	Reference temperature [Cº]
T	Temperature [ºC]
TDR	Reflectometer sensor
T_{heat}	Temperature heater sensor [Cº]
Time	Fraction of day (1/48, 12/48, …, 48/48)) variable
T_{MAX}	Maxima temperature reached [Cº]
T_{SOIL}	Soil temperature [Cº]
u	Sap flux density [m^3 m^{-2} s^{-1}]
u_{adj}	Adjusted sap flux density. [m^3 m^{-2} s^{-1}]
u_{Biot}	Adjusted *Granier* sap flux density [m^3 m^{-2} s^{-1}] (Biot number approach)
u_{Conv}	*Granier* sap flux density [m^3 m^{-2} s^{-1}] (conventional approach)
UD	Universe of discourse.
u_{na}	Not adjusted sap flux density [m^3 m^{-2} s^{-1}]
u_{pred}	Predicted sap flux density [m^3 m^{-2} s^{-1}]
Vd	Relative output to each event e
VPD	Vapour pressure deficit [kPa]
W_i	Actual mass balanced in i time[g]
W_{MAX}	Maximum mass value weighted
W_{MIN}	Minimum mass value weighted
WSB	Weighed soil boundary
x	Actual value of a variable.
x_L	Distance between the measuring point and the source region of the fluxes [m]
x_{max}	Maximum normalised value of a variable.
x_{min}	Minimum normalised value of a variable.
x_n	Normalized value of a variable.
z	Subscript representative of the soil depth
z_{mLy}	Depth between the mLy plate and surface [cm]
z_o	Aerodynamic surface roughness[m]
ΔT	Temperature difference [ºC]
$\Delta T(t)$	Temperature difference at t time [ºC]
$\Delta T_{adj}(t)$	ΔT adjusted by NTG observed at t time [ºC]
ΔT_{MAX}	Maximum temperature difference [ºC]
ΔT_{MAXadj}	Adjusted maximum temperature difference [ºC]
ΔT_{MAXna}	Not adjusted maximum temperature difference [ºC]
$\Delta T_{na}(t)$	Not adjusted temperature difference at t time [ºC].
$\Delta T_{pred}(t)$	Predicted temperature difference at t time [ºC].
θ	Actual mass moisture [cm^3 cm^{-3}]
θd	Daily mean mass moisture [cm^3 cm^{-3}]

θ_{FC} Soil field capacity [$cm^3\ cm^{-3}$]

θh Hourly mean mass moisture [$cm^3\ cm^{-3}$]

θ_{WP} Soil wilting point [$cm^3\ cm^{-3}$]

INTRODUCTION

CHAPTER 1

I. CHAPTER 1: Introduction

I.1.   General framework

The efficient use of water in agriculture is at the forefront position of the issues related to the sustainable exploration of hydric resources. Water scarcity arises not only in arid and drought-prone areas but also in regions where rainfall is abundant. According to Pereira *et al.* (2002), water scarcity concerns the quantity and the quality of the available water. For this reason, several studies point out solutions to cope with insufficiency of agricultural water demand, investigating the ability to improve quality and use a minor quantity of water without producing new environmental impact and reduction of the crop productivity (Pereira *et al.*, 2009; Dias *et al.*, 2010).

The scientific community has been impelled to develop new technologies for the efficient use of water based on the accurate information of crop water requirements at different growth cycles and soil water hold capacity (Pereira *et al.*, 2012). In the face of the apparent performing complexity to determine the crop water requirements, a range of decision-making tools for irrigation schedules have been developed aiming at optimising the water use while maintaining enough levels of crop productivity.

The central challenge for irrigation scheduling based on the crop water requirements and soil characteristics involves the development of specific methodologies for ranges of yield, environments and soil. Unfortunately, the increased sophistication, easy-operationality and easy-maintenance of the devices, have not necessarily improved the accuracy of data collection. In fact, it has facilitated the carry out of measurements by individuals having insufficient experience, care, or understanding of the physics and methodology, resulting in data showing relatively reduced accuracy (Jensen & Allen, 2016). Also, Allen *et al.* (2011a) have summarised common errors to modern crop water requirements methodologies.

Several reasons explain the failure of these approaches, *e.g.*, economic aspects, problematic maintenance, non-existent training and deficient interaction among all agents involved, *i.e.*, researchers, technicians, farmers and governmental agencies (Smith *et al.*, 1996; Blazy *et al.*, 2009; Grové, 2011). Consequently, research and demonstration efforts are sometimes wasted. The challenge to researchers concerns developing a technological alternative for the efficient use of water that is readily adaptable to agricultural environment categorised for the economic, social and technical constraints.

The development of innovative technology for applications in the agricultural environment should take low cost, easy maintenance, and life-long training of the users as mandatory requirements. Also, it should consider the robustness and easy-handling of all devices installed in the field. Finally, it is justifiable to reflect on the interactive communication between researchers, technicians and farmers. A low-cost open system attends to these requests, since providing unrestricted and transparent access to hardware and software designs. It takes advantage of new technologies associated with efficient mathematical tools, which permits building, replicating, modifying or repairing transducers at low cost and streamlining aid of experts or professionals.

The Smart Orchard Irrigation System (SOIS), defined as a low-cost open system, proposed here allows improving the transferability and applicability of the irrigation scheduling techniques based on specific crop water requirements and soil characteristics. In this context, this work addresses the design and implementation of SOIS as a means to manage the watering in orchards and vineyards, demonstrating their adaptability, advantages and challenges.

I.2. Objectives

The general objective of this thesis is to design and to implement the low-cost open, interactive and user-friendly system for orchards and vineyards irrigation management to improve irrigation scheduling, aiming at the efficient use of water in agriculture.

The specifics objectives are:

a) Design the low-cost open system characterised by resorting to easy-to-use and inexpensive materials and methods;
b) Develop a fuzzy logic algorithm for the automatic data analysis of the data originated from the low-cost open system.

c) Optimize the *Granier* sap flow sensors by using thermistors as the temperature sensing components, which will allow improving the computation of the *Granier* equation parameters;

d) Develop and manufacture the material and methods for a novel automatic microlysimeter that is characterised by being deprived of a container, aiming to measure the under-canopy in continuo;

e) Use *Peltier* cells as an alternative soil heat flux sensor, aiming to measure the soil heat flux in two soil depth and estimating the soil latent heat flux.

I.3.   Original Contributions

a) A new system to control the use of water in commercial orchard and vineyard was developed resorting to low-cost hardware and software parts.

b) A fuzzy logic algorithm automation system (FAUSY) for automatic and in real time sap flow data analysis was established and validated.

c) A modified *Granier* sap flow sensor was advanced and validated using thermistors, obtaining success in adopting a new approach to compute the *Granier* sap flow index.

d) A novel automatable weighing device was developed to measure the under-canopy soil evaporation measurement, which can be used in continuous time.

e) A *Peltier* cells based methodology was proposed and tested, which estimates the soil latent heat flux from the story.

I.4.   Outline of the thesis

This thesis is organised into eight chapters. Chapter I describes the problem reading, the objectives required to solve the problem and the framework of the thesis.

The *State of the Art* is overviewed in Chapter II. In this chapter, the first and second sections address the solutions that have been proposed in the scientific literature for the efficient use of water in orchards and vineyards. The usual procedures for the crop evapotranspiration, soil evaporation and transpiration sensing are also described. The second section ends with an overview on the current literature concerning the ET modelling for orchards and vineyards. Finally, the last topic presents the concept of the low-cost open system applied to ET measurement.

Chapter III describes the concept, material and approaches concerning the Smart Soil Irrigation System (SOIS). Firstly, in sequence are described the SOIS concept, its architecture, and the inputs and outputs required for integrating the two components of the evapotranspiration and the physical principles with which the SOIS is constructed, *i.e.,* transpiration and soil evaporation estimates. Also, Chapter III describes the material and methods adopted for the assembly, manufacture and trial implementation, as well, refers to the implemented mathematical tool.

The following chapters IV, V, VI and VII describe the experimental working using partial and global SOIS approach. Finally, chapter VIII highlights the main conclusions and future perspectives.

STATE OF THE ART

CHAPTER 2

II. CHAPTER 2: Crop Evapotranspiration and Efficient Water Use in Orchards and Vineyards

The adequate use of water for irrigation figure weights different water balance components, the relationships between these components and takes into account losses during storage, conveyance and application to irrigation plots (Hamdy, 2007). Also, it involves a broad assortment of disciplines, *e.g*., agronomy, plant physiology and engineering (Nair *et al.*, 2013), including mixed approaches for the rational and sustainable use of water in agriculture, for example, water productivity and water efficiency. As defined by Pereira *et al.* (2002), the term "water use efficiency" should be used to measure the water performance of plants and crops, irrigated or non-irrigated, to produce assimilates, biomass and harvestable yield. While the term "water productivity" should be adopted to express the quantity of product or service generated by a given amount of water used. In the sense of taking a broad view of the water consumption with efficient and productive strategies, the crop evapotranspiration information is an essential term in that equation (Pereira, 2007). Thus, the crop evapotranspiration sensing and modelling are prerequisites for efficient and productive water use.

Allen *et al.* (1998, 2007b) describe the term evapotranspiration (ET) as a combined process, whereby liquid water is transformed to water vapour and removed from the evaporating surface and contained in plant tissues to the atmosphere. Also, ET is driven by atmospheric demand as well as soil water potential and hydraulic conductivity. However, unlike soil evaporation, plant transpiration is regulated by opening and closing of the stomata (Kool *et al.*, 2014). Thus, ET should be computed and monitored by evaluation of the biophysical parameters and variables related to the hydric and heat transference inside of the vadose zone, among plants, soil and atmosphere (Allen & Pereira, 2009; Paço *et al.*, 2012).

The orchards and vineyards, named as sparse canopies, can be described as surface types which are partially covered with plants, permitting a significant part of the available radiative energy heating the bare soil (Hurk, 1996). According to sparse canopies, the sensing and modelling of the transpiration (T) and soil evaporation (Es) in two independent components, *i.e.*, ET partitioning, can be useful for assessing water use efficiency (Kool *et al.*, 2016). Mainly, it can incorporate the effects of the different canopies and soil characteristics in the discrete

estimation of T and Es (Odhiambo & Irmak, 2011), permitting to use different combinations, depending on the scale of interest, cover type, study objectives, and available resources (Kool *et al.*, 2014).

II.1. ET partitioning sensing for orchards and vineyards

The crop evapotranspiration sensing in ET partitioning approach requires the employment of sensors and techniques, with which both components, transpiration (T) and soil evaporation (Es) are measured separately, or the ET component is measured, and one of the elements (T or Es) is taken as the residual of the other two.

The methods discussed in this thesis are those that recurrently are used in commercial orchards and vineyards aiming to estimate the sap flow rate into the tree trunk and under-canopy soil evaporation. Relevant scientific works include typically, the use of sap flow sensors and microlysimeter devices for transpiration and soil evaporation estimates, respectively. Also, the eddy covariance technic among others, due to being mostly used in global ET sensing for research purposes.

II.1.1. Transpiration sensing

The direct measurement of crop transpiration under field conditions can be done using several methods that include, *e.g.*, stem flow gauges, weighing lysimeters and environmental chambers that cover a volume (>1 m^3) of plants (Lascano *et al.*, 2016). However, the most techniques designed to T estimations for orchards and vineyard install sensors in the trunk using heat as a sap motion tracer because the stem is limited by a single route of water extraction along the soil-plant-atmosphere continuum (Fuchs *et al.*, 2017). Fernández *et al.*(2017) summarised this approach in heat balance, heat pulse and constant heater methods, which are fundamentally different in their operating principles (Smith & Allen, 1996; Vandegehuchte & Steppe, 2013), *e.g.*, the localisation of sensors in relation to the conductive organ, the methods to the calculation of the sap flow, the size of the stems and the frequency of measurement. Also, their potential for irrigation scheduling has been assessed (Fernández, 2017), which are chosen to be robust and reliable enough for operation in the field over extended periods, automatable and implemented with low cost and easy-to-use data transmission systems (Smith & Allen, 1996). Thus, these sap flow sensors have many applications conferring a high potential for the efficient use of water in orchards and vineyards (Fernández, 2014).

Currently, two commercially available focal methods are employed to sap flow quantification (Fernández *et al.*, 2017) that are appropriated to use in orchards and vineyards (Kool *et al.*, 2014), respectively, the *Granier* heat dissipation method (*Granier*, 1985, 1987) and the heat pulse-sap velocity method (Green *et al.*, 2003). Given the ordinary replication and automation of these sap flow approaches, they have been widely used on main woody stems to quantify the tree transpiration (*Granier et al.*, 1996).

The well-known *Granier* heat dissipation method (GM) (*Granier*, 1985, 1987) is the most widely applied sap-flux density method because of its simplicity and low cost (Vandegehuchte & Steppe, 2013). It consists of constant heater methods, which are used to quantify sap flow velocity based on temperature dissipation from a constant heating source into the stem. It requires one or more pairs of heated and unheated sensors that are inserted radially into the sapwood. Sap velocity is determined from the temperature differences, using an empirical flow index and equation that is subsequently calibrated to plant size using sapwood area. That equation assumes that the maximum temperature difference corresponds to zero flow conditions and the unheated sensor is the intangible referential temperature.

The heat pulse-sap velocity method (HM) relies on short heat pulses applied into the conducting sapwood layer, being the mass flow of sap is determined from the velocity of the heat pulses moving along the stem (Green *et al.*, 2003). It allows the quantification of sap flow velocity based on temperature response curves to a short heat pulse into the stem, where time delay for temperature rise is assumed to be proportional to sap flow velocity.

The similarities between *Granier* heat dissipation method and heat pulse-sap velocity method stand out in that both methods:

i)   use a part of the conductive organ as a sampling of the whole tree;

ii)   are invasive methods, since the sensors are located within the sapwood;

iii)   use medium to large steam diameters (*i.e*., > 30 mm) (Smith & Allen, 1996);

iv)   require that the area of conductive tissue must be estimated accurately;

v)   can be implemented with automatable and inexpensive technology;

In contrast, the differences when comparing GM and HM approaches are the physical principles of HM in opposition to the GM empirical approach, and the required installation precision of the HM sensors into the tree.

HM is derived from thermodynamic principles, which require elaborate and understanding computation. Thus, it is supposed not to require calibration. On the other hand, the original empirical *Granier* equation cannot be used for GM sensors with deviating design (Lu *et al.*, 2004;

Fuchs *et al.*, 2017) since that any modification of methodology needs recalibration. However, GM approach computation is simple and easily interpreted.

The GM methodology uses sensors separated with a distance free of accuracy (Vandegehuchte & Steppe, 2013), of around 10 cm. Contrarily, HM sensors must be installed in exact measure, since the sensors misalignment can lead to significant errors. HM calculations are highly sensitive to the distance between the heater and the sensors, which can lead to either an over or underestimation of transpiration. Also, the reverse flow and low or very high flux densities cannot be measured because a temperature equilibrium between upstream and downstream sensors does not establish under those conditions. It performs poorly at low flow rates and has unresolved limitations under conditions of high flows (Vandegehuchte *et al.*, 2015; Miner *et al.*, 2017). It suggests that the HM methods have high precision but a bias towards correct plant water use and must be calibrated (Forster, 2017).

A significant limitation that applies to all heat pulse and constant heater methods is found in scaling from sap flow to whole plant T, where individual trees introduce uncertainty due to variation in exposure to solar radiation and aerodynamic turbulence (Kume *et al.*, 2010). Also, the relationships and calibrations may change with soil moisture, LAI, disease (Allen *et al.*, 2011). To conclude, the implanting sensors can cause mechanical damage and interrupt flow by occlusion or blocking of the plant's vascular tissues and the area of conductive tissue must be estimated accurately. Clearwater *et al.* (1999) showed that sap velocity could be severely underestimated if portions of the heated sensor are in contact with inactive xylem or bark.

The *Granier* heat dissipation method has been widely used for larger stems and has been reported to give moderate to reasonable results. For example, olives (Cammalleri *et al.*, 2013; Paço *et al.*, 2014b), Mediterranean evergreen oak savannah (Paço *et al.*, 2009), date palms trees (Sperling *et al.*, 2012), cherries orchards (Li *et al.*, 2010), peach orchards (Paço *et al.*, 2012),vineyards (Fernández *et al.*, 2008; Ferreira *et al.*, 2012). However, some restrictions were observed in using the GM approach. Wilson *et al.* (2001) observed errors associated with scaling single tree estimates and measurement errors associated with ring-porous water conducting elements. Ferreira *et al.* (2008) observed an underestimation of T with GM data when compared to data from eddy covariance (EC) micrometeorological method. Bush *et al.* (2010) suggested that the original *Granier* calibration should not be assumed for all cases. Masmoudi *et al.* (2011) observed that sap flow estimates within young olive trees varied with the sensor position.

In conclusion, weighting the pros and cons, the principal advantages of the GM method as an alternative to others sap flow sensors approach, appears to be the unproblematic installation, low-cost and low requirements for processing and interpreting the collected data (Fernández, 2014). It suggests that the upgrading of *Granier* methods should be a benefit, making the reliable

and robust sensors, capable of working under field conditions for the whole irrigation season, thus, being a useful tool for monitoring the water use in commercial orchards and vineyards.

II.1.2.   Soil evaporation sensing

The importance of measuring soil evaporation (Es) lies in evaluating the effects of Es in the global ET. Es is coupling heat and water transfer between ground and atmosphere (Heitman *et al.*, 2008c), which can be quantified based on the soil water and soil energy balance approaches. In this work context, *i.e*., for orchards and vineyards, it will be lined up the Es sensing methods that are suitable to estimate under-canopy Es, characterised for to vary spatially, depending primarily on soil water distribution, canopy shading, and under-canopy wind patterns (Kustas, 2014). In the soil water balance approach, the under-canopy Es sensing can be determined directly (*e.g*., microlysimeter) or indirectly resorting to sensors that measure the soil water content, computing the water changes in the timeline. Alternatively, Es estimates can resort to the soil energy balance approach for the soil sensible heat measurement along of the soil profile (Gardner & Hanks, 1966).

The microlysimeter based methodology is used to measure the Es, which provides a direct reference for under-canopy Es on the condition that the soil and the heat balance are similar to those in the surrounding area (Lascano & van Bavel, 1986; Plauborg, 1995) and it enables measurements of partial canopy cover conditions due to easy replication in different spatial soil water distribution, canopy shading, and under-canopy wind patterns (Kustas, 2014). Walker (1983) was one of the first to use microlysimeter for under canopy Es measurements. Since then, it has been widely used to measure evaporation from the soil surface of irrigated crops due to the accuracy of measurement and installation low-cost (Parisi *et al.*, 2009).

Daamen *et al.* (1993) reviewed various microlysimeter designs, which ranged from 51 to 214 mm in diameter and 100 to 200 mm in depth and used in field studies for 1 to 10 days. However, the microlysimeters commonly reported in the literature, followed the original design by Boast & Robertson (1982), being typically in diameter as 8 –10 cm and depth range of 7–10 cm (Boast & Robertson, 1982; Evett *et al.*, 2009) and experienced for different materials and sizes (Evett *et al.*, 1995; Todd *et al.*, 2000). Boast & Robertson (1982) pointed out that the microlysimeter gives accurate Es measurements provided the soil cores be replaced at least every 24–48 h to minimise discrepancies with field conditions. Also, it can be considered with reasonable accuracy when reaches to measurements better than 0.1 mm per hour evapotranspiration (Aboukhaled *et al.*, 1982).

Kustas (2014) describes the typical methodology of microlysimeters as a representative vertical section of an undisturbed soil profile, which is inserted into a small cylinder open at the top. The microlysimeter is inserted back into the soil, aligning its upper edge level with the soil surface and weighed either periodically or continuously. The changes observed in weight reflect an evaporative flux. Due to practical implementation, the microlysimeters has been used widely for Es studies in orchards and vineyards, for example, coffee (Flumignan *et al.*, 2011), cherry orchards (Li *et al.*, 2010), olive orchards (Rousseaux *et al.*, 2009; Paço *et al.*, 2014b), peach orchards (Paço *et al.*, 2012), vineyards (Heilman *et al.*, 1994; Trambouze *et al.*, 1998; Yunusa *et al.*, 2004; Zhang *et al.*, 2011; Ferreira *et al.*, 2012; Poblete-Echeverría *et al.*, 2012).

The microlysimeters are appreciated for simplicity and economy (Lascano & van Bavel, 1986), but are also considered time-consuming and constraints in time resolution as a result of manual weighing (Trambouze *et al.*, 1998), limited representation of field conditions due to small sample size (Daamen & Simmonds, 1996) and the inability to measure during irrigation or rain (Flumignan *et al.*, 2012).

The labour-intensive weighing issue has been resolved by placing the microlysimeter on a continuously weighing device (Daamen *et al.*, 1993). Analysis of the costs for the mini-lysimeter system indicates that Es can be measured economically at a reasonable accuracy and sufficient resolution with a robust method of load-cell calibration (Misra *et al.*, 2011), also, resorting to the multiplication of microlysimeters as much as necessary. Grimmond *et al.* (1992) experienced a portable and automatable mini-lysimeters ($< 0.2 \ m^2$), which was compared with evaporative flux measurements obtained using eddy correlation instrumentation. The results showed that the evaporative flux and soil moisture from the mini-lysimeters compared favourably with measurements that are representative of their surroundings. However, the microlysimeters compute the water loss by evaporation in the continuo, being always reset in irrigation or rain events. Unfortunately, nothing has yet been studied to overcome this obstacle. Instead, alternative methods are used.

An alternative indirect method to measure the under-canopy Es are the many soil water content sensors, which compute the change in soil water storage being Es extracted from the water balance equation. The most of these sensors are preferentially adopted compared to the microlysimeters because of being commercially available, practical use and automatable (Persson *et al.*, 2000). For example, time domain reflectometry (TDR), time domain transmission (TDT) and capacitance-based sensors have become typical for measuring soil water content (Ren *et al.*, 1999; Allen *et al.*, 2011; Evett *et al.*, 2012).

Recently, a novel approach for measuring soil evaporation has been proposed, based on the soil energy balance (Heitman *et al.*, 2008c; b) using the soil heat pulse sensor. That approach uses

the sensible heat balance at various depths within the soil, to determine the amount of latent heat involved in the vaporisation of soil water following (Gardner & Hanks, 1966). It should detect "heat sinks" that result from evaporation since it requires large quantities of heat. Thus, the soil latent heat flux is estimated since the soil thermal properties being measured (*i.e*., soil temperature, soil thermal conductivity and soil volumetric heat capacity).

The soil heat pulse sensor was initially developed to determine water content based on soil thermal properties (Campbell *et al.*, 1991), being improved to measure the soil heat flux and estimate the soil evaporation (Ham & Benson, 2004). The procedure for the soil heat pulse consists of three-needle sensors spaced 6 mm apart, in parallel. The three-needles measure temperature and the inner needle also contains a resistance heater for producing a slight pulse of heat required for the heat pulse method (Heitman *et al.*, 2010). At a given time interval (2–4 hours), a heat pulse is executed, and the corresponding rise in temperature at the outer sensor needles is recorded. Soil volumetric heat capacity and thermal diffusivity are determined from the heat input and temperature response following the procedures described by Bristow *et al.* (1994) and Knight & Kluitenberg (2004, 2013), respectively.

The heat-pulse method has yielded reasonable results in field experiments (Heitman *et al.*, 2008a; Sakai *et al.*, 2011; Xiao *et al.*, 2011, 2012). Ren *et al.* (2005) compared the heat-pulse and time domain reflectometry (TDR) approaches in measuring the soil water contents. They observed that the heat-pulse technique seemed better suited than TDR for water content measurements on soils with relatively high organic matter content and showed more sensitivity to spatial soil variability than the TDR method. According to Deol *et al.* (2012), its primary drawback is its inability to measure Es in the first stage when evaporation occurs at the uppermost soil surface. Thus, it would be most useful to monitor evaporation over long drying periods in combination with a different measurement method for the first stage. Also, the soil heat pulse sensor shows to be mathematically complex and challenging to manufacture.

An alternative approach to estimate the soil energy balance is based on the use of heat flux transducers. These devices measure the heat flux density (G_Z) directly and are adequate for soil heat flow measurements (Fuchs & Hadas, 1973; Fuchs, 1986). The heat flowing through the plate results in a temperature difference between the two faces which is proportional to the heat flux density and can be measured with thermopiles. The alternative low-cost *Peltier* cells were introduced by Weaver & Campbell (1985) and had been used instead of heat flow plates (Paço *et al.*, 2014b; Pôças *et al.*, 2014), given have been calibrated with thermopile heat flux transducers manufactured following the methods of Fuchs & Tanner (1968).

In conclusion, from the methodologies described previously, *i.e*., the microlysimeters and the heat-pulse technique, showed to be the most adequate to Es measurement based on the soil

water and soil energy balance approaches, given to be practical and provide straightforward computation, besides of being good accuracy in comparison to the soil water sensors. The microlysimeters are direct, low-cost and associated with a load cell can be made automatable. However, the upgrading of the microlysimeter aiming to improve its performance should be based on allowing for automated and continuous data collection and data transmission, with low power requirements and no interruption in watering events. Also, the use of *Peltier* cells for soil energy balance estimates should be a useful tool for the soil energy balance understanding and estimating the Es contribution to global ET in commercial orchards and vineyards.

II.1.3. ET sensing

The whole ET sensing is based on the soil water balance, as also, the energy balance. The soil water and energy balances are both conservation equations where the evapotranspiration components are computed as the residual of a defined system being all other components known.

The water balance equation takes into account different components, including irrigation (I [mm]), rainfall (P [mm]), run on or runoff (R [mm]), deep soil water flux (D [mm]) and the changing of the soil water storage ($\Delta\theta$ [mm]) (Rosa *et al.*, 2012b; a).

The primary source of error in ET determination by the soil water balance method comprises the uncertainty in drainage from the zone sampled or any upward movement of water from a lower wetter zone into the zone sampled zone (Allen *et al.*, 2011). These errors are difficult to detect, but they can be minimised with proper precautions, for example, by employing appropriate parametric modelling to estimate the deep fluxes (Liu *et al.*, 2006). Also, the soil water balance equation presents a temporal resolution of a few days at best, and difficulties arise because estimates of drainage and surface runoff are usually uncertain (Nicolas *et al.*, 2005).

The surface energy balance includes the terms: net radiation (Rn [W m^{-2}]), soil heat flux (G$_Z$ [W m^{-2}]), latent heat flux (LE [W m^{-2}]) and sensible heat flux (H [W m^{-2}]). These terms can be estimated in loco using eddy covariance (EC) systems, which the LE term can be estimated directly at the surface, and indirectly using the Bowen ratio energy balance method (Farahani *et al.*, 2007).

The Bowen ratio energy balance (β) (Bowen, 1926) can be estimated by measuring differences in water vapour concentration and air temperature at two heights (Holland *et al.*, 2013). LE is calculated from β, Rn, and G$_Z$. It is considered a practical and reliable micrometeorological method, which enables measurement of latent heat flux for periods of an hour or less. The method works best when soil water is not limiting ET, but as water becomes

less readily available and β increases, the relative error in LE increases due to errors as β becomes larger (Jensen & Allen, 2016).

Eddy covariance (EC) system resorts to heat fluxes measuring, as well, it is mostly known for ET measurements. The EC technique is based on a high-frequency measurement, which is necessary to capture small eddies contributing to turbulent transfer. Also, it requires a uniform surface without disruptions between the surface and the instrument height. The EC technique is mostly applicable for tall canopies (Kool *et al.*, 2014), considering that measurement accuracy increases with height. It does not require elaborated scaling considerations to represent spatial areas that are orders of magnitude higher than sap flow or soil water budget methods (Wilson *et al.*, 2001).

EC systems are becoming relatively widely used in ET measurement but require the correction of the energy balance closure, having an easier setup, reduced costs for sensors, and the ability to co-measure H, LE and CO_2 fluxes, depending on the equipment configuration (Allen *et al.*, 2011). Also, it has also been successfully applied to measure Es under forest canopies (Wilson *et al.*, 2001). The EC method has an advantage in that it measures continuously and represents a more significant area. Further work is necessary to identify conditions, including canopy height, that can allow the use of EC for under-canopy Es measurement and to explore possible solutions for its use under less tall canopies (Kool *et al.*, 2014).

In conclusion, the energy balance approach can be used to measure evapotranspiration with much better temporal resolution than the soil water balance approach. Nevertheless, the methods available for implementing energy balance techniques are sophisticated and expensive, and the fetch requirement, which increases as vegetation height increases, makes it difficult to use the boundary layer sampling systems (*e.g.*, Bowen Ratio, Eddy Covariance) to measure ET from narrow or isolated stands of vegetation (Allen *et al.*, 2011).

In general, the ET partitioning sensing has several marked advantages over ET modelling, given that it can provide significant, continuous and direct measurements of ET, T and Es rates within a local field scale. However, it has shown low accuracy for the high spatial variability, being problematic in extrapolating to the field scale. Therefore, the integrated mathematical models have taken place in that framework.

II.2.   ET modelling for orchards and vineyards

The measurement of crop evapotranspiration (ETc) plays an essential role in the improvement of crops water use and irrigation performance. Notwithstanding, ET measurements

are difficult and costly (Farahani *et al.*, 2007). Thus, ET modelling has been taking place by means of the popular approaches, for example, the crop coefficient - reference ET method (Kc-ETo) adopted by FAO56 (Allen *et al.*, 1998). The Kc-ETo approach is mostly preferred for the estimation of the crop water requirements due to its robustness, simple in design and construction, which successfully incorporates some consistent and compensating factors that distinguish the ET of any single crop from that of the reference ET (Pereira *et al.*, 2015). In addition, it provides for straightforward, visually-based derivation and application of the Kc curves over a wide range of climates and locations (Rosa *et al.*, 2012b; a).

Kc-ETo approach computes ETc of a well-watered crop using an empirically defined crop specific multiplication factor (Kc) in combination with a reference ET (ETo). ETo takes into account a hypothetical grass reference surface response to atmospheric conditions by solving the Penman-Monteith equation (Penman, 1948; Monteith, 1965). ETc of irrigated orchards and vineyards depends on the tree size and crop density, which influence the ground cover fraction, and on the wetted surface and frequency of wettings by irrigation and rain (Allen & Pereira, 2009).

The plant transpiration is controlled by stomatal conductance, relates with the variety and also depends upon crop density, age, LAI, and tree architecture (Paço *et al.*, 2014b). Also, T is usually associated with plant productivity, whereas Es does not directly contribute to production (Kool *et al.*, 2014). Given the spatial variability of evapotranspiration for sparse canopies, *i.e.*, orchards and vineyards, Allen *et al.* (1998, 2005) introduced the concept dualKc-ETo approach, such that allows partitioning ETc into crop transpiration ($T = K_{cb} \times ETo$) and soil evaporation ($Es = K_e \times ETo$), where T is the plant transpiration, Es is soil evaporation, K_{cb} is the basal crop coefficient relative to crop transpiration, and K_e is the soil evaporation coefficient.

For transferability purposes, the concept of standard, potential Kc and Kcb values are defined and tabulated for no stress and high crop yielding (Allen et al., 1998; Allen & Pereira, 2009), but appropriate corrections may be required, adopting a stress coefficient (Ks) to obtain the actual Kc ($Kc_{act} = Ks\ Kc$ or $Kcb_{act} = Ks\ Kcb$). The adjustment of tabulated Kc and Kcb values for local conditions are necessary when differences occur in planting density and geometry, vegetation height and canopy architecture, particularly in case of tree and vine crops (Allen et al., 1998; Allen & Pereira, 2009). Nevertheless, the dualKc-ETo approach requires support by a computer model framework because two daily water balances are required, one for the soil evaporation layer and another for the soil explored by the crop roots (Allen *et al.*, 2005). The SIMDualKc tool was developed (Rosa *et al.*, 2012a) to overcome the multifaceted computation. Also, it has the aiming to provide information to researchers and irrigation water management professionals and to make the dualKc-ETo approach operational (Fandiño *et al.*, 2012; Paço *et al.*, 2012; Cancela *et al.*, 2015).

The possibility of directly estimating the crop coefficient from satellite reflectance has been investigated since the similarities with the crop coefficient curve. The principle of the remote sensing for ET estimates relies on the combination of the surface parameters derived from remote sensing data with surface meteorological variables and vegetation characteristics, which allows the evaluation of ET on local, regional and scales (Li *et al.*, 2009).

Satellite-derived vegetation index showed potential for modelling a crop coefficient as a function of the vegetation index (Glenn *et al.*, 2007; Kamble *et al.*, 2013; Lian & Huang, 2016), which is particularly crucial for incomplete cover crops such as orchards and vineyards (Santos *et al.*, 2012; Paço *et al.*, 2014b; Pôças *et al.*, 2014).

Pôças *et al.* (2015) proposed a new procedure for estimating actual basal crop coefficients from vegetation indices, which consider a density coefficient, computed using the fraction of ground cover by vegetation, and it is estimated from vegetation indices derived from remote sensing. Results for an olive orchard have shown that the approaches compared well with results obtained using the SIMDualKc model after calibration with ground observation data. Also, (Paço *et al.*, 2014b) showed that METRIC™ – Mapping EvapoTranspiration at high Resolution using Internalized Calibration (Allen *et al.*, 2007a) could be used operationally to estimate and to map ET of super-intensive olive orchards aiming at improving irrigation water use and management. This approach has a substantial advantage in spatial accuracy because it allows obtaining information for each pixel of a satellite image (Paço *et al.*, 2014b).

Since the recent scientific and technological advances, several researchers have contributed to and embraced the most preferred ET modelling, *i.e.*, Kc-ETo methodology, as well, in combination with remote sensing approach. Nevertheless, this model is a function of general environment parameters (Allen *et al.*, 1998) and in the scope of water use efficiency, it would be necessary the calibration and validation of the (Kc and Kcb)-ETo and remote sensing approaches. The negligence of the validation has resulted in several misunderstanding, which includes the blind application of the model to a field condition without some parameter calibration and verification to ensure on-site behaviour. The dualKc-ETo approach should often be performed through specific observations of the soil evaporation with microlysimeters and of the plant transpiration with sap-flow measurements (Paço *et al.*, 2012; Cammalleri *et al.*, 2013) or with the eddy covariance method in conjunction with the use of devices of sap flow measurement and microlysimeters.

II.3.   Low-cost open system for the water efficient use in orchards and vineyards

The recent confluence of embedded and real-time systems with wireless, small size sensors and networking technologies is creating a promising infrastructure for a technical, economic, and social revolution (Stankovic *et al.*, 2005), inclusive for crop irrigation issue. Sensors and their networks are being used meaningfully in irrigation, fertilisation, horticulture, greenhouse, farming and monitoring of livestock and pastures as reviewed by Mesas-Carrascosa *et al.* (2015). These are some examples: *Precision irrigation systems* (Smith & Baillie, 2009), which crop yields are optimised through systematic gathering and handling of information about the crop and the field (Smith *et al.*, 2010); *Irrigation decision-making systems* applied to support precise guidance for crop irrigation processes (Xu *et al.*, 2011); *Smarts irrigations systems* where inputs from the smart sensor array will determine timing and amounts for real-time site-specific irrigation applications (Vellidis *et al.*, 2008); *Automate irrigation system* with a wireless network of soil moisture, humidity and temperature sensors monitoring the field in real time from any remote location (Khan *et al.*, 2017); *Open source control systems*, which a design takes advantage of the decreasing cost and size of sensors to automate systems, increasing the efficiency and yield of greenhouses (Mesas-Carrascosa *et al.*, 2015; Ali *et al.*, 2016).

Several technologically advanced methods for efficient use of water are starting to be utilised in the more modern orchards and vineyards as well. However, the lack of experience by the local producers, the high cost of the equipment and constant maintenance issues currently limit their applicability (Rousseaux *et al.*, 2009; Gaddam & Esmael, 2014). Consequently, the Kc-ETo and dualKc-ETo approaches are still the methods most often used to water-use efficiency. However, these approaches are function of general environment parameters (Allen *et al.*, 1998), requiring a specific local adjustment (Er-Raki *et al.*, 2009), observing and establishing local cropping data, mainly when addressing discontinuous crop covers, local crop variety, cultural practices and year-to-year variation in weather effects (Allen *et al.*, 2007b). One exception is when applied to a situation that has already been subject to previous calibration and validation, *e.g.*, Fandiño *et al.*, (2015). Further, the accurate characterisation of parameters that influence the measurement of ET is often limited to the use of hardware and software intended for data acquisition and data processing, respectively. It is the case of the developing countries where the principal economic activity is the irrigated agriculture; such technologies have not often been used (Babu, 2013). As cited by (Farahani *et al.*, 2007), there is a real need for innovative methods that can provide sound and affordable estimates of ET that use "plug-and-play" features to link better with on-farm managerial skills.

The low-cost open systems could overcome these constraints. ET estimates driven for the low-cost open system can help in models, where the field information about transpiration and soil evaporation are parameterised and local conditions adjusted in real time. It could keep available for automation and signal sending, either act on models inserted in software or send signals of adjustments to remote sensing. Innovations in low-cost greenhouse design with open source control systems, for example, have shown the potential to increase food security, particularly in areas where global climate change is contributing to additional variability in local weather patterns (Groener *et al.*, 2015).

The low-cost open approach is a decentralised development system that encourages improvements by free collaborations (Fisher & Gould, 2012). If properly adjusted, they can be used to accurately quantify the water consumption of orchards and vineyards (Green *et al.*, 2003; Fernandez *et al.*, 2006). In order to ensure the successful implementation of the low-cost open system approach some requirements should be reinforced (Ali *et al.*, 2016), for example, reasonable price, yet high-performance electrical components (*e.g. Peltier* coolers, load cells, thermistors), designed and constructed using open source hardware and software (Fisher & Gould, 2012), easy to build, easy-programming and launch following detailed tutorials, low-power requirement.

Nevertheless, other issues should be attended. If one way, the data acquisition is straightforwardly solved by low-cost open systems driven by ET measurement, the data processing requires complex interpretations. The quantification of transpiration (T) and soil evaporation (Es) for orchards and vineyards are challenging and continually in improvement. Thus, the techniques of measurements in a low-cost open system approach, although the character inexpensive and straightforward, require automatic adjustment and sophisticated data processing (Do & Rocheteau, 2002b; Mori *et al.*, 2003; Lubczynski *et al.*, 2012; Reyes-Acosta *et al.*, 2012), which became a challenging tactic within universal systems.

The artificial intelligence tools (*e.g.*, fuzzy logic models) have the potential to model complex systems and solving decision problems in the high complexity models , for example, the soil-plant-atmosphere transfer model (Romero *et al.*, 2012). These tools have been used to study the soil and water regimes related to crop growth and support decision-making in precision farming (Huang *et al.*, 2010), to select or reject simulations, to arrange a restricted set of ensemble parameter solutions and to evaluate predicted latent heat fluxes against thermal remote sensing estimates of surface temperature (Mackay *et al.*, 2003).

There are several sensing and modelling systems directed to the efficient use of water in orchards and vineyards. However, it is outlying from the low-cost open system approach encompassing in the scientific domain, and that could be accessible to the agricultural community.

In this work, the reviewed literature described as the preferred methodology, the use of microlysimeters and the *Granier* sap flow sensors for measuring T, Es and ET, and FAO dualKc-ETo approach for modelling the partitioning ET. However, the review showed still some challenges, notably the cost, complexity and automatic data processing, which justifies the study, improvement of devices, not depending on commercial demand as well as, resorting to artificial intelligence tools to enable the automatic data processing using inferential control systems embedded into the low-cost sensors.

MATERIAL AND METHODS

CHAPTER 3

III. CHAPTER 3: Smart Orchard Irrigation System

The Smart Orchard Irrigation System, SOIS for short, is based on open source devices and is intended for long-term capture and recording of soil evaporation and transpiration data on orchards and vineyards. In implementation terms, the SOIS system can be divided into hardware and software. The SOIS hardware comprises the modified *Granier* sap flow sensor, the weighing device and the pair of *Peltier* cells, combined with a set of other complementary devices, notably, Arduino platform, signal amplifiers and signal interfaces. The SOIS software includes data acquisition and sensors operation management, as well as the data processing algorithms that analyse the captured data and provide the needed terms to the decision-making in the watering management. The main SOIS features are robustness, low cost, simple operation, user-friendliness, adaptability to the field environment, together with low power consumption and automatic data processing.

Fig.III.1 illustrates the SOIS architecture. The sensors, interfaces, data recorder, and local and external controllers are the main blocks of the hardware part. The database, the knowledge base, the FAUSY algorithm that generates the set of fuzzy variables and governs the SOIS operation, constitute the software. The sensors assist in converting physical parameters into electrical signals, the interfaces are mainly the circuitry that performs signal conditioning, and the data recorder manages the transmission of data to a database physically built in the local and external controllers.
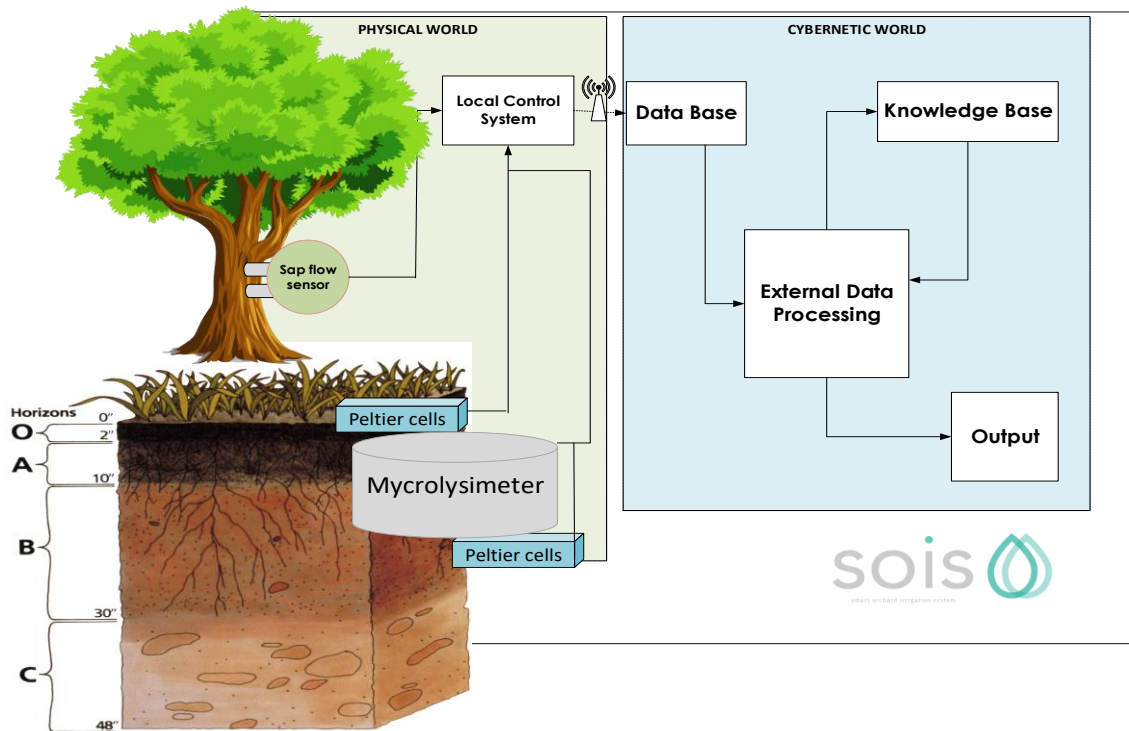
Fig.III. 1: The architecture of SOIS

III.1.   Underlying Physical Phenomena

III.1.1.   Transpiration estimation

The SOIS system relies on thermic and electrical conductivity phenomena to estimate the transpiration and soil evaporation quantities with which one more accurately controls the irrigation process.

The estimates of woody plant transpiration, referring to the sap flow resort to the *Granier* heat dissipation methodology. Therefore, the tree transpiration evaluation is made after heating a point slightly inside of the tree trunk (xylem) by using a heating element and measuring the temperature variation observed in a point 10 cm below that heating spot. The transpiration is inferred after relating the heat transfer with the sap flow.

For this purpose, two temperature sensors are used to measure the temperatures at the heated (T_{heat} [C°]) and the unheated observation points (T_{no_heat} [C°]), from which ΔT [°C] is computed as:

$$\Delta T = T_{heat} - T_{no\_heat} \qquad\qquad\qquad \text{(Eq.III.01)}$$

Conventionally, the *Granier* sap flow index k_{Conv} is obtained with the empirical *Granier* equation:

$$k_{Conv} = \frac{\Delta T_{MAX} - \Delta T}{\Delta T} \qquad\qquad \text{(Eq.III.02)}$$

where ΔT_{MAX} [°C] is the maximum value of ΔT on a daily course and which is related to the minimum or null sap flow rate for that specific day. The flux is calculated from k_{Conv} using a relationship admitted to being species independent (Granier, 1985, 1987; Lu *et al.*, 2004) and based on the *Granier* calibration equation:

$$u = 118.99 \times 10^{-6} k_{Conv}^{1.231} \qquad\qquad \text{(Eq.III.03)}$$

where u [m³ m⁻² s⁻¹] is the sap flux density. The sap flow (F_{Conv} [m³ s⁻¹]) can be calculated from Eq.III.04.

$$F_{Conv} = u \times A_{TK} \qquad\qquad \text{(Eq.III.04)}$$

where A_{TK} [m²] is the area of the conducting xylem section.

Within the system under development this estimation is automatable, requiring a time-indexed t[s] capture of both temperature sensors T_{heat} [C°] and T_{no_heat} [C°], after switching on the heater and then performing the data processing and inferential control. Alternatively, the heater can be switched off for adjustment purposes.

III.1.2. Soil heat flux estimation

The soil heat flux density (G_z [W m⁻²]) estimation resorts to the soil heat flux transducers following the Fuchs & Tanner (1968) calibration methodology, in that the heat flux transducers measure the voltage difference (ΔV [mV]) between two soil surfaces, and it is relating to the difference temperature (ΔT [°C]). The soil heat flux density (Weaver & Campbell, 1985) is computed using Eq.III.05,

$$G_z = -k \, ^{\Delta T}/_{\Delta z} \qquad\qquad \text{Eq.III.05}$$

where k [W m⁻¹ °C⁻¹] is thermal conductivity, $^{\Delta T}/_{\Delta z}$ [°C m⁻¹] is the gradient in the vertical direction and subscript z represents the soil depth, being $z = 0$ the soil surface. The negative sign in that equation is used because heat flows from a higher to a lower temperature, *i.e.*, in the direction of, and in proportion to, a temperature gradient.

The measurement procedure consists of inserting the soil heat flux transducers into the soil at depth z and measuring G_z directly. In the absence of any sources or sinks of heat and using two depths (Δz [m]) to measure G_{z1} and G_{z2} and based on the principle of energy conservation, it is possible to quantify the soil heat storage (S [W m^{-2}]) between two depths with the equation:

$$S = G_{z1} - G_{z2} = G_{\Delta z} \qquad\qquad\qquad\qquad\qquad\qquad\qquad Eq.III.06$$

Also, the computation of S can be obtained from the equation:

$$S = Cv\left(\Delta T / \Delta t \right)\Delta z \qquad\qquad\qquad\qquad\qquad\qquad\qquad Eq.III.07$$

where Cv [J m^{-3} °C^{-1}] is the soil volumetric heat capacity and $\Delta T / \Delta t$ [°C s^{-1}] is the change in soil temperature per unit of time. The value of Cv can be estimated by summing the heat capacities of the various constituents, weighted according to their volume fractions.

III.1.3. Volumetric soil moisture content

The soil water content is directly determined by measuring its weight as a fraction of the total soil weight. Thus, the volumetric soil moisture content (θ [cm^3 cm^{-3}]) is defined as the ratio of water volume to soil volume. The procedure to calculate θ is based on the gravimetric approach (Dane & Topp, 2002), in that the soil weighing is measured at regular intervals. In practical terms, the water content of the evaporating soil layer is at field capacity (θ_{FC} [m^3 m^{-3}]) when it reaches the maximum weight after natural drainage. Thus, the values measured (W_i [g]) in a period with irrigation, allows computing the maximum mass value (W_{MAX} [g]) and relate it to the evaporating soil layer at θ_{FC}.

W_{MAX} is directly related to θ_{FC}, given that the terms (W_{MAX}–W_i) and (θ_{FC}–θ) show to be a linear function, thus, by means of Eq III.08, one can estimate the adjustment of the soil weighing to compute the actual soil moisture, relating to the actual mass of water (θ).

$$\theta = -1 \times \left(\frac{(W_{max} - W_i)\theta_{fc}}{W_{max}} - \theta_{fc} \right) \qquad\qquad\qquad\qquad Eq.III.08$$

Eq. III.09 defines the depletion depth (D_z [mm]), where the subscript z represents the weighted soil depth.

$$D_z = (\theta_{FC} - \theta) \times z \times 1000 \qquad\qquad\qquad\qquad\qquad Eq.III.09$$

III.1.4. Soil evaporation estimation

Soil evaporation estimation is coupled to heat and water transfer measurement, which is quantified based on the soil water and soil energy balances approaches. The first one refers to the continuum measurement of volumetric soil moisture. The last one refers to the continuum measurement of soil heat flow in two depths.

III.1.4.1. Soil water balance approach

The soil water balance approach resorts to a weighing device (mLy) to provide a direct inference of the soil evaporation. The mLy is configured to enable water transference into or out of the weighed soil boundary (WSB), in an open system, which means without a container, thus diverging of the typical microlysimeter. Therefore, some issues should be considered: 1) the interval of measurement of the water balance (mm h^{-1}) should allow sufficient time for the soil water redistribution after watering events; 2) the WSB position below of the drippers should be avoided, allowing that the lateral and vertical (drainage) water losses are not recorded and 3) the horizontal runoff is negligible.

The WSB weighted values are acquired continuously, in which the maximum weight is reached when the soil is in its field capacity condition. Thus, the gains and losses of water are straight balanced via the equilibrium of the soil water tension, where the gains originated from rainfall (P [mm]), and irrigation (I [mm]) reaches to a maximum soil water content equal to θ_{FC}.

Evaporation is determined on an hourly basis from the differences of mLy at the beginning and end of each period. The hourly soil evaporation from the mLy (Es [mm h^{-1}]) is calculated with the equation:

$$E_s = 10 \times \left(\frac{\Delta W}{\rho_w A_{mLy}} \right) \qquad\qquad \text{Eq.III.10}$$

where A_{mLy} is the mLy weighing plate area [cm^2], ρ_w is the density of water (g cm^{-3}) and ΔW is change in weight (g h^{-1}) given as:

$$\Delta W = \frac{s_t^{mLy} - s_{t-1}^{mLy}}{f_{mLy}} \qquad\qquad \text{Eq.III.11}$$

where s_t^{mLy} is the mLy signal (mV) and f_{mLy} is the calibration factor (mV g^{-1}). f_{mLy} is determined in the field after frequent application of known weights on the WSB and recording

the signal response. It should be done at a time of the day when evapotranspiration and wind speeds are negligible. Thus, the difference between the two measured masses divided by the circular cross-sectional area of the cylinder plate above of the balance plate gives the cumulative evaporative flux density during the period when the values are negative.

III.1.4.2. Soil energy balance approach

The principle of relating soil heat flux and soil evaporation is based on the assumption that the energy changed in soil heat flux or heat storage is assigned to latent heat flux. Gardner & Hanks (1966) suggested that it could be adjusted to include LE, *i.e*., evaporation of soil water, to determine the evaporation occurring within the soil. The hypothesis in this approach is that in open environments, it may be needed to account for the possible occurrence of heat sources or sinks in the realm where heat flow takes place. Heat sources include such phenomena as organic matter decomposition, wetting of initially dry soil material, and condensation of water vapour. Heat sinks are associated with evaporation.

Similar to S (Eq.III.07), the heat source-sink term is considered as a function of both space and time. Thus, the variation of S ($S_{\Delta t}$ [W m^{-2}]) is related to the vaporised or condensed water volume per time. After lumping all these sources and sinks into a single term, the soil latent heat flux (LE_{soil} [W m^{-2}]) and rewriting the equation, $S_{\Delta z}$ is computed by Eq.III.12.

$$S_{\Delta t} = S_t - S_{t-1} = LE_{soil} \qquad\qquad\qquad\qquad\qquad \text{Eq.III.12}$$

where LE [W m^{-2}] is the source-sink term (Heitman *et al.*, 2010). Thus, the residual of measurable sensible heat flux terms measured at two different depths and the sensible heat storage represents the soil latent heat flux in the considered depth interval. Negative values (LE^- [W m^{-2}]) are considered latent heat of vaporisation (LE^+ [W m^{-2}]), and positive values are considered latent heat of condensation, whose L [J m^{-3}] is the latent heat of vaporisation, and E [m s^{-1}] is evaporation. Values for L can be calculated from Eq. III.13 (Forsythe, 1964),

$$L = 2.49463 \times 10^9 - 2.247 \times 10^6 T_m \qquad\qquad\qquad \text{Eq. III.13}$$

where T_m [°C] corresponds to the mean temperature for a given depth layer and time step.

III.2.   SOIS hardware

III.2.1. Modified *Granier* sensor

The modified *Granier* sensor (mG) design resorts to the *Granier* heat dissipation method (G), presenting some modifications aiming to improve the conventional *Granier* design. Table III.1 describes the differences between the mG design and conventional design (G$_{Conv}$). The fundamental difference between mG and G$_{Conv}$ concerns that G$_{Conv}$ only provides a temperature difference measurement, while the system being proposed also provides the two absolute temperatures allowing for a more accurate observation of the process. Thus, mG relies on two operations: temperature sensing and heating. Another core difference is the localisation of the thermal sensing component (Fig.III.2(a)). G$_{Conv}$ sensors have the thermal sensing component in the middle of the heating component, and mG have the sensing component in the tip of the needle. Fig.III.2(b) shows the operational effects of that localisation. It allows the sensors to measure the temperatures changes caused by sap motion.

Table III. 1: Technical comparison between the original *Granier* sap flow and the modified *Granier* approaches.

Criteria	Conventional *Granier* approach	Modified *Granier* approach
Sensing component	Type T Thermocouple (Copper/Constantan)	Thermistor
	Wide range of temperature sensing (-200ºC to 350°C)	Narrow range of sensing (-55ºC to 150 ºC)
	Requires a measuring system such as a voltmeter to measure the output voltage.	Requires an external voltage to operate as a measuring device.
	Difficult construction.	Easy construction
	The voltage generated by junctions at different temperatures is relatively low (around 43µV/C). Thus, amplification is required.	The voltage divider with a reference resistor tied to reference voltage usually is enough. Thus, it is not required for amplification.
Heating component	Wire Constantan (range 14 to 20 Ω)	Wire Constantan (range 30 to 40 Ω)
Operational features		
Type of measurement	Differential temperature	Absolute temperature
Temperature sensing location	Inner of the heating tube	Outer of heating tube, on the needle tip.

Temperature sensing is performed with thermistors, which are used to measure the temperature in the trunk in two instances. Thermistors are thermally sensitive semiconductors whose resistance varies with temperature. They are manufactured from metal oxide semiconductor material encapsulated in a heat-resistant and highly stable glass. The temperature

sensor consists of a thermistor (Epcos 100 kΩ 18 mW NTC, 1 % tolerance) inserted in a glass micropipette (41 mm long, 0.9 mm inner diameter). The thermistor is glued into place inside the micropipette using a cyanoacrylate adhesive. The location of the thermistor in the micropipette determines the depth at which temperature measurements can be taken inside the tree.

Differently, as of conventional *Granier* sensors, the thermistors are placed on the tip of the needle as showed in Fig.III.2(b). It is expected that this modification should improve the sensitivity of the temperature changes caused by the sap motion.

a)

b)
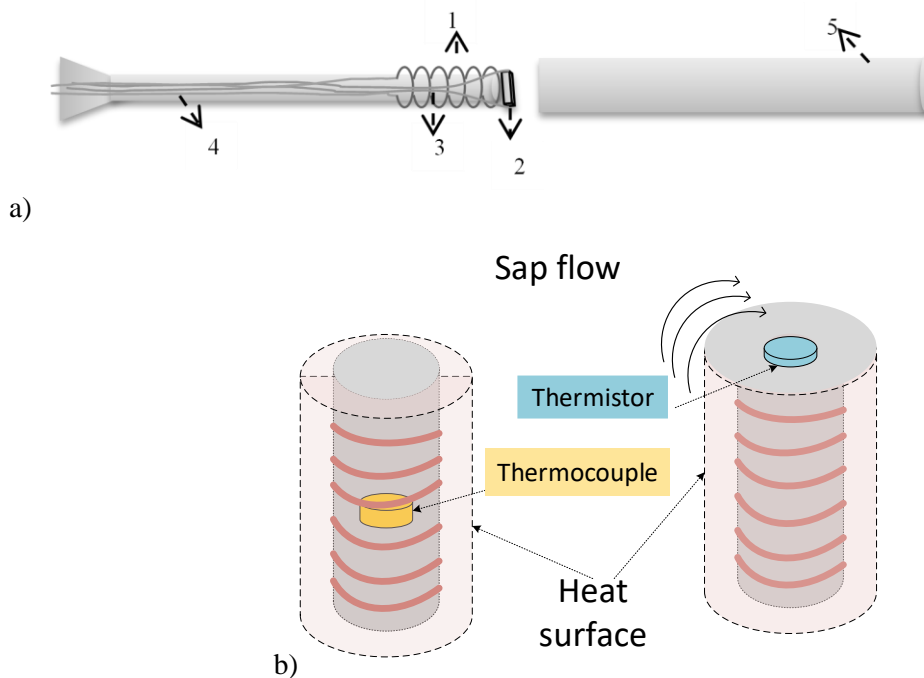
Fig.III. 2: The modified *Granier* sensor (mG) design. a) Building components: 1. Constantan wire; 2. Thermistor; 3. Thermistor terminals; 4. Hypodermic needle; 5. Stainless tube.   b) Schematic structural difference between modified *Granier* sensors and conventional sensors.

The thermistors' terminal extensions (20-gauge, 0.81 mm in diameter) are unwrapped and soldered to their respective thin leads of the thermistor terminals. The connections are insulated with heat-shrink tubing. The micropipette is carefully inserted into a stainless-steel tubing (14-gauge, 2.00 mm in diameter). The tip of the steel needle is sealed with solder to prevent water from reaching the wiring. The heat-shrink tubing is tightened around the needle hub to hold the assembly together and hold tight the thermistor extension wire. For additional water sealing, the seam around the heat-shrink tubing is glued.

The heating element is made with a 0.08 mm, 215 ohms per metre nominal resistance, 44 SWG enamelled nickel-chrome wire. The heating tip is wounded in one thermistor sensor, typically 20 mm long. A second stainless-steel tubing (14-gauge, 2.00 mm diameter) is used to cover the full set. The tip of the second steel needle is sealed with solder to prevent water from

reaching the wiring. The heater is calibrated at 0.2 W being the supply voltage applied with an adjustable regulated power supply. The dissipated power is regulated with an adjustable voltage, and current regulator integrated circuit.

Figure III.3 shows the schematic connections of the thermistors and heating circuits. There is one data acquisition and control module per tree. The temperature measurements are performed after capturing the voltage provided by a voltage divider made of a constant resistor and the thermistor. Each module captures the analogue voltages provided by the thermistor circuit, and the digital output is used to switch on/off the regulated voltage sources.
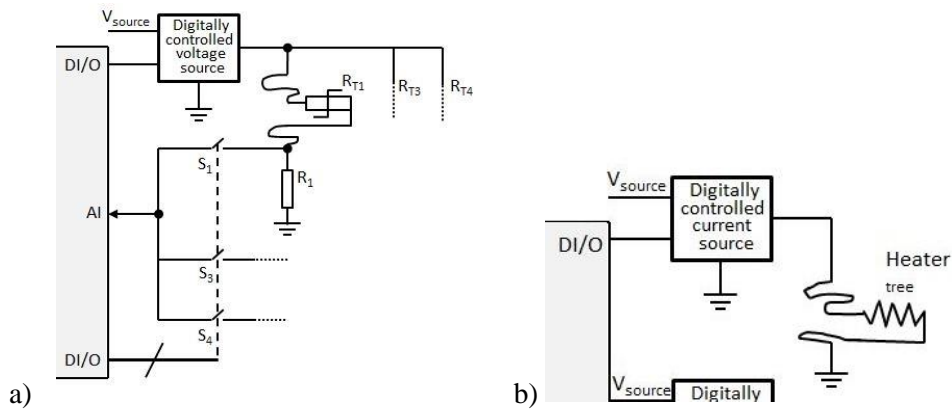
Fig.III. 3: Schematic connections of: a) the thermistors interface; b) the heater circuits.

Once the range of the involved temperatures is not significant (5ºC – 40ºC) and the temperature differences in temporal line to be detected are small (< 1 ºC) the thermistors non-linearity characteristic is not critical in this application. The temperature is read as a voltage given by a passive linear circuit (Eq. III.14)

$$V_{Th} = V_{IN} \times \frac{R_R}{(R_{Th}+R_R)} \qquad\qquad Eq.III.14$$

where V_{Th} [mV] is the output voltage that is a fraction of its input voltage (V_{IN} [mV]) and R_R [Ω] is the reference resistance. R_{Th} [Ω] is the thermistor resistance, which is a function of the temperature.

The sensitivity of the temperature measurement, computed with Eq.III.15, reaches 56.2 mV/ºC, *i.e.*, 11.4 mV per 0.2 ºC, for a 5V voltage source (V_{IN}). The 10-bit ADC of the µcontroller ensures a V_{LSB}[1] resolution of 4.88 mV. The thermal noise of the resistive voltage divider generates (worst case) a voltage of 40 nV/√Hz.

---

[1]LSB (Least significant bit) is the smallest level that an ADC (Analogic – Digital Converter) can convert

$$dV_T/dT = -5 \times \frac{R_R}{(R_{Th}+R_R)^2} \frac{\partial R_{Th}}{\partial T}$$ Eq.III.15

III.2.2. Weighing device

The weighing device (mLy) is used to measure the evaporation from the soil surface of irrigated crops, in order to provide a direct inference of the soil evaporation. Also, it enables the measurements of partial canopy cover conditions due to easy replication in different spatial soil water distribution, canopy shading and under-canopy wind patterns. The mLy consists of stainless-steel shear-beam load cells and levelling mounts, with the difference that there is not a container, thus, permitting complete equilibrium between weighted volume and surroundings. It is configured to enable water transference into or out of the scaled boundary, in an open system that means without a container (Fig.III.4). The design criteria for the mLy developed in this project requires them to be able to monitor evapotranspiration continuously in an hourly periodicity; portable and easy to deploy; economical to construct and install.
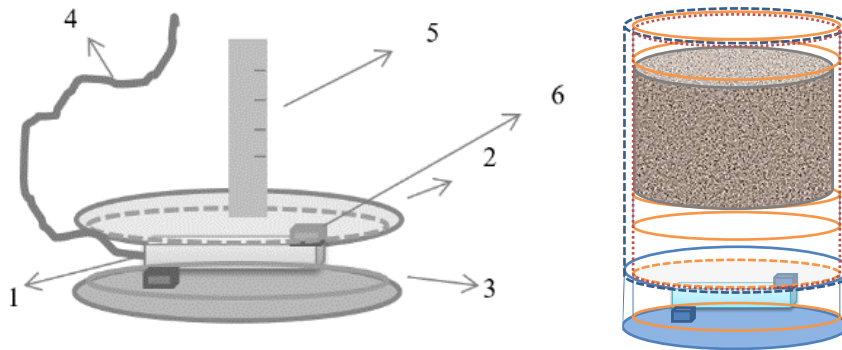
Fig.III. 4: Construction diagram of the weighing device(mLy): 1. Load cell; 2. Superior plate (holding soil component); 3. Inferior plate (base supporting); 4. Power and communication data cable; 5. Height scale; 6. Hex Nut.

III.2.2.1. Load cell specifications

The load cell used as the weighing tool (Fig.III.4) shows a capacity range of 1000 to 10000 grams. Manufacturer's published specifications for the load cell are listed in Table III.2. The load cell is assembled with an end tube cap as a superior plate to hold the soil volume, being the inferior plate used as base support (it shows an area of 105.68 cm^2). The plates are fixed with two screws,

and two hex nuts are added to keep the plates separated from the load cell and guarantee the balance of weight.

Table III. 2: Manufacturer's published specifications for the load cell.

Load Cell Specifications	Values	Unit
Rated Load	10	kg
Rated Output	1.0±0.15	mV V^{-1}
Zero Output	±0.1	mV V^{-1}
Creep	0.03 /30 min	%
Recommended operating voltage	3~12	VDC
Maximum operating voltage	15	VDC
Input Impedance	1115±10	Ω
Output Impedance	1000±10	Ω
Total Size	approx. $8 \times 1.2 \times 1.2$	cm
Cable	0.8×20 (diameter x length)	cm
Input End	Red+ (power), Black-(power)	
Output End	Green+(signal), White-(signal)	
Material	Aluminium Alloy	

The mLy provides an output with a sensitivity of 0.5 µV per 1 g. Fig.III.5 shows the schematic of the mLy output signal amplifier.

The transfer function for this interface is given in Eq.III.16

$$V_{OUT} = V_{IN} \times \left(1 + \frac{R_2}{R_1}\right) \hspace{4cm} Eq.III.16$$

where V_{IN} [mV] and V_{OUT} [mV] are respectively, the amplifier output and input load, term $\left(1 + \frac{R_2}{R_1}\right)$ is the amplifier gain where R_1 [Ω] and R_2 [Ω] are resistors.
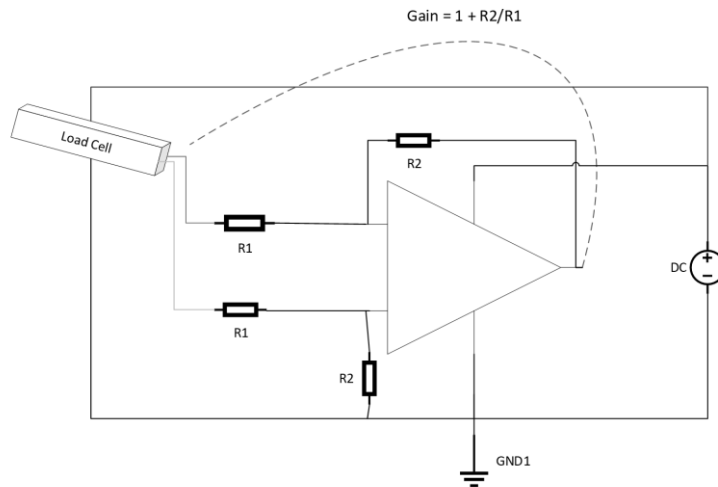
Fig.III. 5: Schematic of the amplifier used in the modified microlysimeter. R1, R2 are resistors. GND1 is the ground. DC (direct current).

III.2.2.2. Accuracy and Sensitivity

The mLy shows as sources of error, nonlinearity, hysteresis, noise, offset and temperature drift. As the linear outputs will be in weight difference and the middle of the full range of 0–10000 g, the errors are irrelevant. The worst-case non-linearity specification is seen over the load cell's full range (Misra *et al.*, 2011).

The signal measured with a load-cell requires calibration to convert the output signal (mV) into an actual weight. Before placing any experimental mLy devices over the load cell plates, the load cells were tested for linearity, (including a zero load) within the range of 0–5000 g. During the calibration of the mLy, the weight of the desired load was first measured with a pre-calibrated electronic platform balance of 10000 g capacity and ±0.01 g sensitivity. For a given load, the load cell signal (mV) was captured at 1–minute interval over a period of 5–10 min. Then the signals were averaged over 5–10 minutes and plotted against load (g).

Fig.III.6 shows the transfer characteristic of the mLy obtained after performing a calibration procedure for which an electronic scale was used. The analysis of the results (slope and intercept parameters) with 12-point calibration equation indicated that the load cell shows satisfactory linearity with a determination coefficient of $R^2 = 0.99$, similar to that presented by Flumignan *et al.* (2012) and Misra *et al.* (2011).
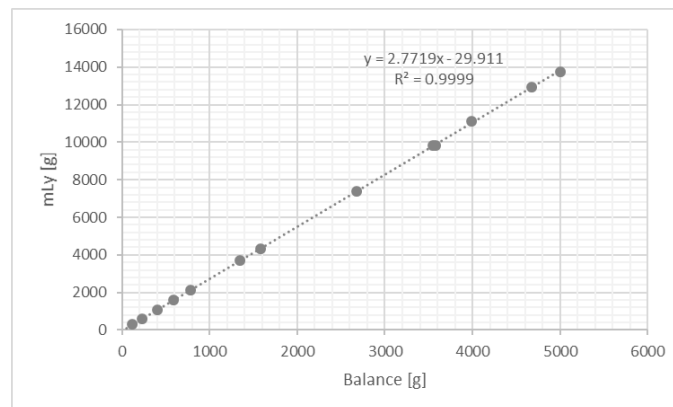
Fig.III. 6: The transfer characteristic of the mLy obtained after performing a calibration procedure with an electronic scale.

The dimensional constraints for the microlysimeter take in consideration the area of the inferior plate (A_{mLy}), the maximum mLy depth installed (z_{mLy}), the maximum weight of saturated soil (W_{MAX}), and the soil bulk density (ρ_b). The weight of the soil column is the product of its bulk density and volume and, the range of soil bulk density to clay soil and sandy soils is between 0.9 g/cm^3 to 1.25 g/cm^3. Therefore, Fig III.7 shows the transfer characteristics that relate to the soil

mass ranging from 951.3 g (0.47 mV) for the dry soil to 2110 g (1.05 mV) for saturated soil mass. The weighted maximum volume is 1057 cm^3, *i.e*., the plate area and maximum heights are 106 cm^2 and 10 cm, respectively.
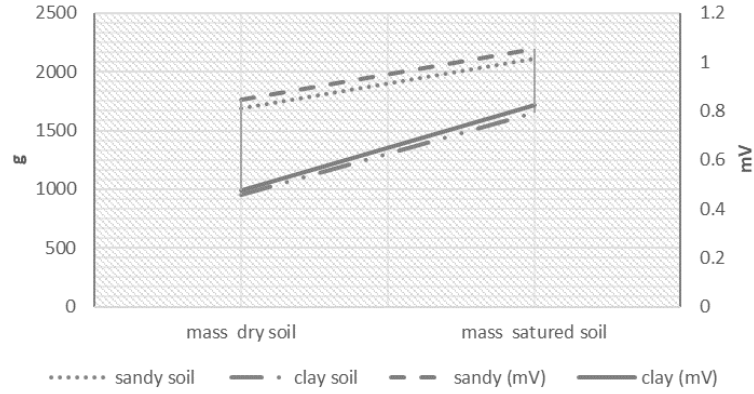
Fig.III. 7: The transfer characteristics related to the soil mass ranging.

The transfer function for the mLy is given in Eq.III.17

$$V_{OUT} = W \times L_S$$ Eq.III.17

where V_{OUT} [mV] is the mLy output, W [g] is the weight, L_S [mV/g] is the load cell sensitivity. From this characteristic and considering that the gain of the analogue signal acquisition front-end is 4000, it can be seen that the mLy measuring sensitivity is

$$L_S = \frac{(1.05-0,47)}{(2110-951.3)} \times 4000 = 2 \text{ mV/g}.$$

The 10-bit ADC of the μcontroller ensures a resolution of V_{LSB}=4.88 mV, thus, the resolution in mm is 1 g $\times$ 4.88 mV / 2 mV = 2.44 g = 0.23 mm.

III.2.3. Calibrated *Peltier* cells

The estimation of the soil heat flux resorts to alternative soil heat flux transducers (Weaver & Campbell, 1985), *i.e.,* the calibrated *Peltier* cells (Pcell). The Pcells, measure the soil heat flux density (G_z [W m^{-2}]) on depth z directly (Fuchs & Tanner, 1968; Fuchs & Hadas, 1973), once that is adjusted with thermopile heat flux transducers manufactured following the Fuchs & Tanner (1968) methods. These devices with dimensions around 40 mm $\times$ 40 mm $\times$ 3.3 mm (Fig.III.8) are thermopiles consisting of many thermocouple pairs separated by two ceramic plates and sealed in a protective cover.
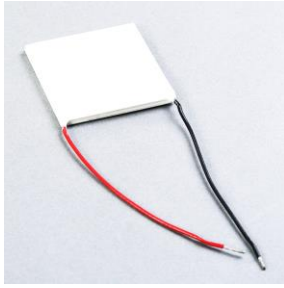
Fig.III. 8: The commercial *Peltier* cell image

The heat flowing through the plates results in a temperature difference between the two surfaces which is proportional to the heat flux density and can be measured with the thermopile. The measured signal requires a calibration related to a commercial soil heat flux plate. The operational ranging is of -25 mV to + 25 mV. The reading range of the SOIS system is 0 to 5000 mV. Thus, the signal is amplified and summed 2500 mV to get relative negatives values.

The calibrated *Peltier* cells (Pcells) are supported on a printed circuit board to connect at the Pcells on µcontroller and enable the readings. Fig.III.9 shows the schematics of the Pcells interface, which one was built to amplify the signal and enable its reading with the µcontroller.
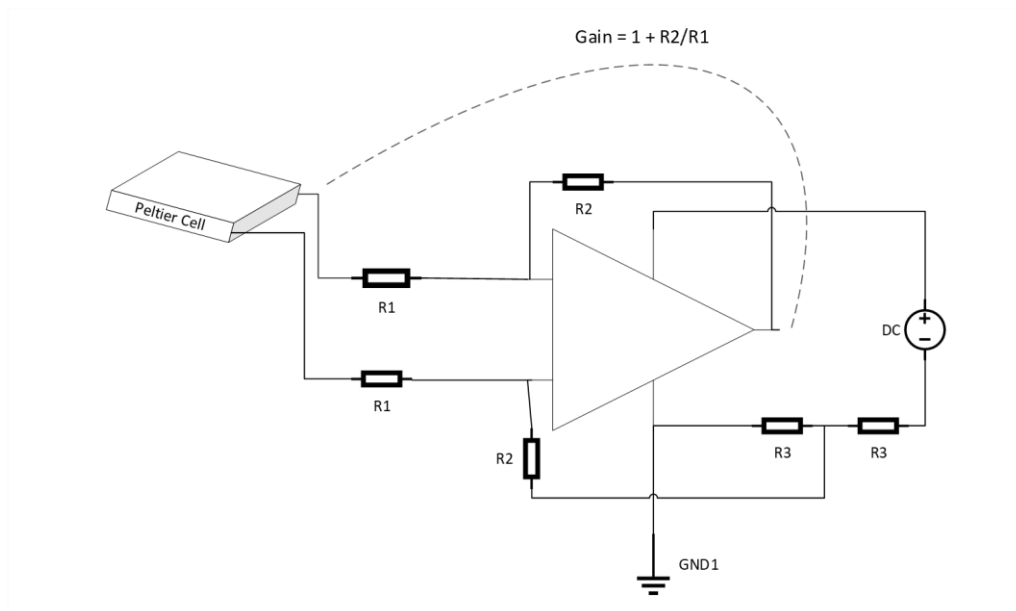
Fig.III. 9: Schematic of the amplifier used in the *Peltier* cell interface. R1, R2 and R3 are resistors. GND1 is the ground.

III.2.4.   Local controller

An Arduino Atmega2560 µcontroller board (*MEGA 2560 Arduino*, 2014) is used to implement the local controller because of its relatively low-cost, large user community, and adaptability. It operates as a logic controller responsible for the overall management of the system operation, data capture and measurement control processes, as well as, receives/sends data from/to the terminal and wired and wireless networks (Fig.III.10). This microcontroller platform is used as a fast prototyping resource, which provides convenient access to the microcontroller input/output pins and connectivity to a personal computer for programming and user interaction.
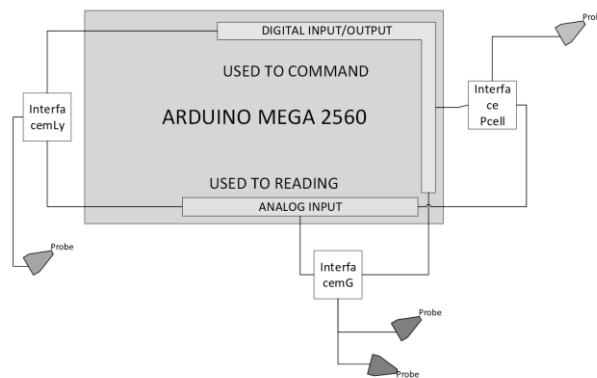
Fig.III. 10: The schematic Arduino Mega 2560 used as the local controller.

The sensors being used operate on low voltages, and output signals are compatible with the Atmega2560 µcontroller I/O ports, including analogue voltages and a selection of digital inputs and outputs. The simple interface to I/O digital and analogical ports permits to control many different SOIS devices.

III.3.   SOIS software

SOIS software (SOS) is the crucial component of SOIS as it establishes rules and procedures to set up the SOIS hardware (SOH), including the systems data management such as data control, data processing and automatic data processing. The latter refers to the non-compulsory automated algorithms to process raw data using relatively simple procedures based on the fuzzy logic approach.

Fig.III.11 illustrates the SOS architecture. It uses the Fuzzy Algorithm Automation System (FAUSY) aiming to supervise, improving, fine-tuning, evaluating the SOIS performance, and promote the automatic learning and decision making.
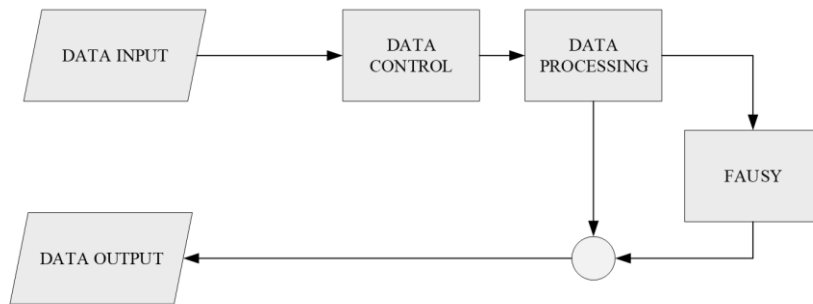
Fig.III. 11: General view of the SOIS software organisation.

III.3.1. Data Control System

The data control system operates in the local controller board, *i.e.*, the microcontroller. The role of the microcontroller consists of controlling the measurement operations for data acquisition, signal pre-processing and management, and data transmission. The data control system is written in a simplified C++ language in a processing-based IDE, which is compiled and loaded on the local machine (*e.g.* Arduino). Fig.III.12 shows the flow chart of the control system.
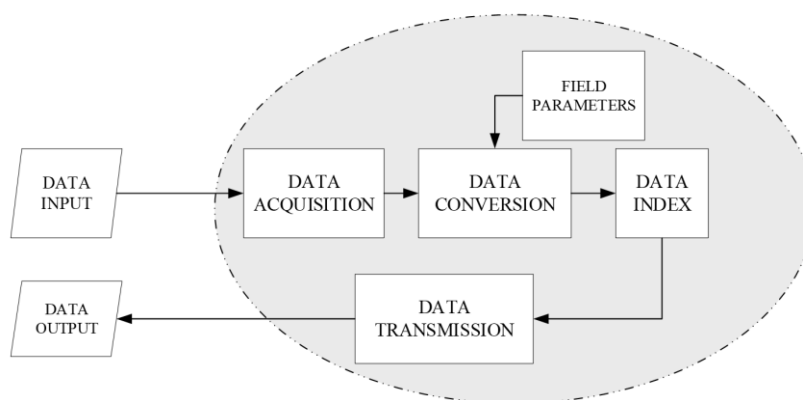
Fig.III. 12: The data control system organisation

III.3.1.1. Data acquisition

The data acquisition block is responsible for controlling signal capturing and obtaining field information inserted manually into the control system. The time base that regulates data collection timing and intervals of data collection is obtained from the sketch built on the Arduino platform.

Preliminary data acquisition is performed for noise filtering purposes. A simple moving average filter is used to minimise random noise while retaining a sharp step response (Smith, 2013). It computes the output signal by averaging a vector of M captured samples via Eq.III.18

$$y[n] = \frac{1}{M} \sum_{k=0}^{M-1} x_{[n-k]} \qquad\qquad \text{Eq.III.18}$$

where x is the input signal, y is the output signal, and n is the discrete-time order.

The following field information are manually inserted during the installation time, *i.e.,* 1) the trunk perimeter ($T_{heater}\text{Ø}$ [cm]) with T_{heat} sensor; 2) T_{heat} sensor azimuth; 3) the diameter of mLy superior plate ($mLy_{\text{Ø}}$ [cm]); 4) the buried depth of mLy superior plate (mLy_Z[cm]); 5) mLy reading for 0 load (mLy_{0W} [mV]); 6) known load (mLy_L [mV]); 7) texture of soil; 8) localisation using GPS; 9) *Peltier* cells calibration equations.

III.3.1.2. Data conversion

The data acquired and filtered previously are converted from sampled electrical signals into digital numeric values, with which the relevant quantities necessary for the irrigation process are estimated. The analogue to digital converter available in the ATMega2560 provides a 10-bit data conversion resolution. The signals of the following sensors are acquired via this converter following the conversion parameters:

a) Thermistors

The computation of the temperature given by the sap flow sensors follows the model of the resistance of a semiconductor at different temperatures by Steinhart–Hart equation (Steinhart & Hart, 1968). The Steinhart–Hart equation is a model of the resistance of a semiconductor at different temperatures. The equation is:

$$\frac{1}{T} = A + B \ln(R) + C (\ln(R))^3 \qquad\qquad \text{Eq.III.19}$$

where: T (K) is the temperature; R (Ω) is the resistance at the measured T, A, B, and C are the Steinhart–Hart coefficients which vary depending on the type and model of the thermistor and the temperature range of interest. However, NTC (negative temperature coefficient) thermistors can also be characterised with the β parameter equation, which is mostly the Steinhart–Hart equation with $A = \frac{1}{T_0} - \frac{1}{\beta}\ln(R_0)$, $B = \frac{1}{\beta}$ and $C = 0$. Thus,

$$\frac{1}{T} = \frac{1}{T_0} + \frac{1}{\beta}\ln(\frac{R}{R_0})$$
                                                        Eq.III.20

where β is the coefficient of the thermistor (4072 is used in this work). R_0 (Ω) is the nominal resistance of the NTC used (100 kΩ at 298.15 K). Since converting Kelvin to centigrade is T [ºC] = T [K] - 273.15, the captured output voltage (V_{OUT} [mV]) is converted to ºC degrees following the Eq.20-21, where V_{IN} is the input voltage (5000 mV is used in this work)

$$R = R_0 \times \left(\frac{V_{IN}}{V_{OUT}} - 1\right)$$
                                                        Eq.III.21

b) Calibrated *Peltier* cells

The *Peltier* cells allow computing the soil heat flux following the calibration equations previously inserted on the microcontroller board. The linear regression equation of calibration uses specific information inserted onboard. Thus, the calibration equation format is:

G_Z [W m^{-2}] =*Peltier* cell signal [mV] $\times$ slope coefficient + G_Z axis interception coefficient   Eq.III.22

c) Load cell

The load cell provides data to compute the soil weight following specific calibration values according to readings obtained experimentally in the field. Two values are captured $L_0 \rightarrow x_1$ [mV], and $L_w \rightarrow x_2$ [mV] from which the load cell conversion factor f_{LC} [g mV^{-1}]is calculated by

$$f_{LC} = \frac{L_w - L_0}{x_2 - x_1}$$
                                                        Eq.III.23

where L_W and L_0 are known weight and no load, respectively, and, x_1 and x_2 are the related readings [mV]. Thus, the equation format is:

W [g] = Load cell signal [mV] $\times f_{LC}$+ L_0.   Eq.III.24

III.3.1.3. Data Index

The data acquired with the SOIS local controller are processed as a text file (.txt) containing columns with index [i], day-of-year (DOY), time and date plus data, whose data are composed by the outputs given by the sensors. The signals are indexed by continuous inputs per intervals monotonically increasing of 1/96 day-of-year (DOY), aiming to guarantee correct matching between inputs in the timeline and avoid extra computational effort in the data processing stage.

The data arrangement resorts to columns in fixed format and order and set up in the μcontroller. For n number of signals, the order of column separated for comma should be a row matrix type, where the raw data is expressed as:

Raw data = [Year, DOY, index (hour fraction), data(signal$_1$), data(signal$_n$), (specific information)].

The lack of information is codified as NaN meaning, not a number. The gaps and spikes identifying are filled recurring to smoothing algorithms, which these values are substituted.

III.3.1.4. Output data transmission

Different communication media, such as radio, memory card, and internet, can be used to transmit the collected Output captured data and field information to a central controlling centre.

The Output captured data comprises the dataset obtained as described in section III.1, which includes: the dual-tree temperatures from T_{heat} sensor (T_{heat} [ºC]) and T_{no_heat} sensor (T_{no_heat} [ºC]); the soil weight (W [g]); the dual soil heat flux from two depths, G_{Z1} [W m^{-2}] and G_{Z2} [W m^{-2}], respectively, and the soil temperature (T_{soil} [ºC]) at depth between the G_{Z1} and G_{Z2}.

The Output field information includes a package containing all information of field parameters manually inserted during the installation time as described in section III.3.1.1.

III.3.2. Data processing

The data processing is the first step to compute in the external machine, the functional quantities (explicative variables) is based on data captured from sensors. Fig.III.13 illustrates the SOIS data processing organisation, which is composed of the modules: data acquisition, data computation, field information parameters and the data output.
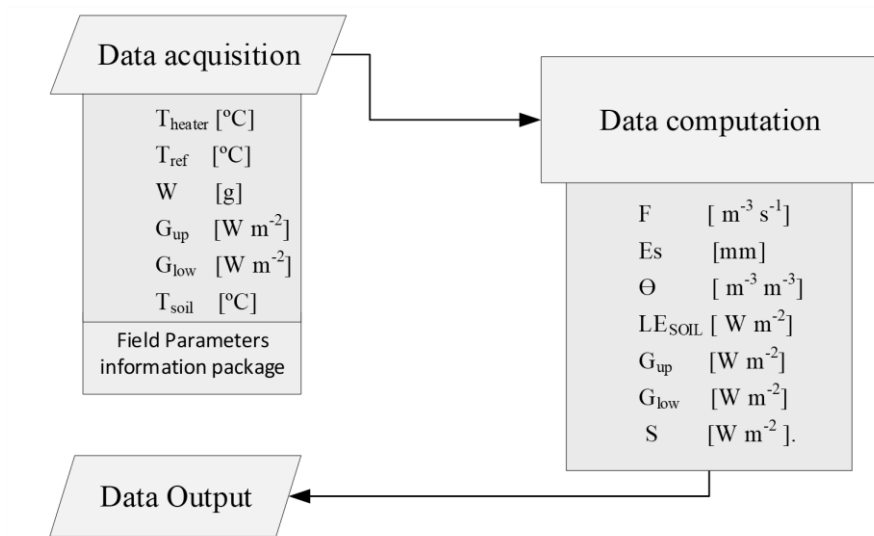
Fig.III. 13: The SOIS data processing organisation

The data acquisition block receives the data set transmitted by the local machine via the available alternative communications media. For this work, the dataset consisted of the dual-tree temperatures from T_{heat} sensor (T_{heat} [ºC]) and T_{no_heat} sensor (T_{no_heat} [ºC]); the soil weight (W [g]); the dual soil heat flux from two depths, G_{Z1} [W m^{-2}] and G_{Z2} [W m^{-2}], respectively, and the soil temperature (T_{soil} [ºC]) at depth between the G_{Z1} and G_{Z2}.

The data computation module computes the explicative variables, which are the measurements transpiration (F [m^3 s^{-1}]), soil evaporation (Es [mm]), soil moisture (Θ [m^3 m^{-3}]), soil latent heat flux (LE$_{SOIL}$ [W m^{-2}]), soil heat flux (G_z [W m^{-2}]) and soil heat storage (S [W m^{-2}]). The field information parameters required to compute the following quantities are described in Section III.3.1.1.

Fig.III.14 (a-c) shows the spreadsheet used to convert measured data in transpiration, soil evaporation, soil latent heat flux, soil heat flux and soil moisture.

a)

Night-time

complete day

T_{heater} T_{ref} T_{heater} T_{ref} k_{Bi}

$T_{MAX} = a \times T_{ref} + b$

Linear regression

$k_{Bi} = (T_{MAX} - T_{heater})/(T_{heater} - T_\infty)$

Computing k_{Bi}

$u = 0.000119 \times k_{Bi}^{1.231}$

Sap flow density

A= Area trunk

$F = u \times A$

Transpiration

Output

b)

A= Area plate

Ten days

W

Compute W_{max}

$(W_i - W_{i-1})/A$

$\Delta\Theta$ [mm]

Soil water change

$\theta = -1 \times \left(\dfrac{(W_{max} - W_i)\theta_{fc}}{W_{max}} - \theta_{fc} \right)$

Θ_{FC}

Θ [m^{3}m^{-3}]

Soil moisture

c)

$\Delta G = G_{up} - G_{low}$ $\Delta S = (\Delta G_i - \Delta G_{i-1})$

G_{up} G_{low} ΔG ΔS
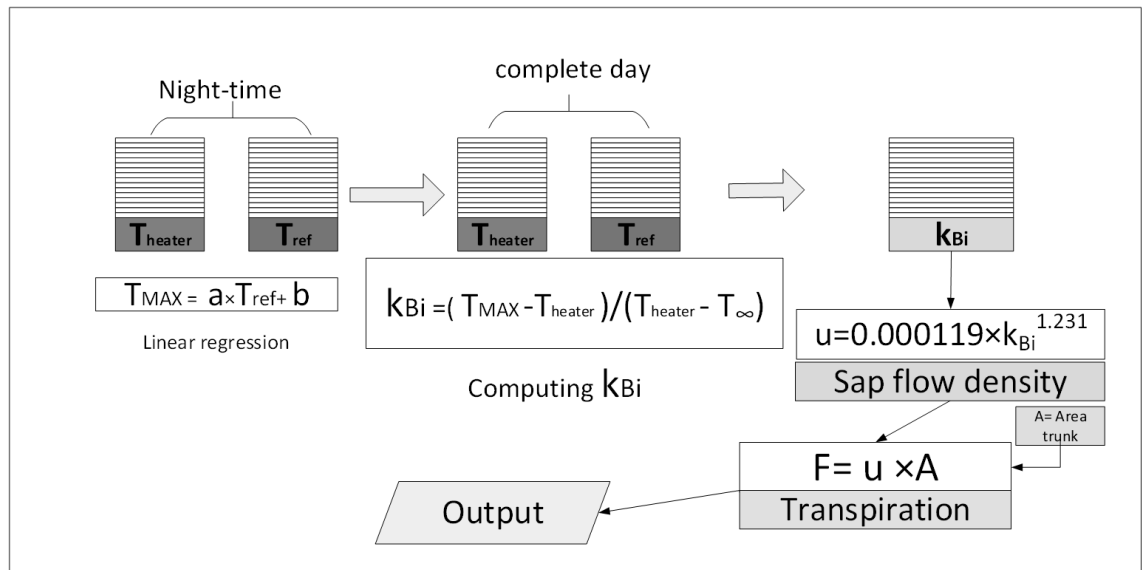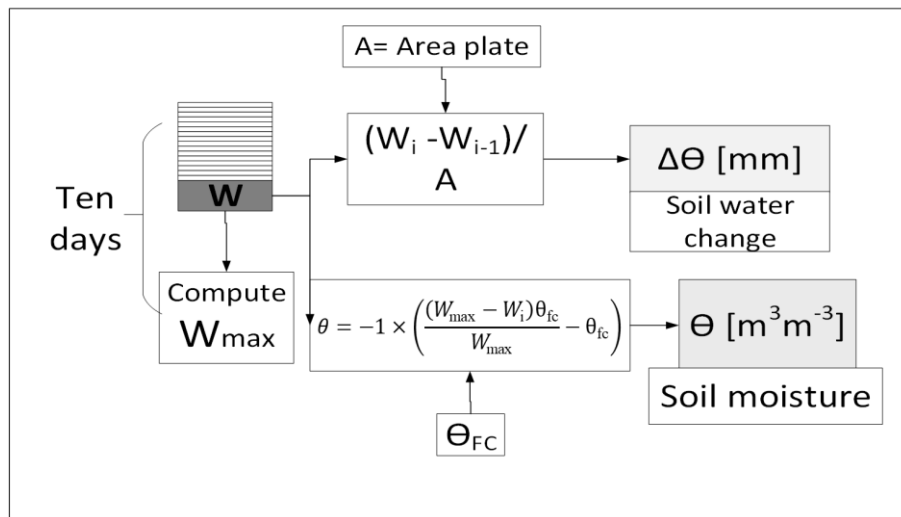
Soil Latent Heat Flux
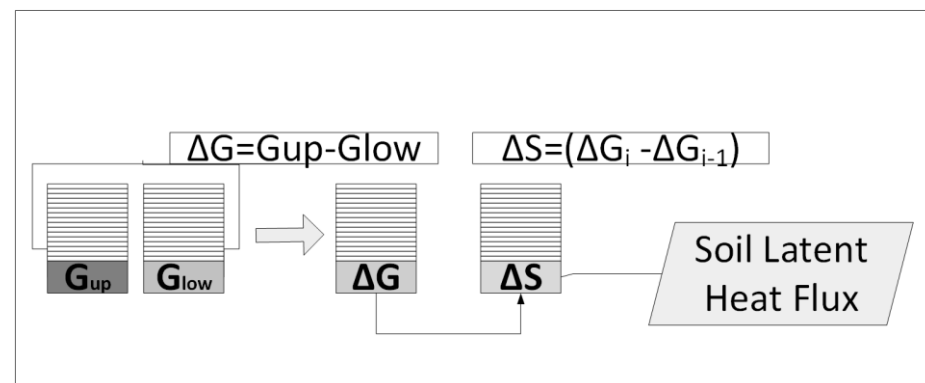
Fig.III. 14: Schematic illustration of computation: a) transpiration; b) soil evaporation and soil moisture; c) soil latent heat flux, soil heat flux and soil heat storage.

III.3.3. Fuzzy Algorithm Automation System

The Fuzzy Algorithm Automation System (FAUSY) is an intelligent system to automate data analysis and prediction embedded in a fuzzy logic algorithm. It is meant to manage the overall orchard and vineyard irrigation process using an approximate and yet effective way of finding the relationship between the environmental variables and SOIS measurements, which are too complex or too ill-defined for precise mathematical analysis. FAUSY is structured in two modules: a) knowledge base and database, and b) inferential machine (Fig.III.15).
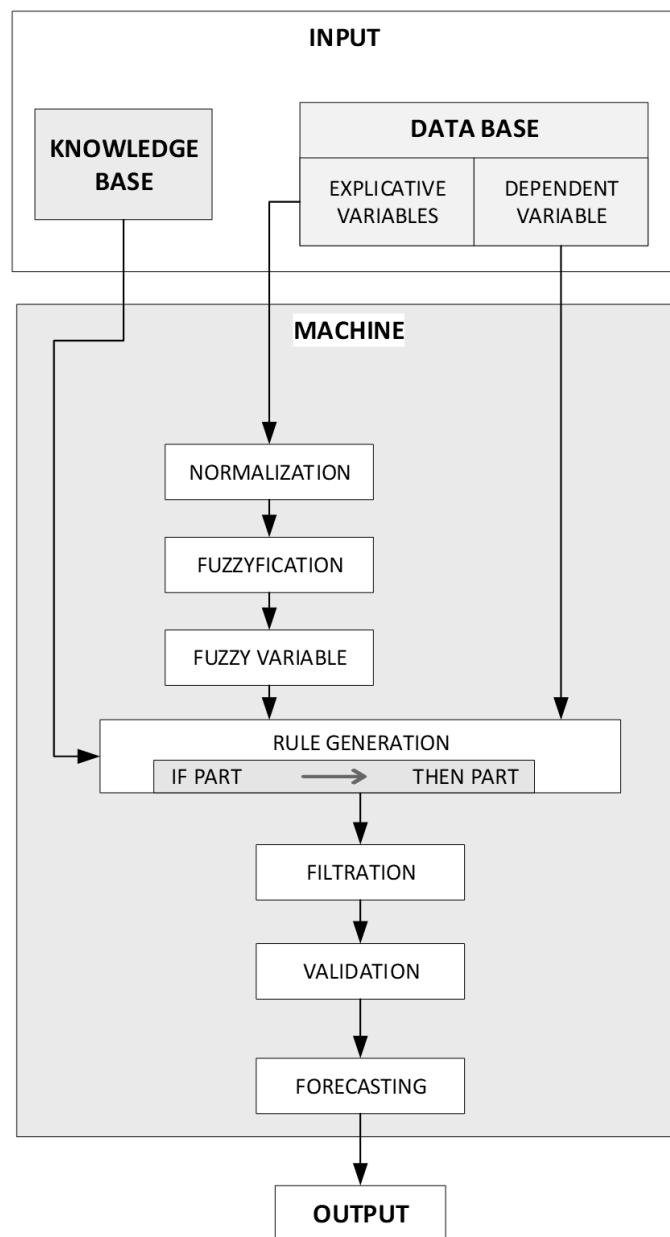
Fig.III. 15: Schematic flowchart of the FAUSY algorithm.

In this process, FAUSY extracts the relationships from a set of input-output environmental observations. Thus, general directions for algorithm-based machine learning in fuzzy systems are outlined. Through an iterative procedure, the algorithm plays with the learning or forecasting via a simulated model. After a series of trial and error control iterations, the outcome of the algorithm may become highly refined and be able to evolve into a more formal structure of rules, facilitating the automation of SOIS data analysis.

III.3.3.1. Knowledge base and database

The knowledge base aims to supply information about the discretisation and fuzzification[2] processes. It is represented by a fuzzy logic approach, which provides a computational framework for fuzzy inference in an environment of rough information. Also, it is used to define and qualify parameters that describe relationships in each event.

The database is structured as a collection of data, where the input/output events are registered and recorded by the algorithm. These records are treated as unsupervised learning, which is used to automatically mapping an input-output event's vector into classes and building systematic learning, *i.e.*, generating rules.

III.3.3.2. Inferential Machine

The inferential machine comprises the procedural steps in the learning time and the generation of output, in the forecasting time. Five steps are operated in learning time.

Step 1: Data normalisation

The database is composed of two categories of indexed variables, explicative (V) and dependent (Vd), and supplied by inputs per Day of Year (DOY). The input indexed dataset should guarantee correct matching between inputs in the timeline and avoid computational effort in the fuzzification stage.

The dependent variables arise from the sensor under analyses. The explicative variables are selected from other available sensors. The explicative variable time is discrete within the interval [1:48] which means one unit each ½ hour, in one day. Otherwise, the continuous explicative variables should be normalised. The normalisation of the database causes a fine-tuning in the

---

[2] Fuzzification is the process of changing a real scalar value into a fuzzy value

fuzzy rules generation, since assuming a normalised relative magnitude for the variables clarifies the comparison process. The explicative variable Time (fraction of day: 1/48,12/48,…,48/48) is selected and associated with each input Vd. It means that the input values of the continuous variables are normalised into an appropriate scale defined by the maximum and minimum values, *i.e.*,

$$x_n = \frac{(x - x_{\min})}{(x_{\max} - x_{\min})}$$ Eq.III.25

where x_n is the normalised value, x is the actual value, and $x_{\min}$ and $x_{\max}$ are the minima and maxima values of x in the actual series. In case information about $x_{\min}$ and $x_{\max}$ is lacking, they should be estimated from the empirical knowledge on the range of these variables. Thus, V attributes are normalised into a real number in the unit interval [0, 1].

Step 2: Fuzzification

Automatic generation of fuzzy rules is based on the fuzzification procedure, in which the input values, supplied in a digital form, are converted to labelled values associated to the degree of membership, namely, fuzzy variables or linguistic variables. These linguistic variables are combined to generate fuzzy rules by the objective of the system, that is casually delivered to other system devices.

The fuzzification procedure consists of the universe of discourse (UD) of continuous explicative variables being divided into fuzzy regions. The UD is divided into a number of overlapping (fuzzy) regions and, to each region, a triangular membership function ($f_{\Delta j}$) is defined. The number of fuzzy regions (n_{fr}), which are overlapped sets of variables, are quantified by $n_{\mathrm{fr}} = $ 2N+1, where N is an adequate numerical choice that ensures an odd number for n_{fr}, with a central region. The accuracy of the algorithm can be regulated through an adequate choice of N since larger values imply higher accuracy levels.

The simple triangular membership function ($f_{\Delta j}$) is efficiently computed as,

$$f_{\Delta j}(x_i, a_j, b_j, c_j) = \mathrm{FS}_j(x_i) = \begin{cases} 0 & x_i < a_j \\ \frac{x_i - a_j}{b_j - a_j} & a_j \leq x_i \leq b_j \\ \frac{c_j - x_i}{c_j - b_j} & b_j \leq x_i \leq c_j \\ 0 & x_i > c_j \end{cases}$$ Eq.III.26

where a_j and c_j are defined by a lower limit of membership with $a_j < c_j$, b_j is defined by an upper limit of membership, and x_i is the input value to fuzzification. The parameters a_j, b_j and c_j of a triangular membership function for the j_{th} fuzzy set (FS_j) can be calculated as:

$b_1 = 0$, $b_2 = b_1 + 1/(n_{fr} -1)$, … , $bn_{fr} = bn_{fr-1} + 1/(n_{fr}-1)$ Eq.III.27

$a_i = b_i - 1$ Eq.III.28

$c_i = b_i + 1$ Eq.III.29

with the interval domain of FS_j [0;1] divided into (n_{fr}-1) equal regions. The information on parameters a_j, b_j and c_j of the function (Eq.III.23) should be included in the knowledge base.

Step 3: Fuzzy rule generation

After the fuzzification procedure, the fuzzy rule generating algorithm can be executed (FigIII.16). The absolute target is to develop a fuzzy model that is capable of learning and afterwards forecasting the dependent variables of a given input set in real time by the fuzzy inferential mapping as

IF part   Inference operator   **THEN** part

The fuzzy-rules generation algorithm runs at the learning time and is based on multi-input/single-output events in the rule matrix. In the rule matrix (Eq.III.30), each column IF represents the inputs of the i explicative fuzzy variables (FV) and the last column THEN is the output Vd relative to i inputs. Each row characterises a generated rule n, which is filtered and recorded as a rule matrix (Eq.III.30).

$$rule\ matrix = \begin{vmatrix} [FV]_{input^1} \cdots [FV]_{input^i} \rightarrow [Vd]_1 \\ \vdots \\ [FV]_{input^1} \cdots [FV]_{input^i} \rightarrow [Vd]_n \end{vmatrix}$$ Eq.III.30

The rule matrix is recorded in the learning time (LT), and it will serve as a mathematical tool for forecast events at the forecast time (FT). Fig.16 illustrates the temporal sequence of learning time and forecast time.
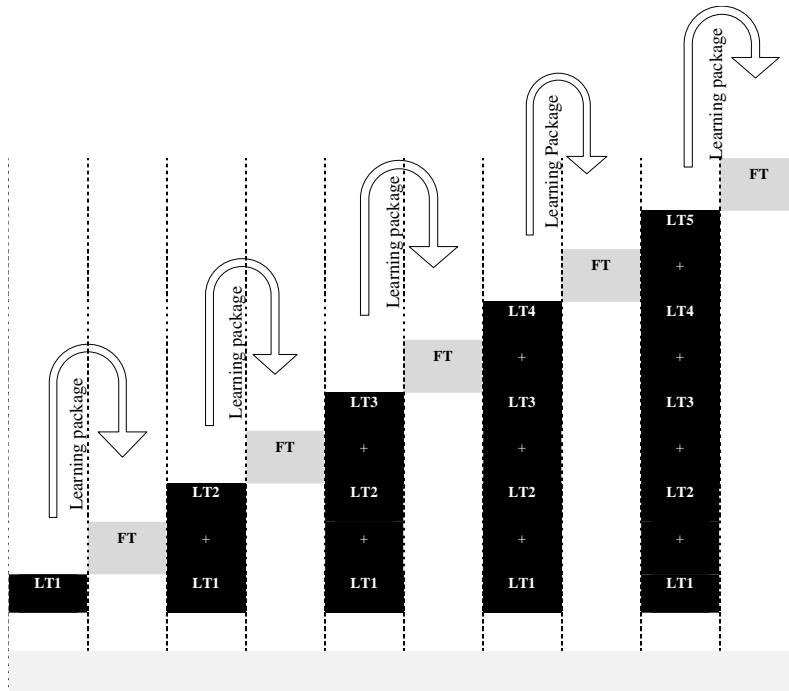
Fig.III. 16: Learning time (LT) and forecasting time (FT) temporal sequence

Step 4: Filtering

Conflicting situations can arise when rules with the same antecedents, *i.e.* the same IF parts, but different consequents (the THEN parts) are generated. In case of a conflict situation, Wang & Mendel (1992) suggested that a degree of membership should be assigned to each rule and that the inconsistent rules with the highest degree should be retained and the other ones rejected. However, because all generated rules convey information, rejects are not possible. Vojtáš (2001) referred that it is essential to have comprehensive and complete semantics because it empowers to compare representative results of computation with real-world data. It should be assured that all occurrences must be computed to describe the *status quo*. Thus, if there are conflicting rules, the model should look for the best solution based on the fuzzy logic theory. The FAUSY conflicting rules are overcome through calculation of the mean consequent part. For example, consider two rules:

$$FV_1 \ldots FVn \rightarrow Vd_x \qquad\qquad\qquad\qquad\qquad \text{Eq.III.31}$$

$$FV_1 \ldots FVn \rightarrow Vd_y \qquad\qquad\qquad\qquad\qquad \text{Eq.III.32}$$

where the aforementioned consequent part is $Vd_x \neq Vd_y$, the rule pair mean is calculated as

$$Vd_{x,y} = \left(\frac{Vd_x + Vd_y}{2}\right)$$ Eq.III.33

Step 5: Performance assessment

The FAUSY algorithm should identify the explicative variables, selected for fuzzy rules set generation, better related to Vd. The performance assessment is done by analysing the residual error (RE) between the predicted and observed values of the dependent variable and through the mean square error (MSE). RE refers to the discrepancy between the observed and predicted outputs

$$RE = |\hat{Y}_i - Y_i|$$ Eq.III.34

where Y_i is Vd observed, and $\hat{Y}_i$ is Vd predicted at the i_{th} event. The mean squared error (MSE) is computed using the equation:

$$MSE = \frac{1}{n}\sum_{i=1}(\hat{Y}_i - Y_i)^2$$ Eq.III.35

where n is the total number of events in the specific time interval. The selection of the best explicative variables set will be defined by the minimum MSE.

If a considerable residual error occurs, then the first set of generated rules in the learning time is not enough to explain the reasoning of the system, or a weak relation is established between the explicative variables and the Vd observed. Therefore, the learning time should be more significant, or the explicative variables should be replaced by new generated fuzzy rules. The decision on how to proceed should be taken by the expert; thus, the expert's information should be added to the knowledge base. Also, if the magnitude of the residual error is minimal, then it is adequate to initiate the forecasting time implementation, which works following the last event in t learning time when learned with the explicative variables.

III.4.   Experiments methodology

This section refers to the material and methods used on the trials (Table III.3), detailing the specific techniques for estimations, the approaches adopted, well as, the field characterisation, detailing the information about the raw materials used and the methodological setting of the trials.

The trials are compared and evaluated using statistical and graphical techniques, which consist of regression analysis, the method of differences and correlations. The graphical methods were required to provide information that could not be otherwise apparent from quantitative

statistical evaluations. Thus, they were used as data evaluation tools, providing visual summaries of essential data characteristics and a basis for interpreting data in line with environmental data, *e.g.*, showing information about concentration ranges, shapes of distributions, extreme values (outliers), relationships between different data sets, and trends, for example, increasing, decreasing, and cyclic trends.

Table III. 3: Summary of the experimental sites

Field experiment	Experimental period	Objectives
Commercial olive orchard located in Alentejo	Days 100 to 160 (2012)	Using the Fuzzy Algorithm for Automatic Data Treatment of Granier Technique; variety "Arbequina"
The green roof lab, Instituto Superior de Agronomia (Lisboa)	Days 153 to 274 (2016)	Built-Up of a Weighing Device to Estimate Soil Water Content and Soil Evaporation
Greenhouse, (INIAV-Dois Portos)	Days 69 to 110 (2018)	Evaluation of the Modified Granier Sensors; variety Galega
Kiwi Orchard, Quinta das Picas (Kiwi Greensun, SA), São Salvador de Briteiros, Guimarães	Days 131 to 246 (2015)	Evaluating installation procedure, heater resistance, sensors design, power requirements, the efficiency of solar panel and robustness, the local machine performance and the automatic algorithm of NTG adjustment.
Vineyard, Adega Catapereiro - EN118 Porto Alto – Alcochete	Days 201 to 240 (2017)	Comparing mG sensors and conventional sensors; variety Fernão Pires
Single lemon tree, Cortegaça, Ovar	Days 126 to 137(2016).	The first experimental evaluation of the whole SOIS approach
Vineyard, Estação Agronómica Nacional – Quinta do Marquês, Oeiras .	Days 245 to 305 (2016)	Experimental evaluation of the whole SOIS approach in a grapevine belonging to the demarcated wine region of Carcavelos of the variety "Galego Dourado"

III.4.1. Fuzzy Algorithm

In this section is described the material and methods employed in the experiment of Chapter IV, entitled *Using the Fuzzy Algorithm for Automatic Data Treatment of Granier Technique.*

III.4.1.1. Data acquisition

The present study has used a dataset acquired by sap flow sensors inserted in tree trunks of a commercial olive orchard located in Alentejo, Southern Portugal (38º 24' N, 7º 43' W, 143 m. a.s.l.), during 61 days in 2012 (DOY 100 to 160). Climate is dry sub-humid, of Mediterranean type, with a dry and hot summer, annual mean rainfall of 600 to 800 mm, most of it falling in

autumn and winter, and monthly mean temperatures varying from 9°C in January to 24°C in July. The production system in the site, an olive orchard of the cultivar *Arbequina* explored by the commercial farm "*Olivais do Sul*", uses a "super high density" management technique, adopting a high density of tree planting (1.35 m × 3.75 m). The olive orchard was irrigated nearly daily during spring and summer, with a drip system having emitters with the discharge of 2.3 L h^{-1} and 0.75 m spacing along the row. It resulted in daily mean irrigation amounts close to 3 mm d^{-1} during the irrigation season.

The experimental plot is part of a large olive orchard of approximately 78 ha. An automatic weather station (Pessl Instruments, model iMETOS Avr, Austria), located at about 12 km distance to the north-northwest direction, was used to collect meteorological data. Meteorological data was also used to compute reference evapotranspiration (ETo) following Allen *et al.* (1998). From these data, relative humidity (RH [%]), solar radiation (R$_s$ [W m^{-2}]) and reference evapotranspiration (ETo [mm h^{-1}]) were selected as explicative variables in the relationship with NTG, since these variables are supposedly those that most influence the occurrence of natural thermal gradients.

The values of ΔT were obtained by 9 sensors (G1, G2, G3, G5, G6, G7, G8, G10 and GN) installed in olive trees just below the bark, with a distance of 10 cm between heated and unheated gauges (Table III.4) (1 cm sensors from UP GmbH, Germany).

Table III. 4: Description of the sensors in the olive trees. [1]: Trunk diameter to height h (30 cm); [2]: heater switched off.

sensor	line	tree	Ø [1]	azimuth
G1	16	34	7.5	NE
G2	16	36	5.4	W
G3	16	38	8.0	E
G5	16	43	7.2	NW
G6	16	44	7.4	NE
G7	13	38	7.1	E
G8	13	39	7.8	N
G10	13	42	7.9	S
[2]GN	**13**	**41**	**7.6**	**E**

The reference sensor (GN) traced the temperature variability (NTG) into the trunk when the heater was switched off. Mean sap flow data was stored every 30 minutes in a data logger (Model CR1000, Campbell Scientific, Inc., Logan, UT, USA).

Three ΔT approaches were used as functions of the variable time (*t*, [s]):

$$\Delta T_{ADJ(t)} = \Delta T_{(t)} - NTG_{OBS(t)} \qquad \text{(Eq.III.36)}$$

$$\Delta T_{NA(t)} = \Delta T_{(t)} \qquad \text{(Eq.III.37)}$$

$$\Delta T_{PRED(t)} = \Delta T_{(t)} - NTG_{PRED(t)} \qquad \text{(Eq.III.38)}$$

where $\Delta T_{(t)}$ [ºC] is the temperature difference acquired by the sensor when switched ON at t time, $\Delta T_{ADJ(t)}$ [ºC] is the ΔT adjusted by the natural temperature gradient observed at t time, $NTG_{OBS(t)}$ [ºC] is acquired by the reference sensor GN when switched OFF, $\Delta T_{NA(t)}$ [ºC] is the not adjusted ΔT, $\Delta T_{PRED(t)}$ [ºC] is the ΔT adjusted by the NTG predicted via algorithm at t time ($NTG_{PRED(t)}$ [ºC]).

To accurately calculate the sap flow, the term ΔT_{MAX} [ºC] must be determined separately for each sensor (*Granier*, 1987). Two estimates of ΔT_{MAX}, *i.e.*, ΔT_{MAX} adjusted (ΔT_{MAXadj} [ºC]) and ΔT_{MAX} not adjusted (ΔT_{MAXna} [ºC]) were calculated for each sensor by searching the maximum temperature difference obtained with a sensor switched ON (heated) over the initial ten days.

Accordingly, by Eq.III (1-4) and for each sensor, the values of k_{Conv}, sap flux density (u [m^3 m^{-2} s^{-1}]) and sap flow rate (F [m^3 s^{-1}]) were obtained by range of temporal sequence (Fig.III.14(a)), namely k, u and F adjusted (k_{Gadj}, u_{adj} and F_{adj}), not adjusted (k_{Gna}, u_{na} and F_{na}) and predicted (k_{Gpred}, u_{pred} and F_{pred}).

The temporal sequence of data collected from sensors in the DOY interval [100,160] was divided into learning time and forecasting time. The learning time operation was defined as the time used for capturing inferences by generated fuzzy rules. Alternatively, the forecasting time operation was defined as the time to estimating NTG occurrences after the environmental variables and fuzzy rules has been generated. The learning time and the forecasting time are illustrated in (Fig.III.16).

The $\Delta T_{MAXna(t)}$ and ΔT_{MAXadj} were extracted from the sensors' measurements in the 10 initial days (Table III.5) and recorded for later computations. Lastly, FAUSY started the forecasting time process by estimating k_{Conv} through $\Delta T_{pred(t)}$ and ΔT_{MAXadj}, for all sensors.

Table III. 5: ΔT_{MAXna} [ºC] and ΔT_{MAXadj} [ºC] obtained from measurements in the 10 initial days (DOY[100;110])

sensor	ΔT_{MAXna}	ΔT_{MAXadj}	$/\Delta T_{MAXna} - \Delta T_{MAXadj}/$
G1	11.740	11.408	0.332
G2	14.880	14.551	0.329
G3	13.510	13.254	0.256
G5	13.260	12.984	0.276
G6	11.990	11.705	0.285
G7	11.660	11.314	0.346
G8	14.140	13.942	0.198
G10	10.790	10.397	0.393

III.4.1.2.Methodology to evaluate FAUSY performance

The evaluation of FAUSY algorithm performance is achieved using the following residual error equations:

$RE_f = \lvert F_{pred}-F_{adj}\rvert$	(Eq.III.39)
$RE_{na} = \lvert F_{na}- F_{adj}\rvert$	(Eq.III.40)
$PFC = (RE_f- RE_{na})100/RE_{na}$	(Eq.III.41)

where RE_f and RE_{na} are the residual errors obtained when comparing the results of the sap flow rate predicted, respectively, by the FAUSY algorithm (F_{pred}) and the sap flow rate not adjusted (F_{na}) with the sap flow rate manually adjusted F_{adj}. PFC is the percentage of FAUSY contribution to the improvement of sap flow rate estimation without requiring manual computations.

The performance evaluation through the RE_f, RE_n and PFC calculations infer if the FAUSY algorithm contributes to the ΔT adjustment and if it can supplant the non-automatic data processing when the sensor is switched on.

III.4.2. Weighing Device

In this section is described the material and methods employed in the experiment of Chapter V, entitled *Built-Up of a Weighing Device to Estimate Soil Water Content and Soil Evaporation*.

III.4.2.1.Experimental set

Five weighing devices (mLy), assembled as described in section III.2.2, were buried into five large metallic trays (2.5 m $\times$ 1.0 m $\times$ 0.2 m), filled with three different substrates, different vegetation combinations and submitted to two irrigation levels, 60 % ETo and 100 % ETo, respectively, composed of five treatments as described in Table III.6.

Table III. 6: Experimental set up in trays with three different substrates, submitted to two irrigation levels and the botanical Latin designations of the plants used. [*1]: Irrigation level based on 60 % (I_{60}) and 100% (I_{100}) of the reference evapotranspiration (ETo)

ID	Treatment	Vegetation	Irrigation level (% ETo[*1])	Substrate
mLy3	T3	False brome	60 %	S2
mLy5	T5	French lavender, Rosemary, False brome, Bryophytes	60 %	S1
mLy6	T6	Rosemary	60 %	S1
mLy8	T8	Rosemary	100 %	S1
mLy11	T11	Bare substrate	100 %	S3

Botanical designation	English common name
Brachypodium phoenicoides	Perennial False brome
Lavandula luisieri	French lavender
Rosmarinus officinalis	Rosemary
Pleurochaete squarrosa	Native bryophytes

The characteristics of the three substrates are described in Table III.7. The substrate used (Intensivas technical substrate – Landlab: http://www.landlab.pt/pt/inicio) consists of fermented pine bark humus, blonde peat, expanded clay and volcanic rock, which attributes the physical characteristics, such as, medium texture and balanced drainage.

Table III. 7: Characteristics of the substrates used in the experimental sets (OM – organic matter, θ_{FC} – field capacity, θ_{WP} – wilting point, ρ_b – bulk density, Ksat – saturated hydraulic conductivity). [*1]: not classified given the high OM content

Substrate	Texture	OM (%)	θ_{FC} (cm³ cm⁻³)	θ_{WP} (cm³ cm⁻³)	ρ_b (g cm⁻³)	Ksat (cm d⁻¹)
S1	[*1]	6	0.33	0.15	0.383	5214
S2	sandy	1	0.22	0.12	0.883	3675
S3	sandy	2	0.29	0.14	0.531	7507

Font: Soil Laboratory INIAV-I.P. Oeiras, 2016

The trays were filled with substrate until a depth of 0.15 m. The substrate above of the mLy plate was allowed to flatten with the surrounding substrate for two weeks before the beginning of measurements. The depth between the mLy plate and the surface (z_{mLy} [cm]) was measured 30 days later, to certify that the depth was kept. Table III.8 shows the effective depth resultant and the horizontal distance between the mLy devices and TDR sensors (TDR; CS616 water content reflectometers, Campbell Scientific, USA) used as a control tool.

Table III. 8: Experimental set up in trays with mLy devices and TDR sensors. *1: Effective depth of the mLy plate (z_{mLy}); *2: Effective depth of the TDR sensors (z_{TDR}); *3: Horizontal distance between the mLy devices and TDR sensors; *4: Irrigation level based on 60 % (I_{60}) and 100% (I_{100}) of the reference evapotranspiration (ETo)

mLy	mLy z_{mLy} *1 (cm)	Area$_{mLy}$ (cm^2)	TDR	TDR z_{TDR} *2 (cm)	mLy↔TDR *3 (cm)	Irrigation level (% ETo*4)	Substrate
mLy3	3.0	105.68	TDR3	15.0	15	I_{60}	S2
mLy5	5.8	105.68	TDR5	15.0	15	I_{60}	S1
mLy6	3.3	105.68	TDR6	15.0	20	I_{60}	S1
mLy8	4.7	105.68	TDR8	15.0	30	I_{100}	S1
mLy11	4.1	105.68	TDR11	15.0	15	I_{100}	S3

The calibration for each of the mLy was performed during the installation. The calibration procedure consisted of specific calibration readings, which two values were captured: $L_0 \rightarrow x_1$ [mV], and $L_w \rightarrow x_2$ [mV] from which the mLy conversion factor f_{LC} [g mV^{-1}] is calculated by

$$f_{LC} = \frac{L_w - L_0}{x_2 - x_1}$$
         Eq.III.42

where L_W and L_0 are a known weight and no load, respectively, and, x_1 and x_2 are the related readings [mV]. The calibration equation format is:

W_i [g] = Load cell signal [mV] $\times f_{LC} + L_0$.   Eq.III.43

where W_i [g] is load measured.

After the five mLy devices calibrated, the calibration equations (Eq.III.43) of mLy devices uploaded to the local controller (section III.2.4) for data processing.

III.4.2.2. Field capacity estimation

The field capacity (θ_{FC} [cm^3 cm^{-3}]) of the substrates S1, S2 and S3 were estimated by assessment of the substrates-moisture characteristic curve (Fig.III.17), taking θ_{FC} at water column of 100 cm (1/10 bar), considering these substrates as similar to a mineral soil with low bulk density (Hillel, 1998), which hold a bulk density (ρb [g cm^{-3}])) lower than 1.0 g cm^{-3} (Table III.6). Also, the water content at wilting pointing (θ_{WP} [cm^3 cm^{-3}]) corresponded to 15848 cm (15.5 bar).
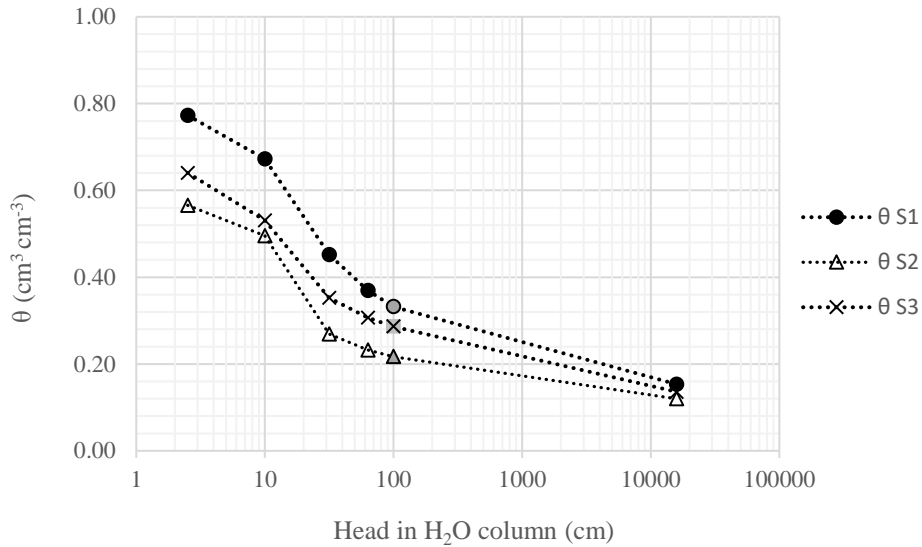
Fig.III. 17: Substrate-moisture characteristic curves for the studied substrates, respectively, S1, S2 and S3; θ – moisture content (cm^3 cm^{-3}). Gray marks: θ$_{FC}$ estimated for the respective substrates.

The estimates of actual substrate moisture (θ [cm^3 cm^{-3}]) proceeded as follows: ten days later, during which irrigation was performed daily, the load measured (W$_i$ [g]) for each mLy and every 15 minutes, were used to compute the maximum mass value weighted (W$_{MAX}$ [g]). The actual substrate moisture (θ [cm^3 cm^{-3}]) was calculated following Eq.III.44,

$$\theta = -1 \times \left(\frac{(W_{\max} - W_i)\theta_{FC}}{W_{\max}} - \theta_{FC} \right)$$
Eq.III.44

where θ$_{FC}$ [cm^{3}cm^{-3}] is the field capacity of the substrate obtained for the substrates-moisture characteristic curve (Fig.III.17) and W$_i$ [g] is the weight measured.

III.4.2.3.Evapotranspiration estimation

The evapotranspiration rate (ET [mm d^{-1}]) of five treatments (T3, T5, T6, T8 and T11) were estimated based on the water balance approach, and using the water balance equation:

ET = I + P + Δθ – D
Eq.III.45

where Δθ [mm d^{-1}] is the water content change, I [mm d^{-1}] is the irrigation depth, P [mm d^{-1}] is rainfall, and D [mm d^{-1}] is the deep percolation.

The Δθ values measured by the mLy devices were computed by means of Eq.III.46, which defines the water content change in mm,

$$\Delta\theta \; [mm] = 10 \times \left(\frac{(W_i - W_{i-1})}{\rho_w A_{mLy}} \right) \qquad\qquad\qquad Eq.III.46$$

where W_i [g] is substrate weight at the end of interval i (hour or day), and W_{i-1} [g] is substrate weight at the end of the previous interval i-1 (hour or day), A_{mLy} [cm^3] is mLy plate area, ρ_w [g cm^{-3}] is water density.

The measurements of $\Delta\theta$ component from TDR sensors were computed by Eq.III.47, which defines the water content change in mm.

$$\Delta\theta \; [mm] = (\theta_i - \theta_{i-1}) \times z \times 10 \qquad\qquad\qquad Eq.III.47$$

where z (cm) represents the measured substrate depth, θ_i [cm^{3}cm^{-3}] is water content at the end of day i, and θ_{i-1} [cm^{3}cm^{-3}] is water content at the end of the previous day i-1.

The irrigation depth per treatment was computed as defined in table III.5, which the daily target irrigation levels were set at 60 % and 100 % of reference evapotranspiration (ETo), namely, 60% (I_{60}) and 100% (I_{100}). The actual meteorological data was used for computing ETo from FAO methodology (Allen *et al.*, 1998), in order to adjust irrigation amounts. Also, meteorological data were collected in an automatic weather station within ISA campus, at a distance of 200 m.

Rainfall data was measured with a rain gauge tipping bucket located in the superior part of a tray and collected from the meteorological data station. The observed deep percolation (D) was measured by tipping bucket rain gauges, positioned under the drop tube, through which the runoff water drained (Fig.III.18).

Fig.III. 18: The tipping bucket rain gauges at the Herbarium building of the University of Lisbon, Instituto Superior de Agronomia (ISA)

III.4.3.   Modified *Granier* sap flow sensor

In this section is described the material and methods employed in the experiment of Chapter VI, entitled *Using Modified Granier Sensors*.

III.4.3.1.Biot *Granier* sap flow index approach

The evaluation of sensors was based on relating the conventional *Granier* sap flow index (k_{Conv}) to the general *Granier* equation (Eq.III.01-03). The conventional approach consists that ΔT [ºC] is computed as:

$$\Delta T = T_{\text{heat}} - T_{\text{no\_heat}} \qquad\qquad\qquad\qquad (\text{Eq.III.48})$$

where T_{heat} [Cº] and $T_{\text{no\_heat}}$ [Cº] are the temperatures sensors measured at the heated and the unheated observation points, from which ΔT [ºC] is computed.

k_{Conv} is obtained with the empirical *Granier* equation:

$$k_{\text{Conv}} = \frac{\Delta T_{\text{MAX(Conv)}} - \Delta T}{\Delta T} \qquad\qquad\qquad\qquad (\text{Eq.III.49})$$

where $\Delta T_{\text{MAX(Conv)}}$ [ºC] is the maximum value of ΔT on a daily course and which is related to the minimum or null sap flow rate for that specific day.

In theory, the term ΔT_{MAX} is intangible and supposed to be the difference temperature when the sap is quiet or in minimum motion and dependent on the term $T_{\text{no\_heat}}$ measured with a different sensor. The determination of these values has been critical since they affect the complete raw sap flow data (Granier, 1987; Lu *et al.*, 2004). Therefore, the T_{heat} sensor should be adjusted to $T_{\text{no\_heat}}$ sensor to estimate the correct ΔT_{MAX} and the actual environment temperature (T_{∞} [ºC]) terms.

Eq.III.49 was built assuming a transient heat-transfer process develops, where the transient cooling process takes place in the interim period before the equilibrium is established. Thus, the term k_{Conv} would represent the ratio of heat transfer by convection to the heat transfer by conduction. In fluid dynamics, this ratio is called the Biot number (Biot) (Incropera *et al.*, 2007), and it should be selected to identify transient conduction problems which convection is the rate controlling process.

Fig.III.19 shows the schematic sap thermal dynamics, imputing physical meaning to Biot, and also shows the limiting steady-state temperature distributions in three points of measurement:

T_{MAX} (maximal temperature reached with null sap flow), T_{heat} (local temperature reached) and T_∞ (environment temperature). The term T_{MAX} [ºC] is the maximum heated surface maintained in the heating process. T_{heat} [ºC] is the temperature exposure to the fluid in environment temperature T_∞.[ºC] fluctuating for some measure intermediate, which $T_\infty < T_{heat} < T_{MAX}$.
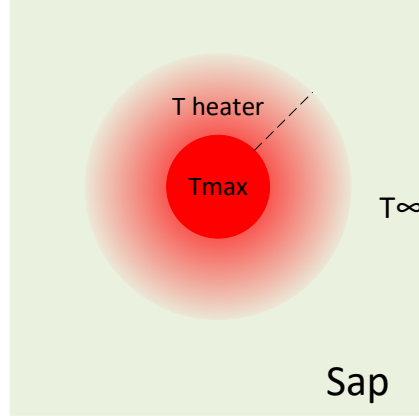
Fig.III. 19: Diagram of the sap thermal dynamic around the heater sensor (T_{heat})

The functional form of the sap thermal dynamic around the heater sensor has been found to be suitable in describing heat transfer in the coupled convective and conductive heat transfer situation, and one can find approximations of the Biot number and its dependency (*i.e.*, T_{MAX} and T_∞ estimates) on the geometry and thermal properties of the system and the flow rate regime. Thus, k_{Conv} is demarcated as analogous to the Biot number (Biot) and computed by:

$$k_{Biot} = \frac{T_{MAX} - T_{heat}}{T_{heat} - T_\infty}$$ Eq.III.50

In this work, the k_{Conv} adjustment (k_{Biot}) consisted in the computation of the linear regression curve of the terms T_{heat} and T_{no_heat} on the night-time period, considering that during this period sap flow is null, and thus, T_{heat} term is equal to the T_{MAX} term.

A linear regression equation (Eq.III.51) can be used to characterise the pair T_{heat} and T_{no_heat} individually, working as a factor of adjustment relating the measurements $T_{MAX(Conv)}$ and T_{no_heat} to the terms $T_{MAX(Biot)}$ and T_∞.

$$T_{MAX(Biot)} = T_{heat(flux\ null)} \xrightarrow{yields} T_{MAX(Biot)} = \alpha \times T_{no\_heat} + b$$ Eq.III.51

where α is the slope of the regression curve and b is the actual $\Delta T_{MAX(Biot)}$. Also, the environment temperature (T_∞) is in principle defined when $\Delta T_{MAX(Biot)}$ is null. Thus,

$$\Delta T_{MAX(Biot)} = 0 \xrightarrow{yields} T_{\propto} = \alpha \times T_{no\_heat}$$ Eq.III.52

The *Granier* sap flow index adjusted (k_{Biot}) in analogy with the Biot number is solved by

$$k_{Biot} = \frac{\alpha \times T_{no-heat} + \Delta T_{MAX(Biot)} - T_{heat}}{T_{heat} - \alpha \times T_{no\_heat}}$$ Eq.III.53

III.4.3.2. Greenhouse trial

This trial was executed in the greenhouse of the Instituto Nacional de Investigação Agrária e Veterinária (INIAV-Dois Portos)[3] on 10 March to 20 April 2018. The experiment consisted in measuring the sap flux density rate (u [m^3 m^{-2} s^{-1}]) with the modified *Granier* (mG). The measurements with conventional sensors and for gravimetric approach were used for comparative purposes.

Five potted olive trees (P01, P02, P03, C01 and C02) were used in this study (Fig.III.20 (a,b)). The potted trees contained a medium consisting of 50% of hummus and 50% of perlite. The potted tree surfaces were covered with cling film to stop evaporation from the medium surface. The sensor-sets and the olive trunk were covered with a thick aluminium foil to limit the effects of sunlight on trunk temperature. Each sensor-set consisted of a pair of sensors, one heater sensor (T_{heat}), and a reference sensor (T_{no_heat}), which were implanted into the olive trunk to a depth of 20 mm, using a 2.0 mm diameter drill bit. The two sensor sets were separated by a vertical distance of at least 10 cm.

Fig.III. 20: Experiment in a greenhouse at the Instituto Nacional de Investigação Agrária e Veterinária (INIAV-Dois Portos): a) Potted olive tree with a *Granier* sensor, heater switched OFF; b) Potted olives trees with a *Granier* sensor, heater switched ON.

Table III.9 describes the sap flow sensor specifications and installation, *i.e.*, heater features, trunk area, azimuth, position, and also, the maximum temperature difference (ΔT_{MAX}) with T_{heat} switched on, and the offset (T_{heat} switched off) obtained in laboratory test, which aimed to verify the sensor heater power and offset level between T_{heat} and T_{no_heat}.

Table III. 9: Description of the resistances of T_{heat}, sensors dimensions, the heat maxima reached in a confined environment, diameter trunk and sensor localisation on the tree. R_{heater}: Nominal Resistance of the heater; V: Voltage applied on resistance; P_{heater}: Nominal power resistance; ΔT_{MAX}: Maximum temperature difference; A_{TK}: Trunk area; h|s: distance between T_{heat} and soil surface; p|s: height of the tree from top to soil surface.

Probe pairs	R_{heater} (Ω)	V (mV)	P_{heater} (W)	ΔT_{MAX} (ºC)	Offset (ºC)	A_{TK} (cm^2)	Azimuth	h|s (cm)	p|s (cm)
P01	34.9	3360	0.32	18.73	0	24	N	26	86
P02	38.7	3640	0.34	11.6	±0.08	18	N	37	120
P03	30.3	OFF		34.18	0.25	24	N	35	100
C01	14.00	1880	0.25			21	N	30	100
C02	14.00	1880	0.25			21	N	40	120

The sap flux density rate was measured with the mG sensors (u_{mG} [m^{3}m^{-2}s^{-1}]) and conventional sensors (u_C [m^{3}m^{-2}s^{-1}]) from March to April 2018. Two pots with mG sensors (P01 and P02) were used to measure u_{mG}. The mG sensors were monitored using the measurement of sap flux density (u_C [m^{3}m^{-2}s^{-1}]) of two commercially manufactured *Granier* sensors (C01 and C02; UP GmbH, Germany). The P03 potted tree was used with mG sensors, in heater off state, to evaluate natural thermal gradients (NTG) occurrences.

The gravimetric test was carried out for the potted trees P01, P02, C01 and C02, one at time, which were transferred onto the weighing platform with 30 kg capacity and 0.5 g accuracy (Radwag -WLC 30/F1/R). The potted trees were irrigated during the previous 24 hours to assurance the same hydric conditions between the treatments. The sap flux density rate (u_{Grav} [m^{3}m^{-2}s^{-1}]) were obtained by weighing the potted olive trees every 30 seconds and averaged to 10 minutes interval. Each monitoring unit was made up of two sensor-set and a data logger.

III.4.3.3.Field experiments

The field trials carried out in the two orchards, *i.e.*, kiwi orchard and vineyard (Fig.III.21(a-b)). The kiwi orchard is located in the Quinta das Picas (Kiwi Greensun, SA), São Salvador de Briteiros, Guimarães – Portugal and the vineyard is located in the Adega Catapereiro - EN118 Porto Alto – Alcochete.
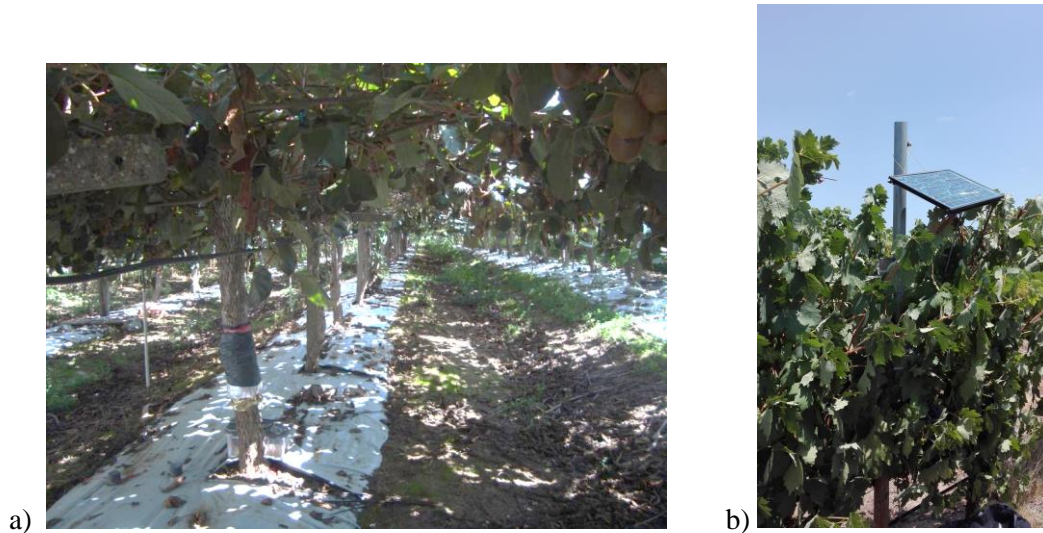
Fig.III. 21: Experimental field set up: a) kiwi orchard in Quinta das Picas, São Salvador de Briteiros; b) vineyard in Adega Carapateiro- EN118 Porto Alto – Alcochete.

III.4.3.3.1.**Kiwi orchard**

The kiwi orchard trial was carried out on 10 May to 2 September 2015. The field trial was preceded by laboratory tests aiming to characterise the sensors to be used in the field and to test the power and heating performance in a controlled environment. Thus, six mG sensors described in the Table III.10 were characterised regarding the resistance, and the electrical current recommended for the heater sensor to reach a constant power of 0.2 W.

Table III. 10: Characteristics of sensors used on kiwi orchard trial. R_{heater}: Nominal Resistance of the heater; I: Nominal electrical current; A_{TK}: Area of the trunk

Probe	R_{heater} (Ω)	I (mA)	A_{TK} (cm^2)	Azimuth	row	tree
G1J	35.1	75	154	N	8	27
G2J	40.5	70	46	N	8	28
G3J	47.3	65	44	N	5	33
G4J	43.2	68	147	N	5	26
G5J	40.7	70	161	N/NO	4	26
G6J	37.7	73	58	N	4	29

The six pairs of sensors presented in table III.9 were installed in the kiwifruit orchard and data was collected for ten days (Fig.III.22). Temperature measurements were acquired with the heater switched on for 15 minutes and likewise, with the heater switched off for another 15 minutes.

Fig.III. 22: The installation of modified *Granier* sap flow sensors on Kiwi plants in Briteiros (Guimarães, Portugal).

III.4.3.3.2.**Vineyard**

The vineyard trial was carried out on 20 July to 28 August 2017, which four pairs of modified *Granier* sensors (SP01, SP02, SP03 and SP04) were installed (Fig.III.23(a)). Also, five pairs of conventional *Granier* sensors (Gr1, Gr2, Gr3, Gr4 and Gr5) were used for comparative purposes (Fig.III.23(b)).

a)   b)

Fig.III. 23: The installation of sap flow sensors on the vineyard -Adega Catapereiro: a) modified *Granier* sensor; b) Conventional *Granier* sensor.

Table III.11 describes the sap flow sensor specifications and installation, *i.e*., heater features, trunk area, azimuth, position and location.

Table III. 11: Characteristics of sensors used on the vineyard – Adega Catapereiro. R_{heater}: Nominal Resistance of the heater; h|s: Distance between T_{heat} and soil surface; A_{TK}: Area of the trunk

Probe pairs	R_{heater} (Ω)	h|s (cm)	A_{TK} (cm^2)	Azimuth	Row	Tree
Gr1	14.1	32	15	NE	Tower	33
Gr2	14.1	30	12	E	Tower	35
Gr3	14.1	35	13	NE	Tower	37
Gr4	14.1	33	18	W	3 right	58
Gr5	14.1	32	12	S	3 left	33
SP01	51.5	31	13	S	3 left	34
SP02	20.2	32	15	E	Tower	36
SP03	14.4	25	16	W	3 right	59
SP04	35.8	27	22	NE	Tower	39

III.4.4. Smart Orchard Irrigation System

In this section is described the material and methods employed in the experiment of Chapter VII, entitled *Using SOIS for Orchards and Vineyard*.

III.4.4.1.Single lemon tree

The first experimental evaluation of the whole SOIS approach was carried out using a single lemon tree localised in Cortegaça, Ovar (40º N, 9 º W), on days 126 to 137 of May 2016. Besides confirming the overall performance of the SOIS system, the objective was also to analyse the physical behaviour of the parameters and extract some further information from the correlation between signals from sensors. For this purpose, a pair of modified *Granier* sensors (mG) was inserted into a lemon tree trunk (20 cm^2), respectively, one heater sensor (T_{heat}), and a reference sensor (T_{no_heat}). These sensors were implanted at a depth of 20 mm, using a 2.0 mm diameter drill bit. The two sensors were separated by a vertical distance of at least 10 cm. The double sensors and the lemon tree trunk were covered with a thick aluminium foil to limit the effects of sunlight on the trunk temperature.

Correspondingly, one weighing device(mLy) and a pair of calibrated *Peltier* cells (Pcells) were positioned 2.5 m away from the lemon tree, which the mLy with superior area plate of 20 cm^2, was buried at 15 cm depth. Also, the Pcells were buried at two depths, 0.1 cm (G_0 [W m^{-2}]) and 15 cm (G_{15} [W m^{-2}]). Fig.III.24 shows a schematic setup of the SOIS system.
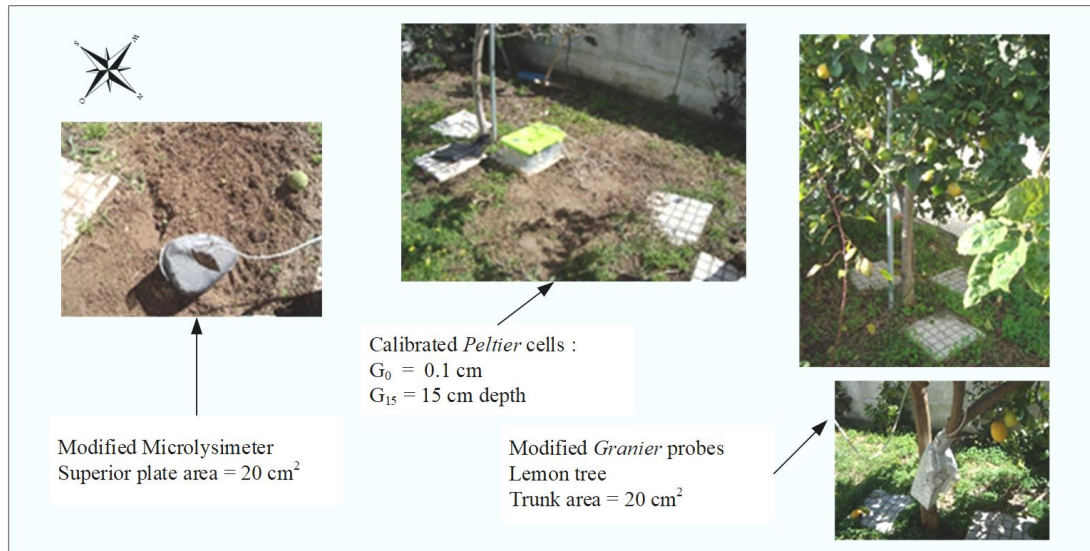
Fig.III. 24: The schematic disposition of SOIS trial with a single lemon tree.

III.4.4.2.Vineyard

III.4.4.2.1.**Field description**

The Vineyard study occurred from September to October 2016 in a grapevine belonging to the demarcated wine region of Carcavelos of the cultivar "Galego Dourado" (Fig.III.25). The vineyard is localised at the Estação Agronómica Nacional – Quinta do Marquês, Oeiras (38°42'10.6"N 9°19'14.7"W). The area presents a high-water deficit during summer and with the climatic formula Csa, according to Köppen e Geiger climatic classification. The annual mean temperature and rainfall for the year of 2016 at the nearest meteorological station were around 17.6 °C and 776.5 mm, respectively. The vineyard was not irrigated, but rainfall occurred during the study. The area is South exposed with prevailing winds from the North, which exert an action to protect the vineyards against the negative influence of the proximity of the sea.

Fig.III. 25: Vineyard field experiment in the Estação Agronómica Nacional – Quinta do Marquês, Oeiras.

The experimental plot is part of a large vineyard of 12.5 ha. The plant density is 3336 plants/ ha, and the plantation spacing of the crop is 2.5 m per 1.1 m. The rows are oriented in the NW–SE direction. The soil is classified as red limestone (marls) Mediterranean by Cardoso (1965). The table III.12 describes the physical characterisation of the soil.

Table III. 12: Physical characterisation of soil in the vineyard field experiment – Quinta do Marquês, Oeiras.

Depth (cm)	0-30	30-80
Particles >2 mm (%)	3.6	3.7
Coarse sand (%)	19.4	11.1
Fine sand (%)	32.3	26.5
Silt (%)	9.8	8.6
Clay (%)	38.5	53.8
Textural classification	Sandy Clay	Clay
particle density (g/cm^3)	2.2	1.8
Bulk density (g/cm^3)	1.2	1.0
Total porosity (%)	48.8	46.2
Max capacity water (%)	44.0	47.5

Font: Soil Laboratory INIAV I.P. - Oeiras, 2016.

III.4.4.2.2. **Installation of eddy covariance sensors**

The direct measurement of evapotranspiration was carried out using the eddy covariance technique. The sensors were placed in a metal observation tower at the height of 2.5 m (at about twice the mean height tree from ground) oriented towards the prevailing winds over a parcel about

2.4 ha (Fig.III.26 (a)). It would, therefore, be necessary to ensure a fetch, in the direction of prevailing winds, equal to or higher than 200 m.

The eddy covariance sensors (EC, W m^{-2}) were placed as showed in Fig.III.26 (b). The measurements obtained by this methodology consisted of latent heat flux (W m^{-2}) and sensible heat flux (W m^{-2}). The wind speed and temperature fluctuations were measured by a three-dimensional sonic anemometer (CSAT3-3D, Campbell Sci., USA). Water vapour concentration was measured with an open path, infrared absorption gas analyser (IRGA) (LI7500, LiCor Inc., USA). The eddy covariance post-processing was done to obtain 15-minute mean fluxes.

Fig.III. 26: Instrumental eddy covariance measurements (EC) in Vineyard field experiment – Quinta do Marquês, Oeiras. a) EC localisation on the parcel. b) the sensors and the metal observation tower at the height of 2.5 m

It is fundamental to ensure that the fluxes measured by the eddy covariance systems correspond to the fluxes originated from the surface of the crop. The horizontal plan on the surface should be uniform, without advection effects or obstacles. Thus, the EC approach assumes the existence of a homogeneous surface, which a distance between the local of measurement and the parcel borderline(fetch), in the predominant direction of the wind sufficiently large to consider horizontal gradients inexistent. The proportion height of measurement to fetch of 1:100 is an indication to obtain valid measurements with the EC approach (Paço, 2003).

A footprint analysis was performed based on Schuepp et al. (1990), for the vineyard measurement conditions aiming to determine the relative contribution of fluxes from points at different distances from the measuring point. The determination of surface roughness parameters, *i.e.* the height displacement of the reference plane (d) and the aerodynamic surface roughness (z$_o$)

were based on the simple relationships of the height of the cover (h). In the vineyard under study, since it was a sparse canopy and considering the height of the cover, it was then appropriate to consider a ratio d/h equal to 0.65, where d is 0.975 m, and h is 1.5 m. The use of 0.075 for the ratio z_0/h (h=1.5 m; z_0 = 0.1125 m) was considered appropriate, taking into account the degree of precision required and the sensitivity of the footprint function calculation.

Figure III.27 shows the location chosen for placing the tower, and the existing fetch that can be observed for each wind direction, respectively, N= 124 m, NW = 210 m, W = 120 m. It is observed that for the directions of the dominant wind the fetch requirement is widely satisfied.
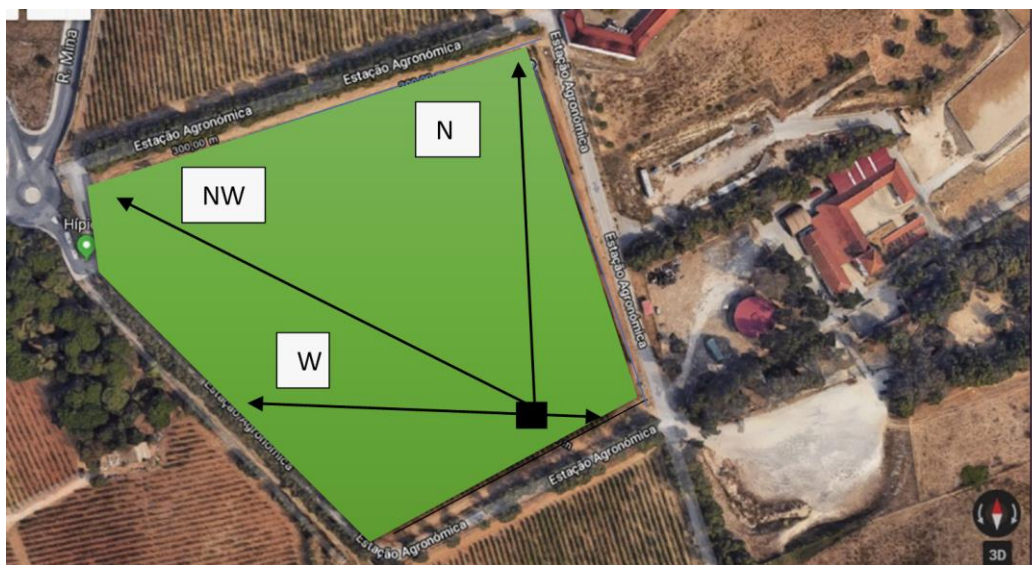
Fig.III. 27: Vineyard scheme and location of the tower used for micrometeorological measurements.

The meteorological data were acquired from the Wunderground meteorological station of Nova-Oeiras (ID: IOEIRAS1, Wunderground.com, site owned and operated by The Weather Company, LLC), in the coordinates N38°41'34", W9°19'31" and altitude of 104 m. Reference evapotranspiration (ETo) was calculated as described in Allen *et al.* (1998).

III.4.4.2.3. **Installation description**

Six pairs of modified *Granier* sensors (mG) were installed to estimate the transpiration, SP32L, SP27L, SP25L, SP23R, SP22R and SP21R, respectively. The mG sensor pairs consisted of one heater sensor (T_{heat}) and another the reference sensor (T_{no_heat}), which were implanted into the vine trunks to a depth of 20 mm, using a 2.0 mm diameter drill bit. The two sensor sets were

separated by a vertical distance of at least 10 cm. The double sensors and the vine trunks were covered with a thick aluminium foil to limit the effects of sunlight on trunk temperature.

Additionally, four weighing devices (mLy1, mLy2, mLy3 and mLy4) and four pairs of calibrated *Peltier* cells (Pcell1, Pcell2, Pcell3, Pcell4) were installed under-canopy to estimate the soil water balance and the soil heat storage, respectively. The mLy devices and their respective pairs of calibrated *Peltier* cells were buried in the row, positioned midway between trees (under-canopy). Fig.III.28 illustrates the layout in the field of a designed set up. The specifications and assembly of the modified *Granier* sensors, weighing devices and calibrated *Peltier* cells are described in section III.2.
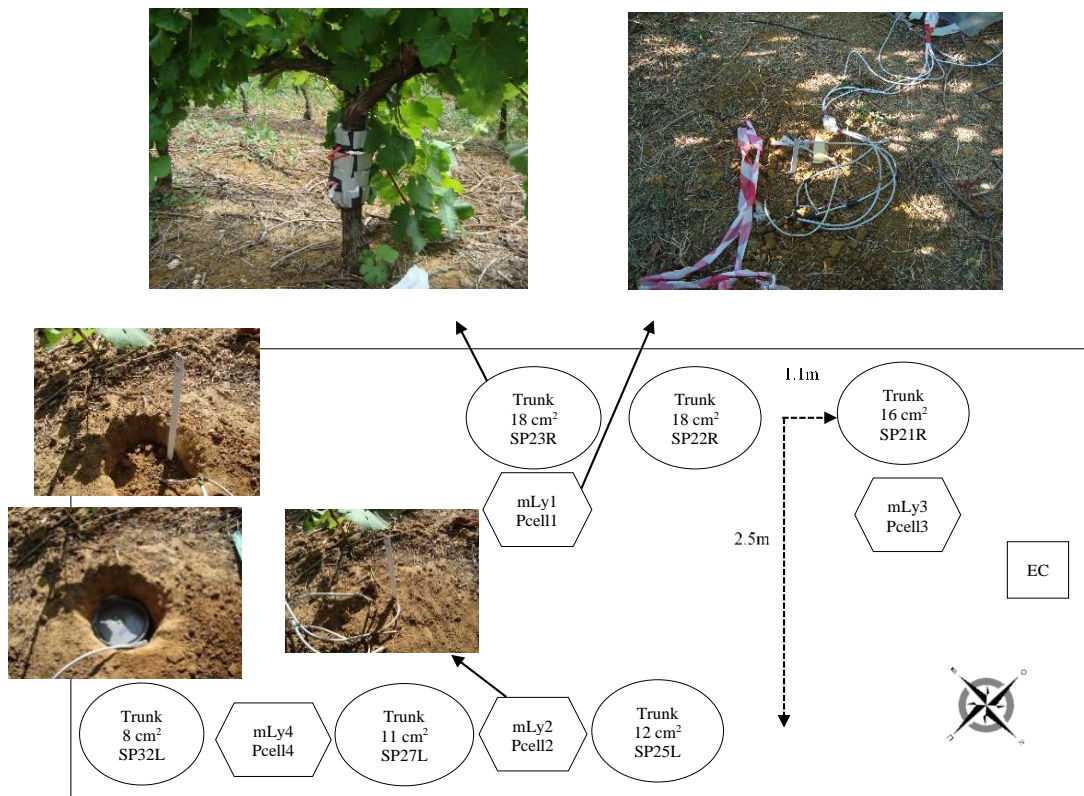
Fig.III. 28: Schematic of the SOIS set up in the vineyard field experiment– Quinta do Marquês, Oeira

The mLy and Pcell devices performed the measurements to estimate soil moisture (θ [m^3 m^{-3}]), soil heat flux (G [W m^{-2}]) and soil heat storage (S [W m^{-2}]) . The soil evaporation (Es [mm h^{-1}]) and the soil latent heat flux (LE$_{SOIL}$ [W m^{-2}]) were analysed based on soil water balance and soil energy balance, respectively. The evaluated data records were obtained separately from the mLy4 and pair of Pcell4.

Table III.13 describes the sensor nomenclatures and their respective setting up information. The information regarding the mG sensors are T_{heat} azimuth, the distance between T_{heat} and soil surface and the sapwood area. The sap flow was calculated considering the full sapwood area as sap conductor, following ink test observations by Silvestre (2003). Also, Table III.12 describes the information concerning mLy and Pcells sensors, which consist of the buried depths into the soil, the mLy superior plate area and the equations of calibration for each *Peltier* cell. The Pcell calibration equations were obtained as described in section III.2.3.

Table III.13: Specifications of modified *Granier* sensors and weighing devices installed in the vineyard field experiment -Quinta do Marquês, Oeiras

Modified *Granier* sensors		SP21R	SP22R	SP23R	SP25L	SP27L	SP32L
Sap flow sensors azimuth		NE	NE	NE	SW	SW	SW
Sapwood area (cm^2)		16	18	18	12	11	8
^{*1}h|s		40	35	40	46	43	45
Modified microlysimeters	**mLy1**	**mLy2**		**mLy3**	**mLy4**		
Effective soil depth layer (cm)	13	6		10	11		
Effective superior plate area (cm^2)	15.4	15.4		15.4	15.4		

Calibrated *Peltier* cells	Buried at z depth (cm)	Equation of Calibration
Pcell1a	0.1	$4.325 \times (\text{signal [mV]}) - 1.3148$
Pcell1b	13.0	$4.325 \times (\text{signal [mV]}) - 1.3149$
Pcell2a	0.1	$4.790 \times (\text{signal [mV]}) - 2.0100$
Pcell2b	6.0	$4.044 \times (\text{signal [mV]}) - 0.9920$
Pcell3a	0.1	$4.760 \times (\text{signal [mV]}) - 2.0160$
Pcell3b	10.0	$3.459 \times (\text{signal [mV]}) - 1.5920$
Pcell4a	0.1	$4.921 \times (\text{signal [mV]}) - 1.7600$
Pcell4b	11.0	$3.921 \times (\text{signal [mV]}) - 2.7360$

^{*1}**h\|s: distance between T_{heat} and soil surface**

RESULTS AND DISCUSSION

CHAPTER 4

IV. CHAPTER 4: Using the Fuzzy Algorithm for Automatic Data Treatment of *Granier* Technique

IV.1.   Experimental purpose

In theory, the sap flow measurement based on the *Granier* method is functional and easily automated. However, it requires massive data processing and analysis for its systematic use while these tasks are difficult to automate since they require frequent user intervention (Do & Rocheteau, 2002a). Beyond that, it is assumed that the temperature measurements are not changed by the occurrence of natural temperature gradients (NTG [ºC]) in the trunk. Nonetheless, NTG occurrences are easily verified by turning off the sensor heating (Do & Rocheteau, 2002b). The variations of the circadian temperature curve induced by the NTG contribute to errors occurring in determining the maximum temperature difference (ΔT_{MAX} [ºC]) and consequently in the sap flow calculation since the error is propagated to the *Granier* sap flow index (k_{Conv}). These errors are difficult to be detected and corrected in automatic calculus (Lu *et al.*, 2004; Allen *et al.*, 2011); thus, the process frequently needs a human decision, which constitutes an obstacle to automation. This is particularly pertinent for long temporal series.

The approach proposed here suggests the Fuzzy Algorithm Automation System (FAUSY) for adjusting the biased data automatically and in real time, thus allowing the correction of NTG in plant transpiration measurements. Also, the algorithm is expected to smooth the input of resulting transpiration values used for water balance and ET calculations. After the integration of time series and optimisation techniques, using means of learning from the environment in the present and past time, it is expected to obtain an innovative automatic data processing for the *Granier* method applied to olive trees. This work led to a scientific paper (Siqueira *et al.*, 2014) (see annex1).

The material and methods for that trial are described in section III.4.1.

IV.2. Results and discussion

IV.2.1. Setting parameters

The search space of the learning parameters is potentially huge, as a countless number of associations can be performed between environmental parameters and different learning time steps. Thus, it was essential to set parameters by the knowledge base and observations. In view of this, it was observed (Fig IV.1(a-b)) that potential relationships between the natural temperature gradients (NTG) and the explicative variables available, namely reference evapotranspiration (ETo), solar radiation (R_S) and relative humidity (RH), could be established over the intervals of days: [100,110] and [150,160].

a)
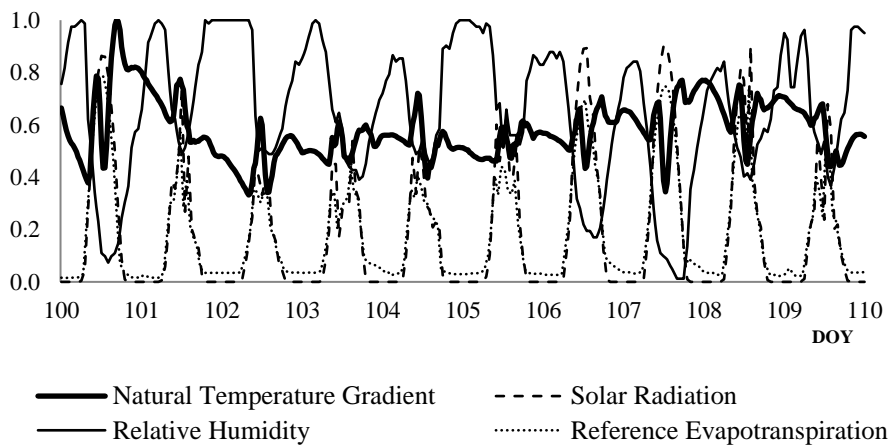
b)
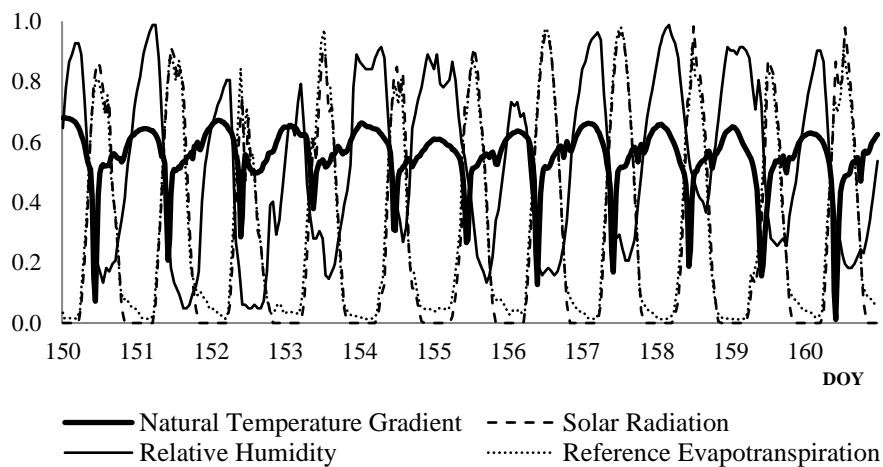
Fig.IV. 1: Visual analysis of the daily behaviour of natural temperature gradients and the accessible explicative variables (normalised data) in the timeline, namely, reference evapotranspiration (ETo), solar radiation (Rs) and relative humidity (RH) over the interval of days: a) [100,110] and b) [150,160].

These time intervals were selected from several intervals established for learning time to show the unpredictability of the process. However, the relationship was better between the NTG and variables ETo, R_s, RH at the time interval [150,160], than at time interval [100,110]. It corroborates the need for a phased learning time procedure (Fig.III.16), aiming to attenuate the unpredictability over time. Following this first assessment, the fuzzy rules were generated considering the relationship between variables ETo, R_S and RH and NTG, for the time interval [100,110].

Three different t time variable combinations, $i.e.$, combinations between explicative variables ETo, R_S and RH were set: (t-4), (t-2) and (t) steps backwards over time (SBT). SBT means the collected data in different time, $i.e.$, the algorithm searches for data four, two or zero steps backwards from t time.

In time interval [100,110], FAUSY searched for the best-related variable between the available explicative variables and the dependent variable NTG. Table IV.1 shows the mean square error (MSE) for the variable combinations: $R_{S(sbt4)} \times R_S \times RH_{(sbt4)} \times RH$; $R_{S(sbt2)} \times R_S \times RH_{(sbt2)} \times RH$; $R_S \times$ RH and $ETo_{(sbt2)} \times$ ETo.

Table IV 1: Mean squared error (MSE) of the four variable combinations during the DOY interval [100, 110] (learning time).

Variable combinations	MSE
$R_{S(sbt4)} \times R_S \times RH_{(sbt4)} \times RH$	0.0021
$R_{S(sbt2)} \times R_S \times RH_{(sbt2)} \times RH$	0.0030
$R_S \times RH_{(t)}$	0.0060
$ETo_{(sbt2)} \times ETo)$	0.0099

In addition, Fig.IV.2 illustrates that the rules generated with R_S and RH led to mean smaller absolute residual errors than the rules generated with ETo. The reason arises probably from the fact that although ETo integrates the same meteorological information, it also integrates the reference crop, which is different from the adjusted coefficients of the crop under study.

The NTG development, in its turn, is influenced by the effect of tree shadowing and row orientation of the crop, with shadow changing over the day, thus dynamically modifying the NTG value near the sensors. This supports the observed fact that NTG forecasting related to ETo is undefined and that the fuzzy rules associated with the explicative variables (R_S plus RH), by themselves, show the best fitting. Accordingly, the variable combination $R_{S (sbt4)} \times R_S \times RH_{(sbt4)} \times RH$ produced the lowest MSE (0.0021) for [100,110], being this variable combination chosen for learning time.
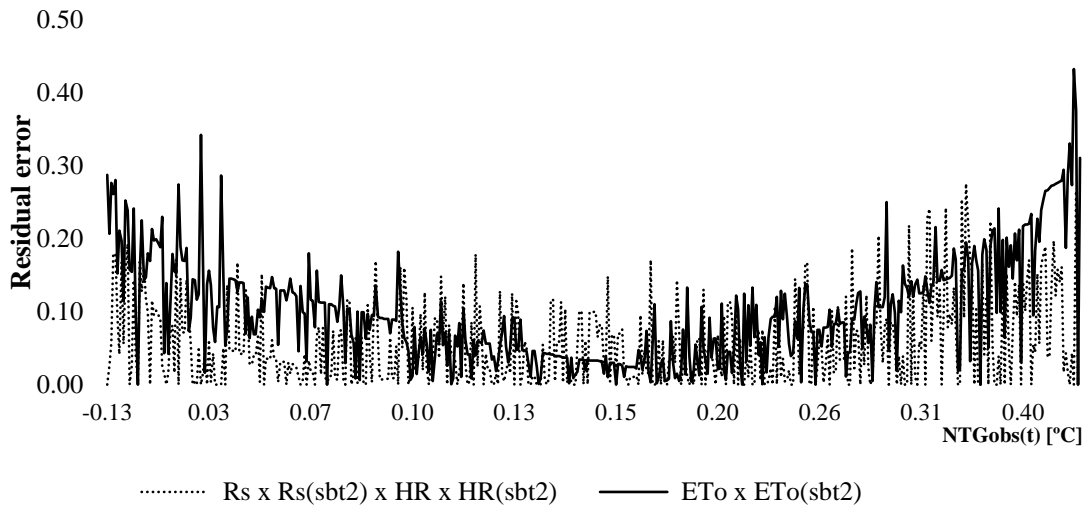
Fig.IV. 2: Comparing between the residual error obtained for the dependent variable NTG and the explicative variable combinations: Rs(t) × RS (sbt2) × RH(t) × RH (sbt2) and ETo (t) × ETo (sbt2).

IV.2.2.   Comparison between manual and FAUSY treatments

FAUSY results were compared with those obtained with manually processed data. In the time interval [110,160], the performance of the FAUSY algorithm was analysed by residual error (Eq.III (39-41)). The mean values of residual errors obtained for NTG with the FAUSY treatment and without any correction (RE_f and RE_{na}, respectively) are shown in Table IV.2.

Table IV 2: Performance of FAUSY algorithm computed by residual error equations (4-6) computed from mean transpiration [mm d^{-1}]

sensor	Mean Transpiration [mm d^{-1}]			Mean Residual Error [mm d^{-1}]		FAUSY Contribution	
	F_{na}	F_{adj}	F_{pred}	RE_{na}	RE_f	RE_f(%)	PFC (%)
G1	1.831	1.672	1.718	0.159	0.046	2.75	71.07
G2	0.594	0.500	0.514	0.094	0.014	2.80	85.11
G3	1.215	1.139	1.155	0.076	0.016	1.40	78.95
G5	1.259	1.170	1.200	0.089	0.030	2.56	66.29
G6	1.120	1.022	1.054	0.098	0.032	3.13	67.35
G7	0.861	0.711	0.731	0.150	0.020	2.81	86.67
G8	1.246	1.213	1.240	0.033	0.027	2.23	18.18
G10	1.703	1.459	1.499	0.244	0.040	2.74	83.61
Mean	**1.23**	**1.11**	**1.14**	**0.118**	**0.028**	**2.53**	**76.14**

In Table IV.2, the column PFC (Percentage FAUSY contribution) shows the improvement obtained with FAUSY. The residual error obtained for NTG with the FAUSY treatment (RE_f) presented lower values than the not adjusted procedure (RE_{na}). The FAUSY algorithm simulated the sap flow rate of sensors with a mean residual error of 0.028 mm d^{-1}, lower than the mean residual error of sap flow rate obtained without NTG corrections (using $\Delta T_{na(t)}$), which was estimated as 0.118 mm d^{-1}. PFC shows that a significant improvement is obtained when using the FAUSY algorithm, compared to the situation of no NTG correction (76.14%, where 100% represents the manual NTG correction), meaning that the algorithm is potentially advantageous for daily sap flow rate estimations.

The best results for daily transpiration [mm d^{-1}], when comparing manual with FAUSY data treatment, were found for sensor G7, with a PFC equal to 86.67% and the slope coefficient reduction from 1.19 (linear regression between F_not adjusted) to 1.03 (R^2=0.96) (Fig. IV.3 (a,b)). Sensor G8 showed an irrelevant adjustment, with a PFC of 18.18% and corresponding slope coefficient of 1.03 (R^2=0.99) (FigIV.3 (c,d)). Results for sensor G5 have shown an intermediate behaviour, with PFC = 66.29%, the slope coefficient reduction from 1.06 (linear regression between F_not adjusted) to 1.03 (R^2=0.99) (Fig. IV.3 (e,f)).

These dissimilarities are observable in Table III.4, which presents the difference between ΔT_{MAXadj} and ΔT_{MAXna}, showing that sensor G8 had the smallest difference and sensor G7 the largest, respectively, 0.198 ℃ (G8) and 0.346 ℃ (G7). It is likely because the biased ΔT_{MAX} values are propagated in the k_{Conv} calculations. Thus, the magnitude of adjustment of ΔT_{MAX} is proportional to the magnitude of the ΔT adjustment and, consequently, to the k_{Conv} calculations. Furthermore, ΔT_{MAXadj} has been used to calculate k_{Conv} adjusted predicted (k_{Gpred}), and therefore, FAUSY uses information in the initial learning time (initial 10 days) to learn with explicative variables and obtain an estimate of the ΔT_{MAX} value observed.

The differences observed in the FAUSY contribution obtained for the different sensors corroborate the fact that NTG is spatially and temporally variable. For that reason, for a more accurate approach, each sensor should use itself as a referential sensor, thus switched off at specific periods. This is possible if there is an algorithm (*e.g.*, like the FAUSY algorithm) capable of replacing the periods when the heater is on. Operating in this mode or after calibration, and about other NTG correction systems, it is possible to discard the need for additional equipment (*e.g.*, that needed to shut down the heating system periodically or additional unheated sensors), relying only on the use of meteorological variables, commonly available on experimental sites.

In a global view of the process, the FAUSY contribution to automate the process could be demonstrated by prompt searching over possible explicative variables, returning the lowest residual error possible. This fact corroborates the rapidness of the automation process, since the simple residual error calculation may be accepted as an efficient statistical tool.

Additionally, in the manually adjusted procedure, the k_{Conv} calculation was computed after the complete data set had been collected; consequently, it was not possible to compute it in real time. Alternatively, the FAUSY routine computed k_{Conv} at the same input data time, after the learning time, which allowed for real-time automation and availability. As FAUSY relies only on measurable environmental conditions, it can theoretically be applied to other woody species and different conditions, although it must be more extensively tested since this is the first application performed and factors influencing NTG (*e.g.*, distance from the soil of the sensors, presence/absence of irrigation) can change. The algorithm is also potentially applicable to other sap flow measurement methodologies to perform possible adjustments and further automate measurements.

a)

Sensor G7

b)

c)

Sensor G8

d)

e)

Sensor G5

f)
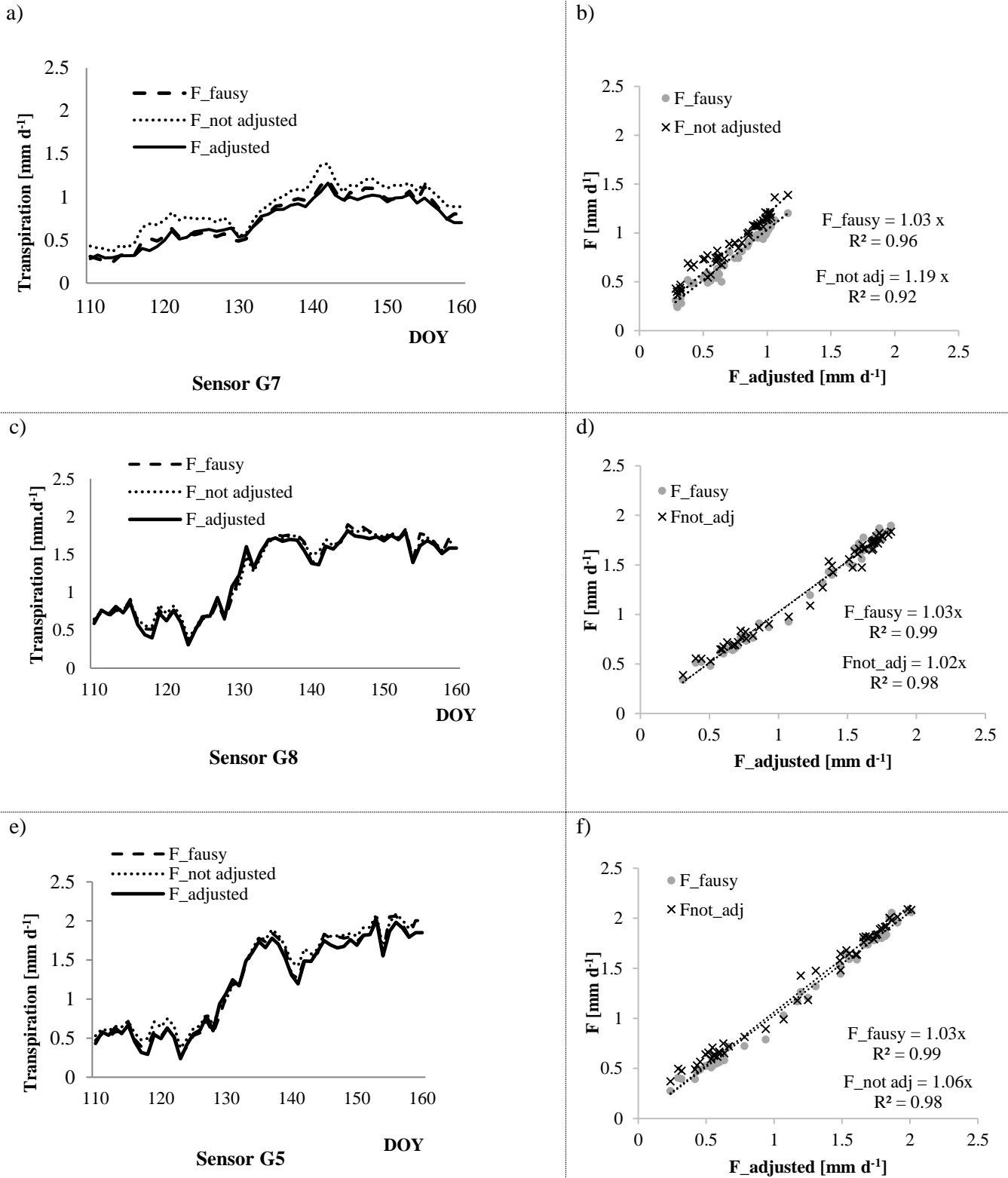
Fig.IV. 3: Comparison of transpiration estimates (F [mm d⁻¹]) with the FAUSY algorithm (F_fausy [mm d⁻¹]), using the not adjusted procedure (F_not adjusted [mm d⁻¹]) and the adjusted procedure (F_adjusted [mm d⁻¹]) and the respective linear regression curves for sensors: (a-b) sensor G7; (c-d) sensor G8; (e-f) sensor G5.

IV.3. Conclusions

The study presented in this chapter addresses the generation of fuzzy rules and the application of fuzzy logic to *Granier* sap flow data treatment. In this context, the FAUSY algorithm shows to be an innovative and practical approach for system optimisation, contributing positively to the estimation of adjusted ΔT values corrected for natural temperature gradients, therefore allowing to automate the data analysis process since it relies only on the use of meteorological variables, commonly available on experimental sites. Also, it allows to overcome the significant restrictions of extensive data processing, especially when practical applications in irrigation management are intended, given that allowed for a less time-consuming process, yet not discarding the human decision capacity. In addition, it provides the opportunity for earlier reaction to data because it allows for a real-time treatment possibility.

The FAUSY algorithm is potentially applicable to other sap flow measurement methodologies and other woody species, although further testing is needed.

CHAPTER 5

V. CHAPTER 5: Built-Up of a Weighing Device to Estimate Soil Water Content and Soil Evaporation

V.1.　　Experimental purpose

The experiment using weighing devices (mLy) was developed at the top of the Herbarium building of the University of Lisbon, Instituto Superior de Agronomia (ISA) (Fig.V.1). This trial aimed to quantify the water requirements of green roofs with native plants and biocrust mosses through the water balance using the weighing device (mLy) described in section III.2.2. For that purpose, daily evapotranspiration (ET) was measured in the trays from June 2016 to September 2016 using automatic weighing in intervals of 15 minutes, giving information on water content (cm^3cm^{-3}) and water balance ($mm\ h^{-1}$ and $mm\ d^{-1}$). The material and methods for that trial are described in section III.4.2.

Fig.V. 1:The green roof lab-rooftop of the Herbarium building of the University of Lisbon, Instituto Superior de Agronomia (ISA) (https://www.facebook.com/thegreenrooflab/?ref=bookmarks).

V.2.   Results and discussion

The evaluation of mLy devices were based on the observation of the volumetric substrate moisture content data (θ [cm^3 cm^{-3}]) in time series using as a control tool, the time-domain measurement method via the reflectometers sensors (TDR; CS616 water content reflectometers, Campbell Scientific, USA), which the mLy weighing plates were buried at least 10 cm above of the TDR sensors (Table III.7). Also, the mLy devices were evaluated about their contribution to the estimates of daily evapotranspiration.

V.2.1.   Volumetric substrate moisture content evaluation

The volumetric substrate moisture content data (θ [cm^3 cm^{-3}]) obtained with the weighing devices (mLy) and the reflectometers sensor (TDR), were compared and evaluated using the bias analysis and graphical techniques. The mLy data and TDR data were recorded between the days 210 and 232, obtained with 15-min measurement intervals and scaled to the hourly (θh [cm^3 cm^{-3}]), daily (θd [cm^3 cm^{-3}]) and global ($\bar{\theta}$ [cm^{3}cm^{-3}]) means, according to the analysis required.

The global mean volumetric substrate moisture ($\bar{\theta}$ [cm^{3}cm^{-3}]) for five treatments (T3, T5, T6, T8 and T11) were compared between mLy and TDR data (Table V.1). The root mean square error (RMSE) between mLy and TDR data for the five treatments ranged from 0.03 to 0.17 cm^{3}cm^{-3}. Treatment T6 showed the highest RMSE (0.17 cm^{3}cm^{-3}), and treatment T11 showed the lowest RMSE (0.03 cm^{3}cm^{-3}), respectively. The statistical comparisons indicated that, for treatments T11 and T8, mLy and TDR data showed better compatibility than did other treatments, with RMSE estimated as 0.03 and 0.05 cm^{3}cm^{-3}, respectively.

Table V. 1: Bias analysis using root mean square error (RMSE) as a statistical indicator for comparison of the global mean volumetric substrate moisture ($\bar{\theta}$ [cm^{3}cm^{-3}]) between mLy devices (mLy) and Reflectometer sensor (TDR)

Treatment	Global mean ($\bar{\theta}$ [cm^3 cm^{-3}])		RMSE [cm^3 cm^{-3}]
	mLy	TDR	
T3	0.20	0.12	0.07
T5	0.24	0.18	0.08
T6	0.24	0.07	0.17
T8	0.26	0.23	0.05
T11	0.21	0.19	0.03

The hourly mean volumetric substrate moisture (θh [cm^3cm^{-3}]) for five treatments (T3, T5, T6, T8 and T11), were clustered on an hourly basis and compared between the mLy and TDR data. Fig.V.2 shows the bias analysis with the RMSE computation, which mLy data showed a temporal variability along day, compared with TDR data. In early in the morning, all treatments showed a high bias of the water content estimates in relation to TDR measurement but declining abruptly until reaching at a lower bias between 7 and 18 hours, returning to rise in the sunset. In fact, at night-time, when usually the ET rate is lower than daytime, the substrate held the moisture under the vegetation due to the microclimate effect, avoiding the lixiviation to lower layers where were sited the TDR sensors. In the daytime, the higher ET rate contributed to the moisture uniform to the whole profile.
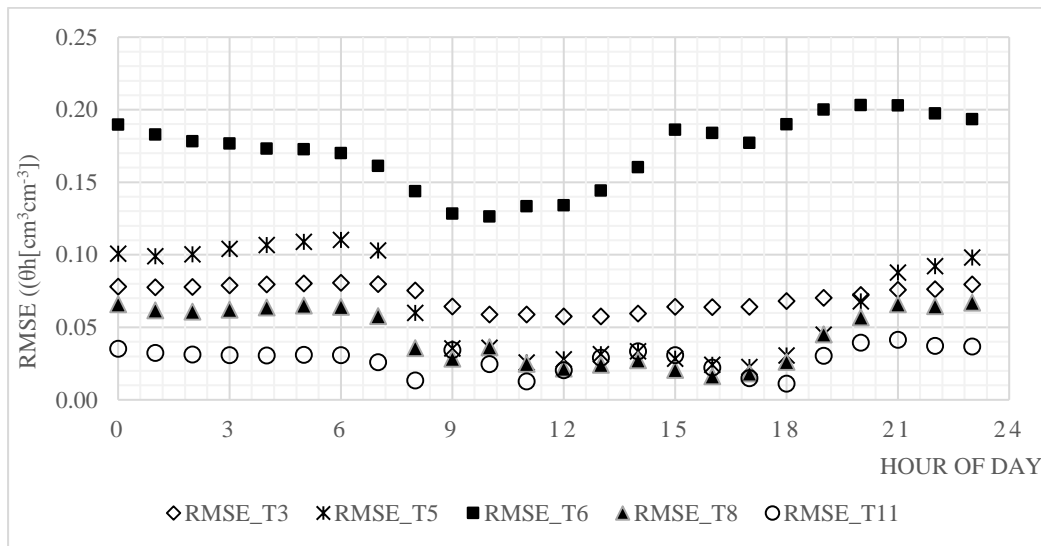
Fig.V. 2: Bias analysis (root mean square error (RMSE)) of the hourly mean volumetric substrate moisture (θh[cm^3cm^{-3}]) for the treatments: T3, T5,T6,T8 and T11 with mLy and TDR data clustered on an hourly basis.

mLy devices are more sensitive to the temporal moisture changes since the events of water content change are more evident at the surface, which exists a higher heat transfer than lower layers. Conversely, the TDR sensors were not able to indicate the water change near the surface, given that were located in a more in-depth site (Table III.7), which the water content changes are less evident and sometimes insignificant in dairy watering. The treatment T11 presented the smallest RMSE, given to not exist vegetation and the osmotic potential being null. Thus, the distribution of water has been standardised with the lower wetter zone by means of matric and gravitational potential.

The hourly mean volumetric substrate moisture (θh [cm^3cm^{-3}]) for five treatments (T3, T5, T6, T8 and T11), was scaled to a daily basis (θd [cm^3cm^{-3}]) and compared between the mLy and TDR data. Fig.V.3(left vertical axis) shows the bias analysis with the RMSE computation, which mLy data showed a temporal variability for the days 210 and 232 compared with TDR data.

The treatment T5, T8 and T11 showed more significant bias in the earlier part of the measurement period than later days in relation to corresponding TDR measurement but declining smoothly until reaching at a lower bias between the days 228 and 232. In fact, the irrigation depths (I_{60} [mm d^{-1}] and I_{100} [mm d^{-1}]) performed in the later days according to ETo [mm d^{-1}] indicated in Fig.V.3 (right vertical axis) (see section III.4.2.3) was lower than in the early days. Thus, a lower θ magnitude has held a low bias magnitude. However, the treatments T3 and T6 presented different circadian RMSE curves. T6 presented the highest bias between mLy6 and TDR6 data, and the bias between mLy3 and TDR3 data showed a constant RMSE in the time series until rising in the days 227 and 228. The bias observed in T3 was caused by the measurement error due to occasional disturbers (*e.g.*, birds visitation) and taking the lowest effective depth between mLy plate and surface.
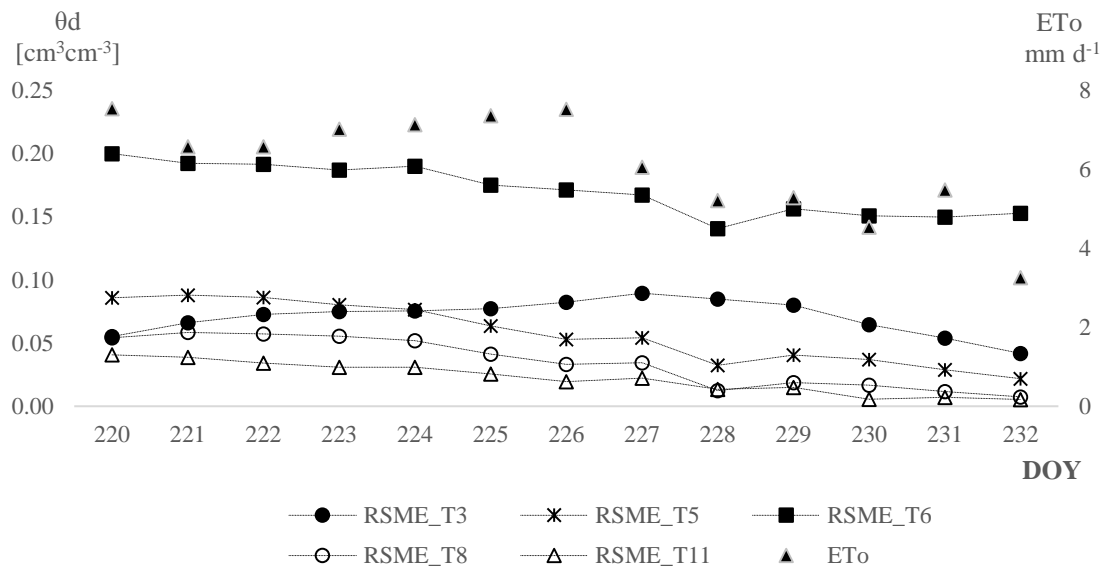
Fig.V. 3: Bias analysis (root mean square error (RMSE)) with mLy and TDR data. Left vertical axis: hourly mean volumetric substrate moisture scaled to a daily basis (θd [cm^{3}cm^{-3}]) for the treatments: T3, T5, T6, T8 and T11. Right vertical axis: reference evapotranspiration estimates (ETo [mm d^{-1}]).

Fig.V.4 (a-e) show θh observed for the treatments T3, T5, T6, T8 and T11. Also, it was compared with the irrigation depth performed along these days, respectively 60 % ETo (I_{60} [mm d^{-1}]) for the treatments T3 (Fig.V.4 (a)), T5 (Fig.V.4 (b)) and T6 (Fig.V.4 (c)), and 100 % ETo (I_{100} [mm d^{-1}]) for treatments T8 (Fig.V.4 (d)) and T11 (Fig.V.4 (e)).

.

a)

b)

c)

d)

e)
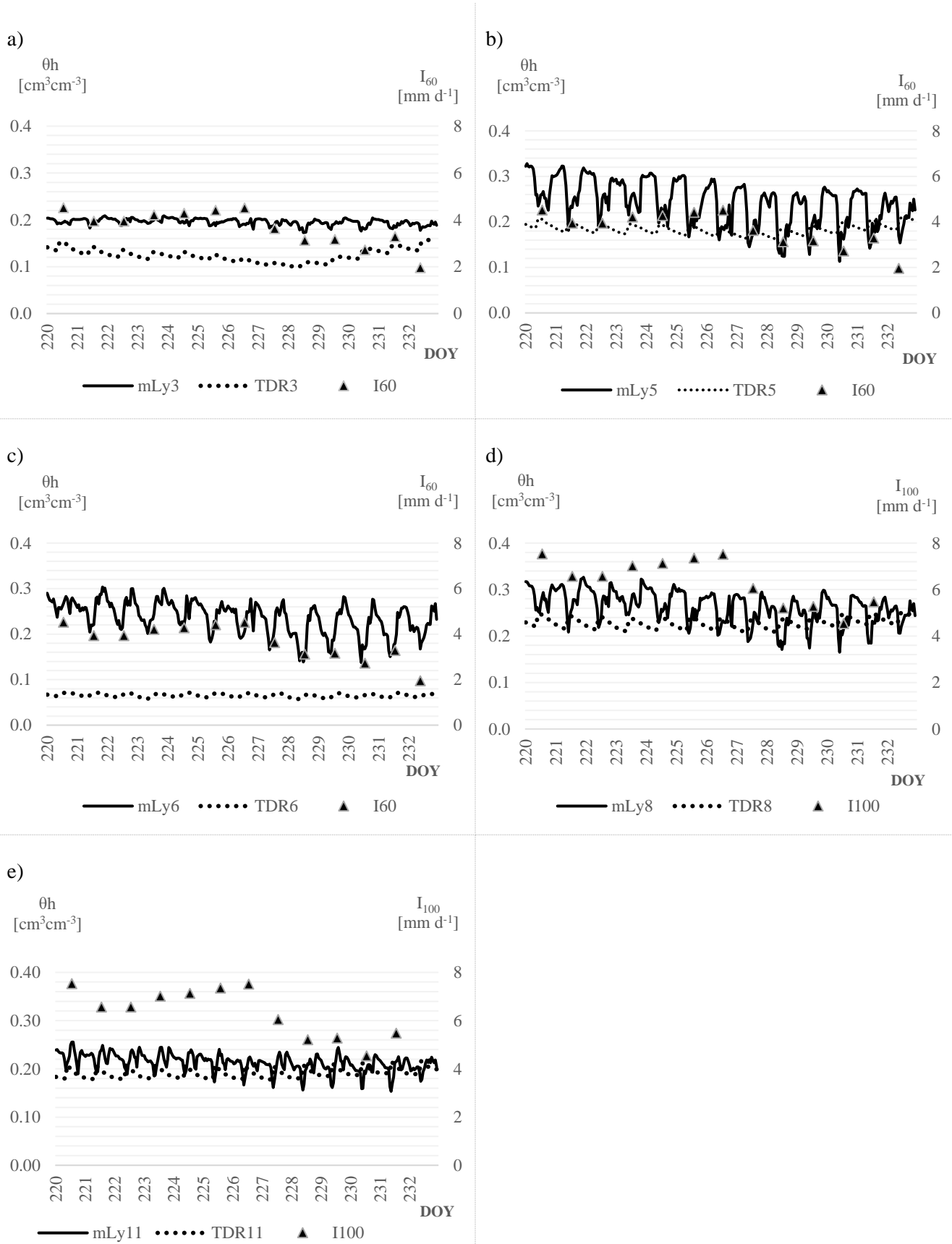
Fig.V. 4: Circadian curve analysis from the day 220 to day 232 for the treatments: a) T3; b) T5; c) T6; d) T8; e) T11. Left vertical axis: hourly mean volumetric substrate moisture content (θh [cm³ cm⁻³]) measured with mLy (full line) and TDR (dash line) sensors. Right vertical axis: irrigation depths: a) I_{60} [mm d⁻¹] (60%ETo); b) I_{60} [mm d⁻¹] (60%ETo); c) I_{60} [mm d⁻¹] (60%ETo); d) I_{100} [mm d⁻¹] (100%ETo); e) I_{100} [mm d⁻¹] (100%ETo). Reference evapotranspiration (ETo [mm d⁻¹]).

The maximum (θh_{MAX} [cm^3 cm^{-3}]) and θh minimum (θh_{MIN} [cm^{3}cm^{-3}]) estimates computed from mLy and TDR data are illustrated in Fig.V.4 (a-e). Fig.V.4 (a) shows that the mLy3 presented the lowest oscillation between θh_{MAX} and θh_{MIN} ($\Delta\theta h_{MAX-MIN}$ [cm^3 cm^{-3}]), ranging between 0.17 and 0.21 cm^{3}cm^{-3}, which presented compatible with $\Delta\theta h_{MAX-MIN}$ of TDR3 ranging between 0.10 and 0.16 cm^{3}cm^{-3}. In the other treatments, the $\Delta\theta h_{MAX-MIN}$ values with mLy data showed higher than the $\Delta\theta h_{MAX-MIN}$ values with TDR data, with mLy5 as the highest range (0.11-0.33 cm^{3}cm^{-3}) and TDR5 ranging between 0.16 and 0.21 cm^{3}cm^{-3}.

The dissimilarities of the moisture substrate circadian curve between the treatments T5, T6 and T8 and compared with T11 are due to the type of substrate used in each treatment, combined with the vegetal covering. In fact, T11 was stuffed with a substrate (type S3) of high hydraulic conductivity (see Table III.6), thus making easy the drainage. Nevertheless, T5 was performed with lower irrigation depth (60 % ETo) than T8 (100 % ETo), and yet so, it ranged in the highest proportions. Indeed, T5 is performed with a dense vegetal covering, including native bryophytes, increasing the moisture retention capacity. The lower values showed by TDR data, compared with mLy data are given that TDR sensors tend to underestimate in high organic matter content due to exhibit reduced dielectric signatures, as suggested by (Ren *et al.*, 2005).

Fig. V.5 illustrates the signalisation of daily irrigation events in treatment T11 defined for the temporal domain (blue dash arrow). Sensor TDR11 signalled these irrigation events with about one hour earlier (short red line) when compared with the signal from weighing device mLy11 (long red line). The sluggish redistribution of water was observed with the mLy11 sensor (long red line), which detected a first peak (1° green arrow), identifying the maximum water holding by the substrate.
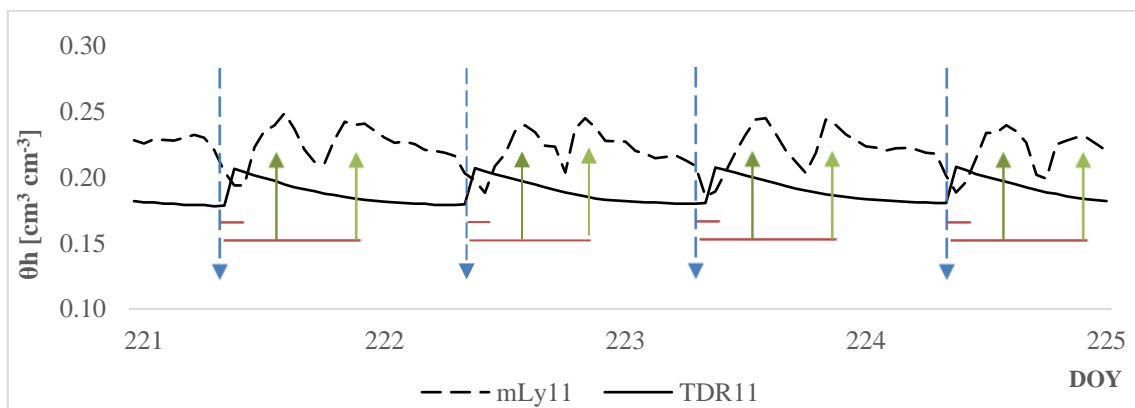
Fig.V. 5: The hourly mean volumetric substrate moisture content θh [cm³cm⁻³] from day 221 to day 225, with the weighing device data (mLy11) and the reflectometer sensor data (TDR11). Irrigation event (Blue Dash line); Spent time to water redistribution (red line); Maximum values measured with mLy11 (green arrows)

The second peak (2º green arrow) could be caused by decreasing evaporation in the sunset time and the homogenising of water content with the lower wetter zone through matric potential. Indeed, as also it was observed in Fig.V.2, all treatments with mLy devices have risen the water content in sunset time, but mLy11 decreasing the water content after the second peak time, due to there no be vegetation cover. The vegetation cover could have actuated as a thermal insulator between the atmosphere and the ground contributing to the microclimatic effect.

V.2.2.   Daily evapotranspiration rate evaluation

The daily ET [mm d^{-1}] was evaluated from the day 220 to the day 232 based on the water balance approach (Eq.III.45) and compared with the daily ETo [mm d^{-1}] described in the section III.4.2.3. The daily water change content ($\Delta\theta$d [mm]) was computed from the TDR sensors with Eq.III.46 and from the mLy devices with Eq.III.47.

Fig.V.6 (a-e) shows the daily ET estimates of the treatments T3, T5, T6, T8 and T11 from mLy and TDR data. The linear regressions between ETo and ET computed for $\Delta\theta$d from mLy data (black line), and TDR data (black dash line) are demonstrated for all treatments. The treatments T3 (Fig.V.6 (a)), T5 (Fig.V.6 (b)), T6 (Fig.V.6 (c)) and T8 (Fig.V.6 (d)) presented the data dispersion below of ETo estimates (red dash line) for both mLy and TDR data. T11 (Fig.V.6 (e)) showed a data dispersion near the ETo estimates, presenting the highest ET estimates with mLy11 and TDR11.

Comparing the results observed in T8 and T11 with both mLy and TDR data, it concludes that the substrate type combined with vegetation covering takes an essential role in keeping the moisture closer the surface and the vadose zone and preserved by the vegetation covering, given that the highest ET rate was obtained from T11 (no vegetated).

The global mean ET ranged from 2.98 to 5.20 mm d^{-1} with mLy data. Also, TDR data ranged from 3.22 to 5.70 mm d^{-1}. The highest values were obtained in the trays T8 and T11, following the treatments T3, T5 and T6 with the lowest estimates for both mLy and TDR data.

a)

b)

c)

d)

e)
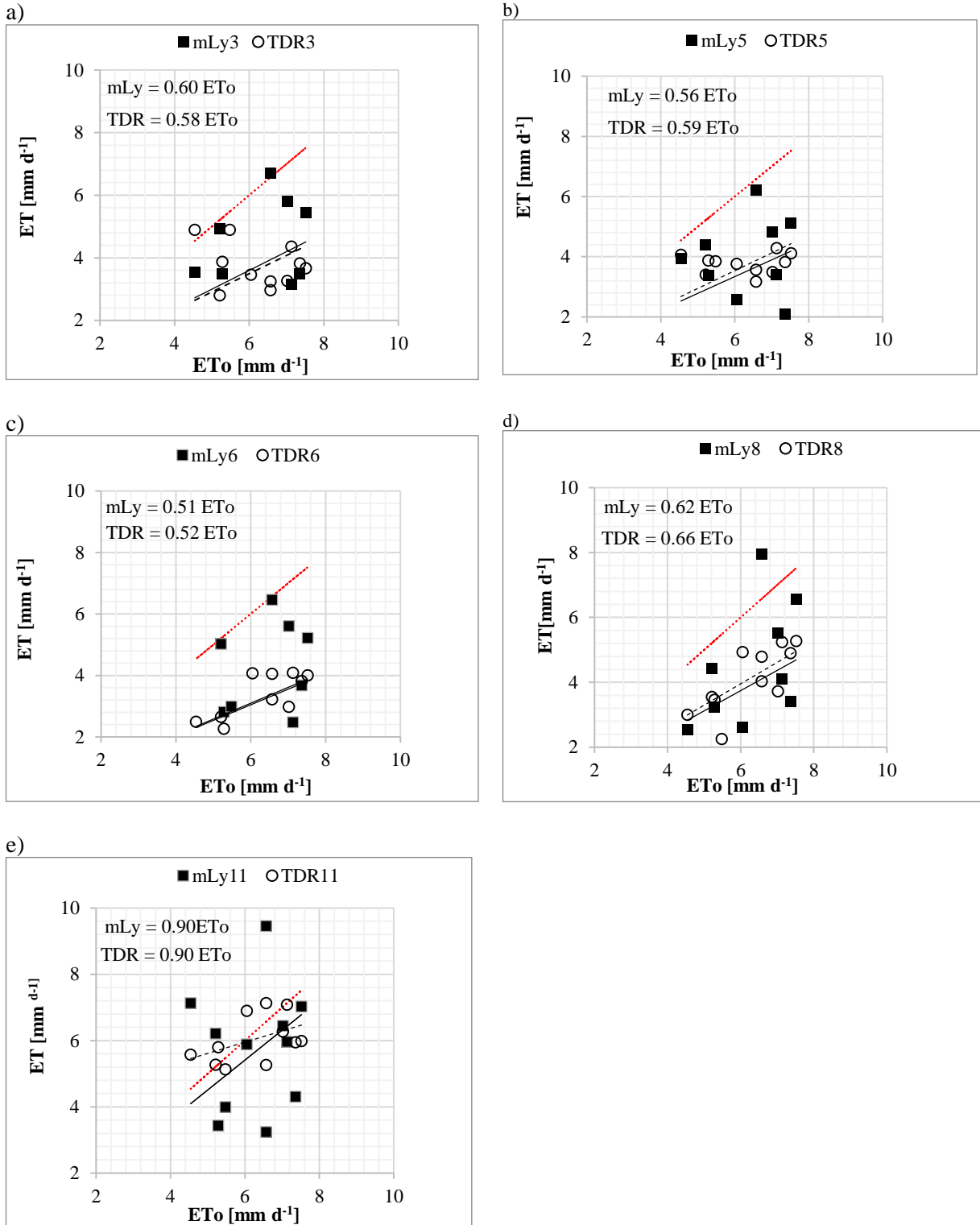
Fig.V. 6: Linear regression between diary evapotranspiration estimates (ET [mm d^{-1}]) and reference evapotranspiration (ETo [mm d^{-1}]) observed with mLy devices (mLy) and reflectometer sensors (TDR) on treatments: a) T3; b) T5; c) T6; d) T8; e) T11. ETo estimates (red dash line), TDR estimates (black dash line), mLy estimates (black line).

Nevertheless, Paço *et al.* (2014) showed for the evapotranspiration in the green roof structure, considering the same period (DOY 192-198), that the mean ET_{obs} was 3.5 mm d^{-1} for the lower irrigation level. Also, for the higher irrigation level, ET was 4.1 mm d^{-1}. Thus, the ET observed can be estimated with the mLy devices since the obtained values reached comparable magnitude.

V.3. Conclusions

It is concluded that the mLy devices, developed and tested in this study, provided relatively accurate and reliable measurements of evapotranspiration. The statistical comparisons indicated that the mLy devices performed compatible to the TDR sensors, but mLy showed a better response to temporal variability of water content than the TDR sensors. It suggests that mLy devices are more sensitive to moisture changes than TDR sensors since the water change events are more pronounced near the surface where the mLy are located. However, additional observations of the micrometeorological air and root zone variables are needed to clarify the behaviour of the new weighing device.

It was possible to verify that the proposed mLy devices can be used as a practical, easy-manufacture and low-cost tool to efficiently indicate the hourly depletion of water. However, it should be noted that the mLy devices have not been evaluated over long time periods and thus these results are only strictly applicable for short-term (days to weeks) studies. The challenge consists of keeping the mLy without local perturbations for long-term.

CHAPTER 6

VI. CHAPTER 6: Using Modified *Granier* Sensors

VI.1.   Experimental purpose

The work presented herein aimed at evaluating and validating the prototypes of the modified *Granier* sensors (mG) described in section III.2.1. The sap flow measurements were collected using mG sensors in the following experimental sets: 1) potted olives trees in a greenhouse at Dois Portos, 2) kiwi orchard in Briteiros, and 3) vineyard in Alcochete.

The trial executed in the greenhouse located at the Instituto Nacional de Investigação Agrária e Veterinária (INIAV-Dois Portos), aimed to analyse the *Granier* model, observing the *Granier* sap flow index performance obtained from sensors in comparison with the transpiration observed from the gravimetric approach. Also, that experiment aimed to compare the modified *Granier* (mG) sensors with a commercial kind obtained from UP GmbH, Germany. Finally, the quantification of sap flow compared to the vapour pressure deficit (VPD [kPa]) estimations were evaluated, as well.

The trials carried out in the kiwi orchard, and the vineyard aimed to assess the procedures of installation and performance of the local machine, heater resistance, sensors design, power requirements, the efficiency of solar panel and robustness of the whole system. The kiwi orchard is located at Quinta das Picas (Kiwi Greensun, SA), São Salvador de Briteiros, Guimarães – Portugal and the vineyard is located at the Adega Catapereiro - EN118 Porto Alto – Alcochete. The experimental results obtained in the kiwi orchard were previously published (Siqueira *et al.*, 2015) and presented at 2015 Conference on Design of Circuits and Integrated Systems (DCIS) (see annex).

The material and methods for that experimental purpose are described in section III.4.3.

VI.2.   Results and discussion

VI.2.1.   Greenhouse trial

The results obtained in the greenhouse trial were sectioned in two analyses: 1) evaluation of sensors with the Biot *Granier* sap flow index approach and, 2) comparison between modified *Granier* and conventional *Granier*. The methodology of that study is described in the sections III.4.3.1 and III.4.3.2.

In order to evaluate probable NTG occurrences, the temperature differences measured were computed in the P03 potted olive tree. P03 sensors (T_{heat} switch off) reached to the mean offset of ±0.10 ºC. Thus, the NTG occurrences were unconsidered for this study, given that the offset captured is due to maladjustments between sensors and not to NTG, as confirmed in a laboratory test, which reached to highest values (0.25 ºC) (see table III.8).

VI.2.1.1. Evaluation of sensors with the Biot *Granier* sap flow index approach

Accordingly, the Biot *Granier* sap flow index (k_{Biot}) was analysed regarding the adjustment of T_{MAX} [ºC] and T_{no_heat} [ºC]. This evaluation focused on the *Granier* model (Eq.III.03), where the *Granier* sap flow index is computed in two approaches, conventional *Granier* sap flow index (k_{Conv}) and Biot *Granier* sap flow index (k_{Biot}) with the modified *Granier* (mG) sensors. k_{Conv} was computed based on Eq.III.49 and reformulated as:

$$k_{Conv} = \frac{(\Delta T_{MAX(Conv)} + T_{no\_heat}) - T_{heat}}{T_{heat} - T_{no\_heat}} \qquad\qquad Eq.VI.01$$

k_{Biot} was computed based on the linear regression curve(lrc) between two terms: T_{heat} [ºC] and T_{no_heat} [ºC], registered at night-time. $T_{MAX(Biot)}$ [ºC] and T_{∞} [ºC] are computed from that lrc obtained for each pair of mG sensors. The lrc were obtained from P01 (days 85 and 86 (2018)) and P02 (days 86 and 87 (2018)), respectively, with Eq.VI.02-05.

$$T_{MAX(Biot)}(P01) = 0.9540 \times T_{no\_heat}(P01) + 4.5088 \quad (R^2 = 0.9996) \qquad Eq.VI.02$$

$$T_{MAX(Biot)}(P02) = 1.0414 \times T_{no\_heat}(P02) + 7.2937 \quad (R^2 = 1.0000) \qquad Eq.VI.03$$

$$T_{\infty}(P01) = 0.9540 \times T_{no\_heat}(P01) \qquad\qquad Eq.VI.04$$

$$T_{\infty}(P02) = 1.0414 \times T_{no\_heat}(P02) \qquad\qquad Eq.VI.05$$

Fig.VI.1(a,d) shows the adjustment magnitude obtained with the Biot and conventional approaches. $T_{MAX(Biot)}$ and $T_{MAX(Conv)}$ offset computed with the sensor P01 ranged between 0 ℃ to –0.22 ℃ (Fig.VI.1 (a)). Conversely, the sensor P02 showed a $T_{MAX(Biot)}$ - $T_{MAX(Conv)}$ offset alternating between –0.16 ℃ to +0.16 ℃, capturing positive bias during 13:00 to 21:00 hour of day and inverting to negative bias during 21:00 to 13:00 hour of day (Fig.VI.1 (b)). Also, Fig.VI.1 (c,d) show the T_∞ adjustments, wherein the offset between T_∞ and T_{no_heat} obtained with both sensors P01 and P02 performed differently. Sensor P01(Fig.VI.1 (c)) showed smaller T_∞ values than T_{no_heat}, and sensor P02 (Fig.VI.1 (d)) reached to higher T_∞ values than T_{no_heat}. Given that different sensors reach to different responses, as well, integrate different effects when in surrounding with sap, the sensors have to be adjusted individually.
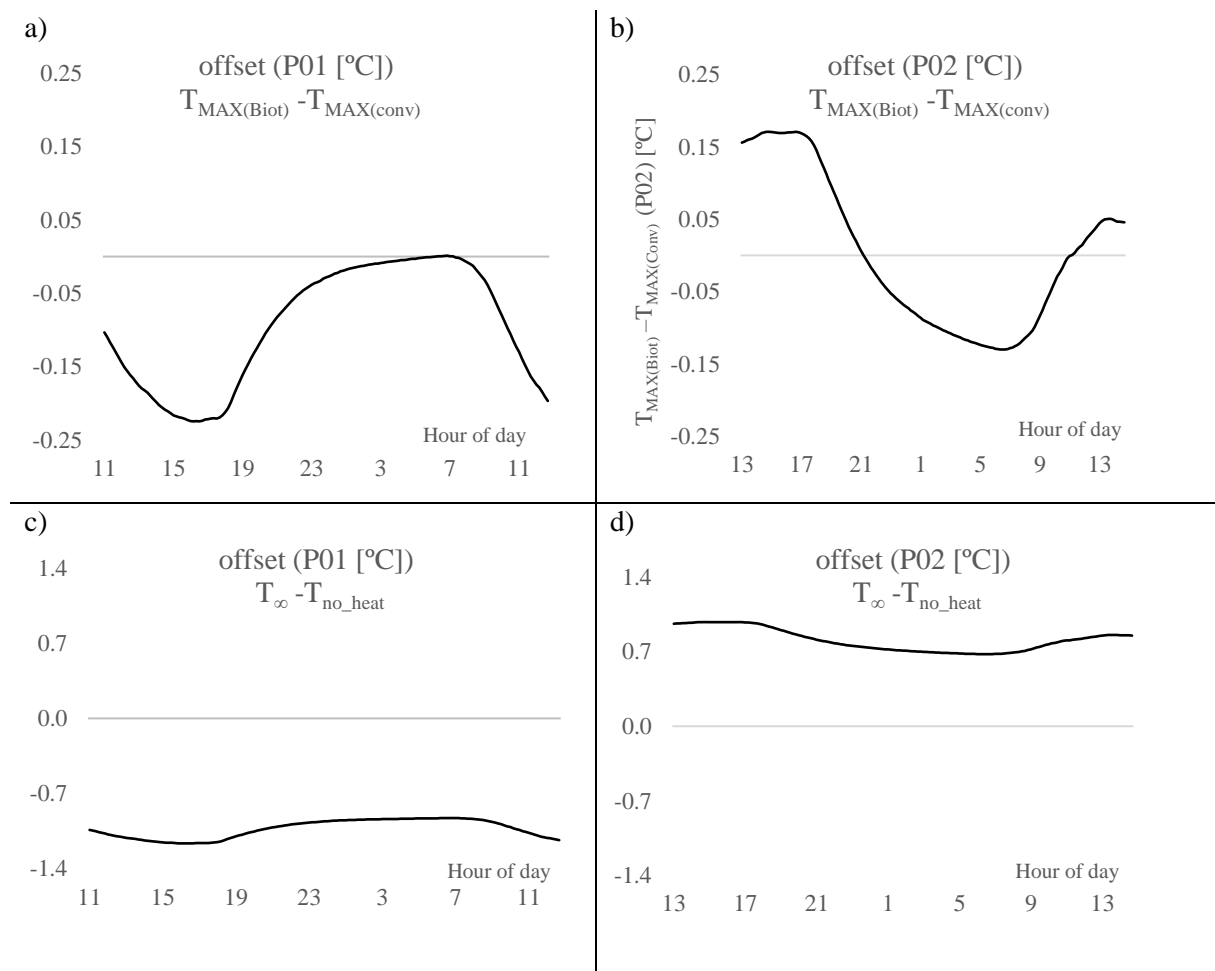
Fig.VI. 1: Comparative offset between conventional and Biot approaches. a) offset between $T_{MAX(Conv)}$ and $T_{MAX(Biot)}$ obtained with the sensor T_{heat}(P01); b) offset between $T_{MAX(Conv)}$ and $T_{MAX(Biot)}$ obtained with the sensor T_{heat}(P02); c) offset between T_{no_heat} and T_∞ obtained with the sensor T_{no_heat}(P01); d) offset between T_{no_heat} and T_∞ obtained with the sensor T_{no_heat}(P02).

The validation concerning the Biot approach was performed with the gravimetric test, aiming to evaluate the agreement grade with the actual sap flux density estimates (u_{Grav} [m³ m⁻² s⁻¹]) and the relevance of adjustments referred in Fig. VI.1 (a-d). The sap flux density rates were calculated from k_{Conv} and k_{Biot}, respectively, u_{Conv} [m³ m⁻² s⁻¹] and u_{Biot} [m³ m⁻² s⁻¹], and they were compared with $u_{Grav.}$, using the pairs of sensors P01 and P02.

Fig.VI.2 (a) shows the circadian curve obtained with u_{Biot} and u_{Conv} data (sensor P01) in comparison to u_{Grav} data in days 85 and 86 (2018). The best agreement occurred in u_{Biot} values, given that u_{Conv} data overestimated the sap flow rate 4 times when compared to u_{Grav} (Fig.VI.2 (b)). Nevertheless, u_{Biot} showed values closer to the u_{Grav} data range, estimated as 1.5 times the u_{Grav} values. The adjustments based on the Biot equations in sensor P01 (Eq.VI.02 and Eq.VI.04) contributed to a reduction of 2.7 times on the overestimate obtained with the conventional approach, which the offset magnitudes were estimated as – 0.2 °C and –1.2 for $T_{MAXheat(P01)}$ and $T_{no\_heat(P01)}$ data, respectively. Also, both u_{Biot} and u_{Conv} estimates presented good correlation (Fig.VI.2 (b)), showing to be useful to sap flow estimates when using sensors calibrated.

Fig.VI.2 (c) shows the circadian curve obtained with u_{Biot} and u_{Conv} data (sensor P02) in comparison to u_{Grav} data. It was observed that the best agreement occurred in u_{Biot} values, presenting a good correlation (Fig.VI.2 (d)). However, u_{Biot} data overestimated the sap flow rate 1.44 times, when compared to u_{Grav}. Nevertheless, u_{Conv} showed values closer to the u_{Grav} data range, underestimated as 0.82 times the u_{Grav} values, albeit presenting a weak correlation compared to u_{Grav} measured from gravimetric approach (Fig.VI.2 (d)).

The low sap flow rates observed in the P02 potted tree compared to the P01 potted tree are plausible, given the small trunk area (see Table III.8). Also, it is verified that u_{Biot} computed with the k_{Biot} approach reached null sap flow in the night-time. The same did not occur with u_{Conv} computed with the k_{Conv} approach.

Fig.VI.2 (a) illustrates that a peak was observed between 16:00 to 19:00 hours. The analysis in Fig.VI.3 shows that ΔT values decreased, ranging initially from 3.16 to 3.08 °C, and at that point, increased up from 3.08 to 3.28 °C. It could be due to the dissonant thermal properties variation between T_{heat} and T_{no_heat} sensor places, caused by the surrounding disturbance, *e.g.*, natural thermal gradients, as mentioned by Lu *et al.*(2004), as well as, motion influenced by the thermal properties of the wood surrounding T_{heat}.

a) Tree P01
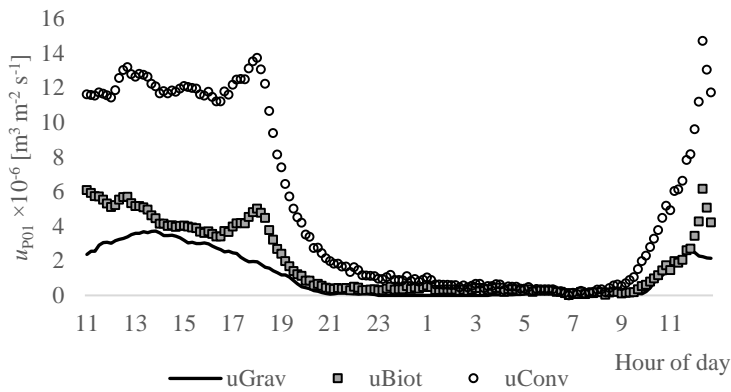
b) Tree P01
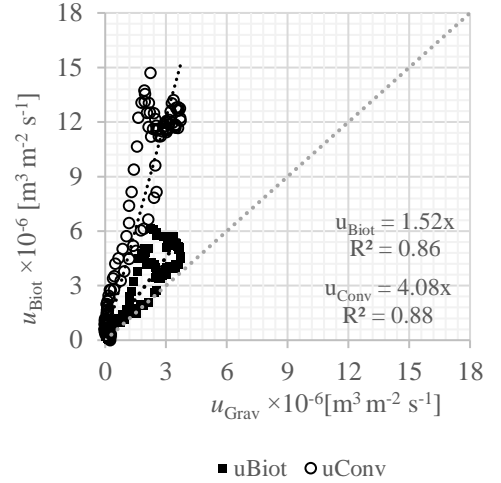
c) Tree P02
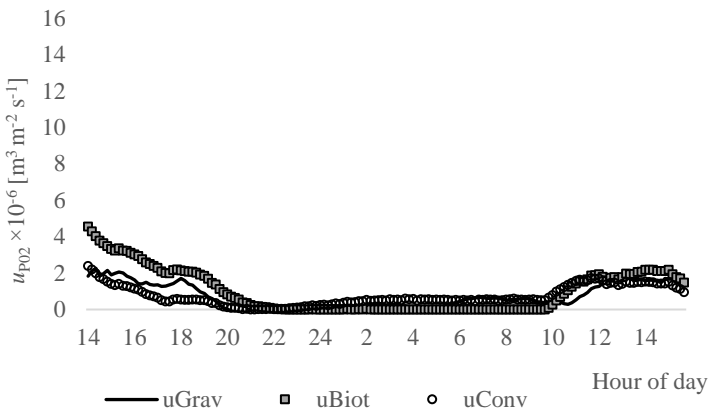
d) Tree P02
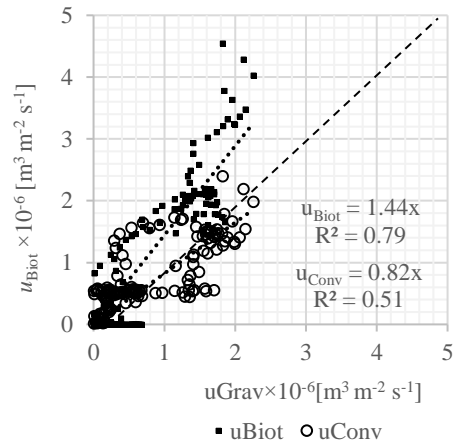
Fig.VI. 2: Comparative diagram between the sap flux density computed from the Biot approach (u_{Biot} [m³ m⁻² s⁻¹]) and computed from the conventional *Granier* approach (u_{Conv} [m³ m⁻² s⁻¹]) in comparison to the sap flux density observed for gravimetric test (u_{Grav} [m³ m⁻² s⁻¹]) on the sensor: a) P01, circadian curves (days 85 and 86 (2018)); b) P01, regression curve u_{Grav} versus u_{Biot} and u_{Conv}; c) P02, circadian curves (days 86 and 87(2018)); b) P02 regression curve u_{Grav} versus u_{Biot} and u_{Conv}.
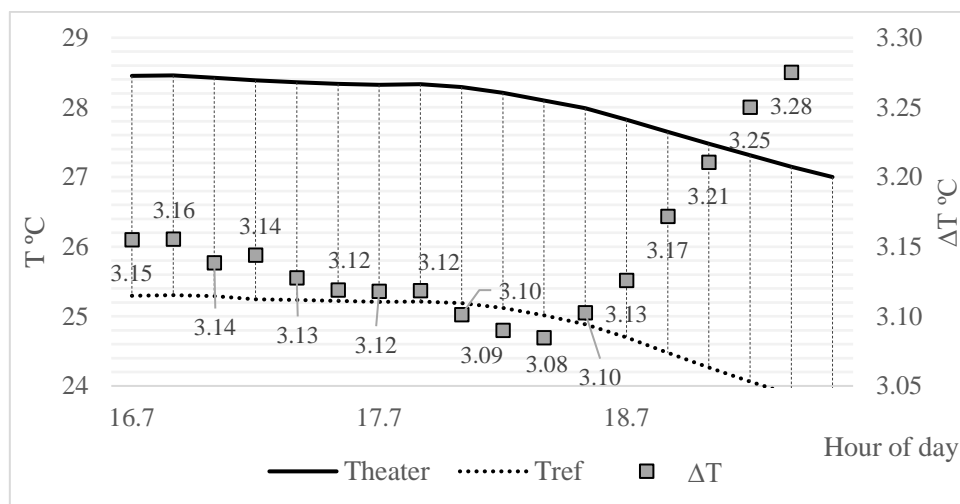
Fig.VI. 3: Observations of the temperature differences decrease (ΔT [ºC]), ranging from 3.16 to 3.09 ºC before to up to higher values ranging from 3.09 to 3.28 ºC.

The conventional sensors C01 and C02 were evaluated in the days 107 – 108 and 108 –110 (2018), respectively, with the gravimetric approach. Fig.VI.4 (a) show the circadian curve obtained with u_{Conv}(C01) [m³ m⁻² s⁻¹] in comparison to $u_{Grav.}$[m³ m⁻² s⁻¹] data. The conventional approach was used to compute the *Granier* sap flow index (k_{Conv}), which overestimated as 7.82 times and presenting a weak correlation compared to u_{Grav} measured from gravimetric approach (Fig.VI.4 (b)). Fig.VI.4 (c,d) show the circadian curve and linear regression obtained with u_{Conv}(C02) [m³ m⁻² s⁻¹] in comparison to $u_{Grav.}$[m³ m⁻² s⁻¹] data. u_{Conv}(C02) showed values closer to the u_{Grav} data range but presented no regression with u_{Grav} measured from gravimetric approach (Fig.VI.4 (d)).
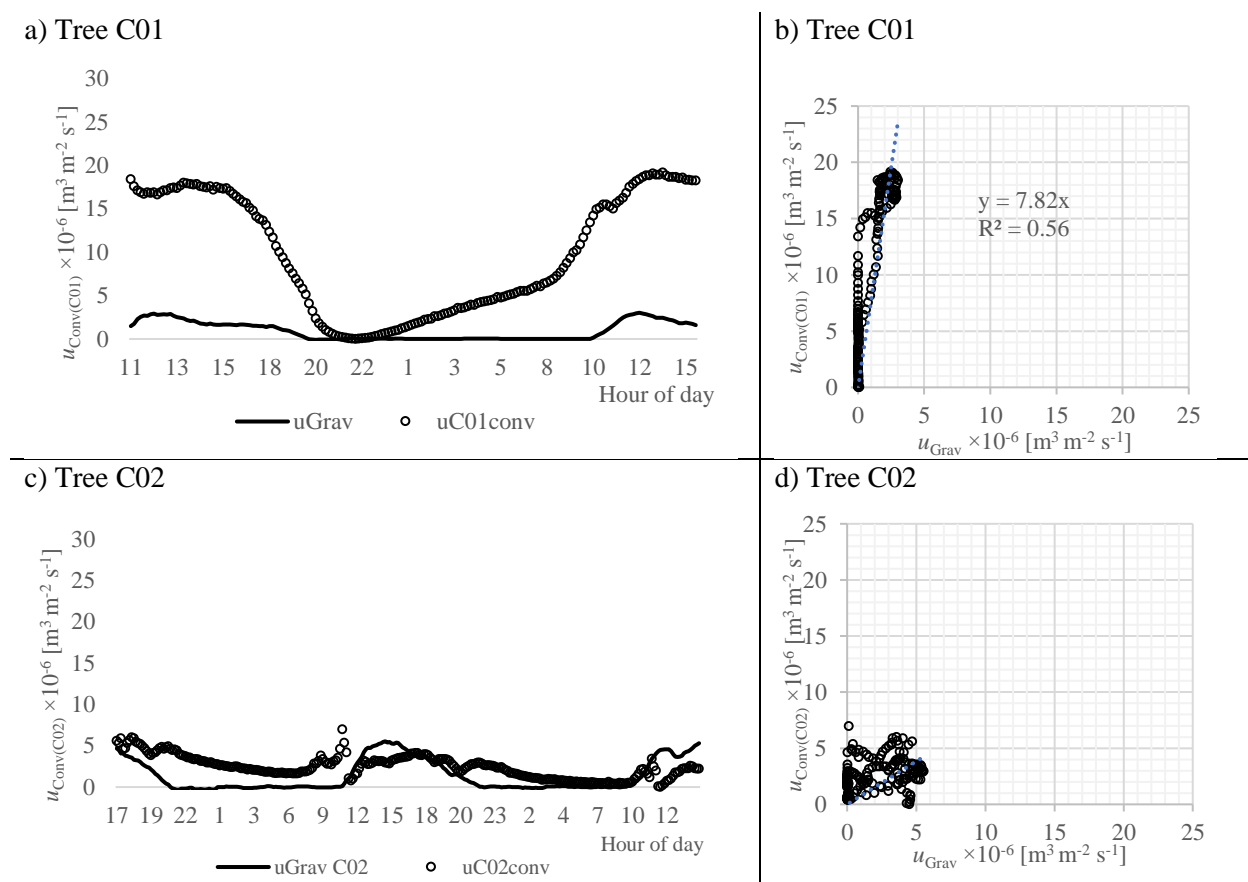
Fig.VI. 4: Comparative diagram between the sap flux density computed from the conventional *Granier* approach (u_{Conv} [m³m⁻³s⁻¹]) in comparison to the sap flux density observed for gravimetric test (u_{Grav} [m³m⁻³s⁻¹]) on the sensor: a) C01, circadian curves (days 107-108 (2018)); b) C01, regression curve u_{Grav} versus u_{Conv}; c) C02, circadian curves (108-110 (2018)); b) C02 regression curve u_{Grav} versus u_{Conv}.

Sap flow estimates are considered challenging, mainly due to the empirical equation that transfers the temperature values to sap flux density being strongly sensitive to ΔT_{MAX} (Rabbel *et al.*, 2016) and the reference temperature collected from another sensor. According to Lu *et al.*(2004), T_{MAX} should be determined separately for each sensor because T_{MAX} is a sensor-specific result. It could be due to manufacturing and installation being occasionally different (*e.g.*, effective resistance of the heater). In a

better way, k_{Biot} approach reduced the bias between T_{heat} and T_{no_heat} sensors, as well, encompassed the characteristics of the conventional daily ΔT_{MAX} determination and upgraded to a stable ΔT computation in the night-time, obtaining ΔT with zero flux conditions, *i.e.* $\Delta T_{MAX(Biot)}$. This was made possible because mG sensors measure absolute temperatures. Thus, based on the analyses of sap flow data of P01 and P02 olive trees, this study showed that $T_{MAX(Biot)}$ and $T\infty$ adjustments based on Biot approach provide the best estimates, allowing for a robust, physically-based ΔT_{MAX} determination, reliable absolute sap flux density computations and with the ability of self-regulating under nocturnal sap flow.

VI.2.1.2.Comparison between modified *Granier* and conventional *Granier* sensors

Fig.VI.5 shows the sap flow circadian curve (F [mm h⁻¹]) captured from the sensor-set P01, P02, C01 and C02. The comparison analysis was limited to the P01 and C01 potted trees because these are comparable sap flow and had similar dimensions as well, *i.e.* similar trunk section area and tree height (see Table III.8).
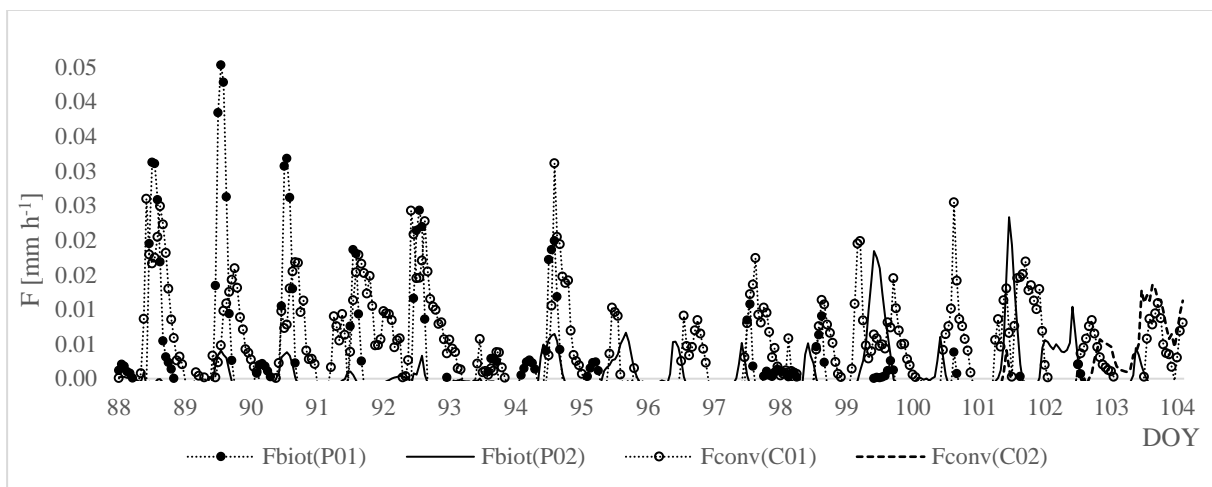
Fig.VI. 5: Comparative diagram between the *Granier* sap flow indexes with the sensors (P01, P02, C01 and C02) from day 86 to day 102.

Fig.VI.6 illustrates the comparison of the sap flow estimates with the gravimetric approach from C01 sensor ($F_{grav(C01)}$ [mm h⁻¹]), the Biot approach from P01 sensor ($F_{biot(P01)}$ [mm h⁻¹]) and the conventional approach from C01 sensor ($F_{conv(C01)}$ [mm h⁻¹]). Albeit the gravimetric data ($F_{grav(C01)}$) were originated from the C01 olive tree, the magnitude $F_{grav(C01)}$ data showed to be like $F_{biot(P01)}$ data. The $F_{conv(C01)}$ data inconsistency is due to conventional sap flow index (k_{Conv}) computation, which the k_{Conv} equation terms were not adequately adjusted. Indeed, the $\Delta T_{MAX}(C01)$ was higher 3ºC in the gravimetric

test day (days 107 and 108) than previous days. Unfortunately, it is not possible to compute the C01 sap flow index via the Biot approach in conventional *Granier* sap flow sensors, as they do not provide absolute temperature values.
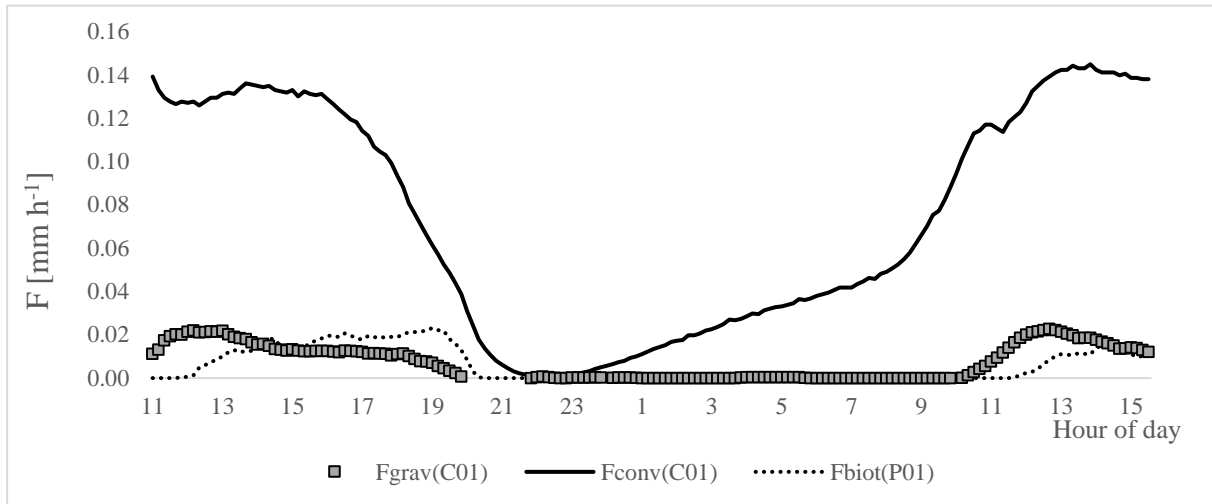
Fig.VI. 6: Comparative diagram between the sap flow measured in potted olive tree (P01) and computed for Biot approach ($F_{biot(P01)}$ [mm h^{-1}]), and the sap flow observed for gravimetric test ($F_{grav(C01)}$ [mm h^{-1}]) in potted olive tree (C01) and computed for conventional *Granier* approach ($F_{conv(C01)}$ [mm h^{-1}]) in the days 107 and 108.

FigVI.7(a-c) shows the hourly mean values of the transpiration obtained with sensors P01($Fbiot_{P01}$[mm h^{-1}]) and C01($Fconv_{C01}$[mm h^{-1}]) in comparison with the hourly mean values of the air vapor pressure deficit (VPD [kPa]) estimates from data collected from day 86 to day 108 (2018), at INIAV-Dois Portos meteorological station at 150 m from the greenhouse. $Fbiot_{P01}$, $Fconv_{C01}$ and VPD data were clustered on an hourly basis.

The Fbiot (P01) circadian curve is related to VPD estimates (Fig.VI.7(a)). In fact, the low values of VPD (< 0.66 kPa) should is related to low sap flow rates, as it is verified in Fbiot (P01). Also, $Fconv_{C01}$ (Fig.VI.7(b)) presented satisfactory data consistency, when compared to the VPD circadian curve.

The Fbiot(P01) and Fconv(C01) data were compatible within the magnitudes of their values (Fig.VI.7(c)), which were contradictory with the previous conclusion in Fig.VI.6, given that the averaged values $Fconv_{C01}$ have minimized the error caused for the overestimated values occurred in the days 107 and 108. Usually, errors of such magnitude are acceptable for practical applications in the agriculture.

Fbiot (P01) showed very low sap flow values, especially between 12 and 18 hours (local time) reaching to almost zero, which possibly influenced the stomatal closure (Ferreira & Katerji, 1992; Paço,

2003). However, Fconv(C01) has not presented the similar sensibility. The reason resides in the geometry of the mG sensor that permits measuring the actual temperature of the sap. It can more easily detect the elevation of temperature from the T_{heat} sensor, which should be closer to T_{MAX} temperature estimated, thus, reducing k_{Biot}.
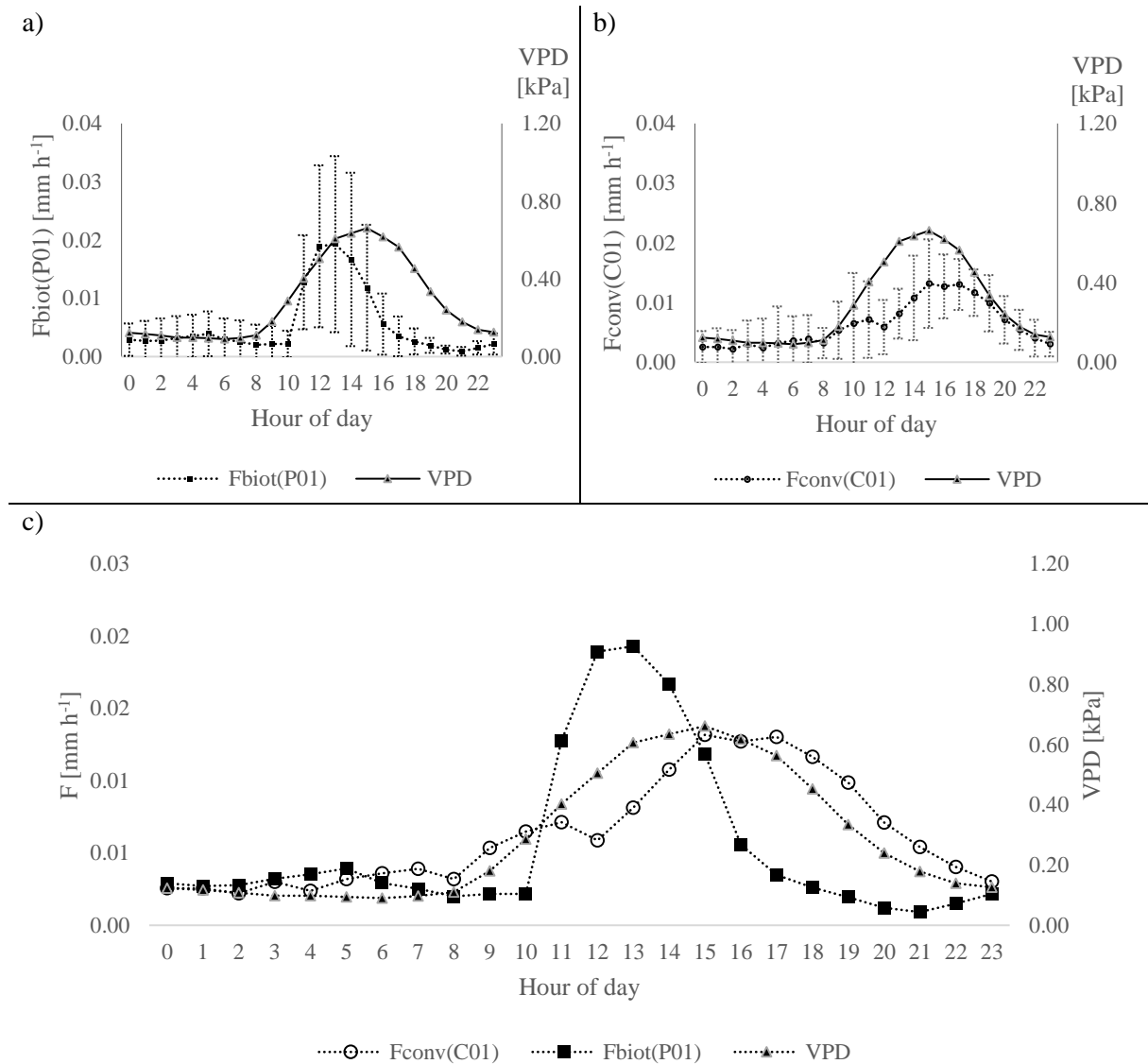
Fig.VI. 7: Comparison of the hourly mean air vapour pressure deficit (VPD [kPa]) from data collected at INIAV-Dois Portos meteorological station (days 86 to 108 (2018)) with: a) sap flow from modified *Granier* sensors (Fbiot$_{P01}$ [mm h^{-1}]); b) sap flow from the conventional *Granier* sensor (Fconv$_{(C01)}$ [mm h^{-1}]); c) Comparison between Fbiot$_{(P01)}$, Fconv$_{(C01)}$ and VPD estimates.

VI.2.2. Field experiments

The field experiments aimed mainly at 1) evaluating the heating capacity of sensors when inserted into the tree trunk; 2) by the comparison between mG sensors and conventional sensors and 3)

evaluating an algorithm to adjust NTG occurrences. Table VI.1 summarises the field trial, their locations and the objectives.

Table VI. 1: Identification of the field trials using the modified *Granier* sap flow

Trial	Location	Objectives
Kiwi Orchard	Quinta das Picas (Kiwi Greensun, SA), São Salvador de Briteiros, Guimarães – Portugal	Evaluating installation procedure, heater resistance, sensors design, power requirements, the efficiency of solar panel and robustness, the local machine performance and the automatic algorithm of NTG adjustment.
Vineyard	Adega Catapereiro - EN118 Porto Alto – Alcochete	Comparing mG sensors and conventional sensors

VI.2.2.1. Kiwi orchard

The kiwi orchard trial, which the methodology is described in the Section III.4.3.3.1, was preceded by laboratory tests aiming to characterise the sensors to be used in the field and to test the power and heating performance in a controlled environment. Also, aimed at characterising the temperature measurement sensors, in particular, the offset.

The T_{heat} (heating capability not used) and T_{no_heat} sensors were inserted into a sealed tube previously filled with warm moist sandy soil and acquiring the two (T_{heat} and T_{no_heat}) temperature measurements in continuous time. The temperature was measured for 4500 seconds. The water temperature was monitored using a reference thermometer (sensitivity ± 0.2ºC -Pocket Digital Probe Thermometer Slimline).

Fig.VI.8 (a) shows the evolution of the two measured temperatures. It can be seen that there is a good agreement between the two values, which differ with a mean offset of 0.09 ºC (Fig. VI.8 (b)).

a)   b)
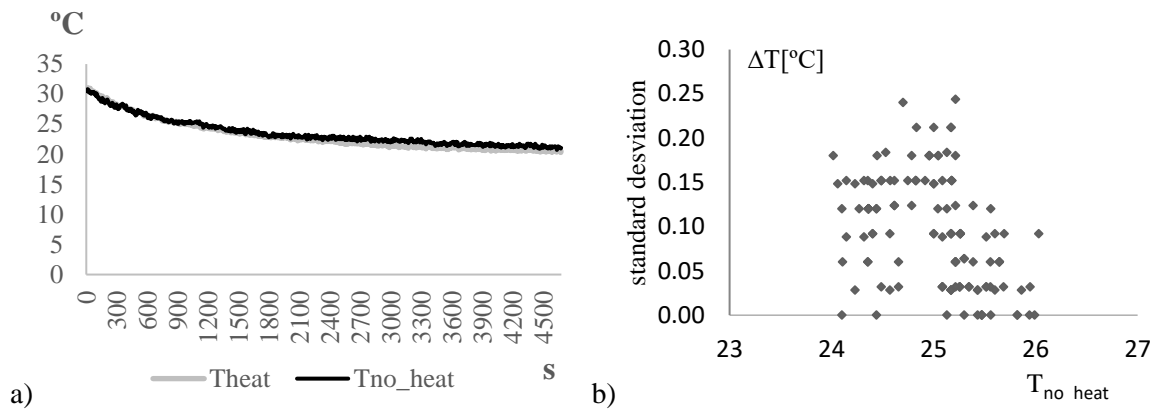
Fig.VI. 8: a) Evolution of the temperatures provided by two tree sensors; b) Distribution of the relative error obtained when measuring the same temperature with the heater sensors (T$_{heat}$[ºC]) and referential sensor (T$_{no\_heat}$ [ºC]).

Fig.VI.9 shows the T$_{heat}$ and T$_{no\_heat}$ temperatures relative error obtained for the 6 made pairs of sensors (Table III.9), with no calibration, in comparison to the temperature provided by a reference thermometer. It can be seen that the maximum obtained error is estimated as 0.9 ºC (G1J$_{no\_heat}$). As the most critical measurement is the difference of temperatures between sensors in a pair and not the absolute temperature, each pair should be then calibrated by an algorithm with that aiming, to obtain a minimum difference ≤ 0.2 ºC, according to the system resolution.
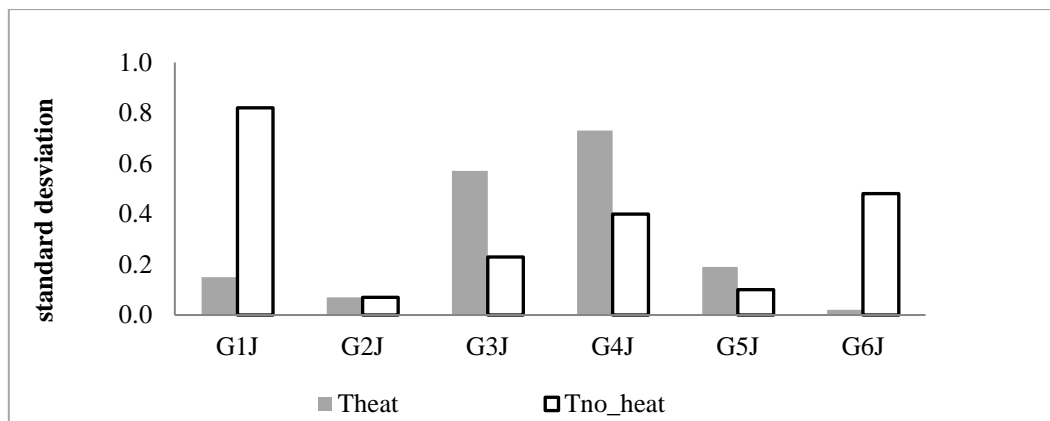
Fig.VI. 9: Distribution of the relative error obtained when measuring the same temperature with heater sensors (T$_{heat}$[ºC]) and referential sensors (T$_{no\_heat}$ [ºC]).

The G2J$_{heat}$ and G2J$_{no\_heat}$ sensors were inserted in a tube filled with cork since can simulate the xylem features (Fig.VI.10). The aiming consisted in evaluating the capability of heating in a confined environment.

Fig.VI. 10: The heater sensors (G2J$_{heat}$[ºC]) and referential sensor (G2J$_{no\_heat}$ [ºC]) inserted into a tube filled with cork

The experiment consisted of activating the heater, regulating its temperature (T$_{heat}$) around 26 ºC and acquiring the two (T$_{heat}$ and T$_{no\_heat}$) temperature measurements for 12 hours. Fig.VI.11 shows the evolution of the applied power and temperatures measured. After one hour with the heater switched-on, its temperature was regulated with an on/off controlling process. During this period the two temperatures increased and then were maintained at an approximately constant value each, with a difference between the two observed as 5 ºC. The power was regulated at 0.15 W, which all heater sensors correctly regulated the heating power around 0.15 W, such as designed for this trial.
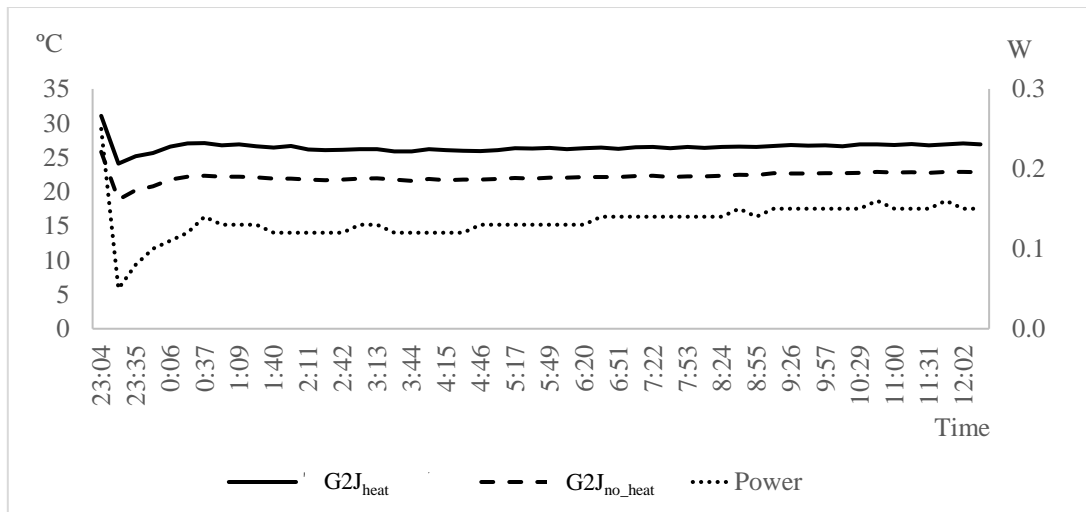
Fig.VI. 11: Evolution of the power applied to the modified *Granier* sensor and temperatures measured with the two tree sensors (G2J$_{heat}$[ºC] and referential sensor G2J$_{no\_heat}$ [ºC]).

The results observed in laboratory experiments showed a precision of 0.2 ºC, in agreement with what is required by applications of this nature. The heater reaches a constant power to maintain a constant temperature, as required for the *Granier* methodology and therefore is adequate for the measurement of sap flow by this technique.

The six pairs of sensors tested in the laboratory were installed in the kiwifruit orchard and data was captured for ten days. Temperature measurements were acquired with the heater switched on for 15 minutes and likewise, with the heater switched off for another 15 minutes. The averages of the temperatures provided by all T_{no_heat} sensors ranged between 21 ºC and 23 ºC.

Fig.VI.12 (a, b) shows the evolution of the difference of temperatures captured with two sensors, G5J (Fig.VI.19(a)) and G6J (Fig.VI.19(b)) in 2015, Aug18, before (ΔT) and after (ΔT_{adj}) offset correction. The square waveform results from switching on ($\Delta T \neq 0$) and off ($\Delta T = 0$) the heater. It can be seen that after offset correction the differences observed with the heater off are reduced to 0ºC. The cyclic ON/OFF heating contributes to adjust the thermistor offset and the possible NTG´s occurrences.

The automatic process of ΔT adjustment is implemented with the temperature measurements in the tree trunk following the steps:

1. Turn the heater off;
2. Measure both T_{heat} [Cº] and T_{no_heat} [Cº] temperatures for 15 minutes;
3. Compute the mean offset (offset [ºC]);
4. Turn the heater on during 15 minutes;
5. Measure both T_{heat} [Cº] and T_{no_heat} [Cº] temperatures;
6. Calculate $T_{heater}adj$ [Cº] = T_{heat} [Cº] – offset [ºC];
7. Calculate: $\Delta Tadj = T_{heater}adj$ [Cº] – T_{no_heat} [Cº]
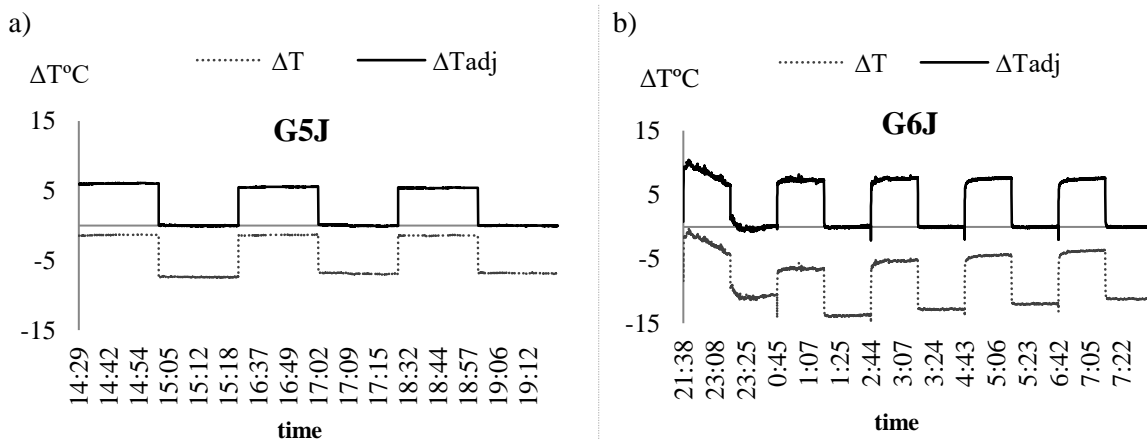
Fig.VI. 12: Differential temperature measurements for sap flow estimation before (ΔT (dash line)) and after (ΔT_{adj} (full line) offset correction: a) G5J sensors, b) G6J sensors.

Preliminary results obtained in the field showed that the thermistor offset could be fixed as well as the NTG occurrences by the FAUSY algorithm (section III.3.3). Moreover, the mG sensors

demonstrated to be able to measure temperature in the trees and adequate sap heating to allow ΔT measurements (*e.g.*, increasing the temperature above 6º C in the G5J and G6J sensors).

In short-term, the trial aims were reached for these first prototypes. However, these sensors presented low performance due to the inefficient power source (batteries and solar panels). Also, the electronics parts (e.g., interfaces, microprocessor) were not in conformity with the field conditions. These observations aided in the improvement of the next prototypes, which are described further in the text.

VI.2.2.2. Vineyard

This vineyard trial, which methodology is described in the Section III.4.3.3.2, aimed to perform the comparison between modified *Granier* (mG) and conventional *Granier* sensors and to analyse the physical phenomena of heat transfer between the heater sensor and sap. Three pairs of modified *Granier* and three pairs of conventional *Granier* sensors were used for this purpose.

The modified *Granier* sensor (mG_{SP02}) performance was compared with that provided by the conventional sensor (C_{Gr3}) described in Table III.10.

The temperature difference data (ΔT [ºC]) obtained with mG_{SP02} and C_{Gr3}, were compared and evaluated using the bias analysis and graphical techniques. The mG_{SP02} data and C_{Gr3} data were recorded from the day 232 to the day 240 (2017), obtained with 15-min measurement intervals and scaled to the hourly mean (ΔT_h [ºC]). The ΔT_h (mG_{SP02}) and ΔT_h (C_{Gr3}) data were clustered on an hourly basis.

The range of differences observed between the maximum and minimum temperature is related to the capacity of the sensor of transmitting the heat dissipation caused by the sap flow. The mG_{SP02} sensor showed lower heating capacity when compared with C_{Gr3} sensor yielding lower ΔT values than C_{Gr3} sensor (Fig.VI.13).

The heating capacity of the mG_{SP02} sensor has provided a minimum of around 7 ºC and maximum about 9 ºC, contrasting with C_{Gr3} (minimum around 6 ºC and a maximum of 12 ºC). Probably, this is caused by operational features of mG sensors described in section III.2.1, as the position of temperature sensing thermistors in the tip of the sensor allowed to capture more accurately the measures of sap temperature. Also, it explains the higher resolution of the mG_{SP02} sensor when compared with the C_{Gr3} sensor, corroborating with the high sensitivity of mG observed in the greenhouse trial (section VI.2.1.2).

A peak was observed systematically around 14:00 hours, after the local solar noon time (at 13:38) (Fig.VI.13). Possibly, this was caused by stomatal closure, which reduced transpiration, therefore

increasing ΔT. This mechanic stomatal closure, occurring soon after solar noon, is known to occur in olive trees as referred in Fernández *et al.* (2006), especially under stress conditions. The vineyard was not being irrigated in the days from 232 to 240, and it is lively to admit some water stress. In comparison, it was not observed any peak in the CGr3 sensor, given the low sensitivity in measuring the sap temperature, as observed in Fig. VI.7 (c).
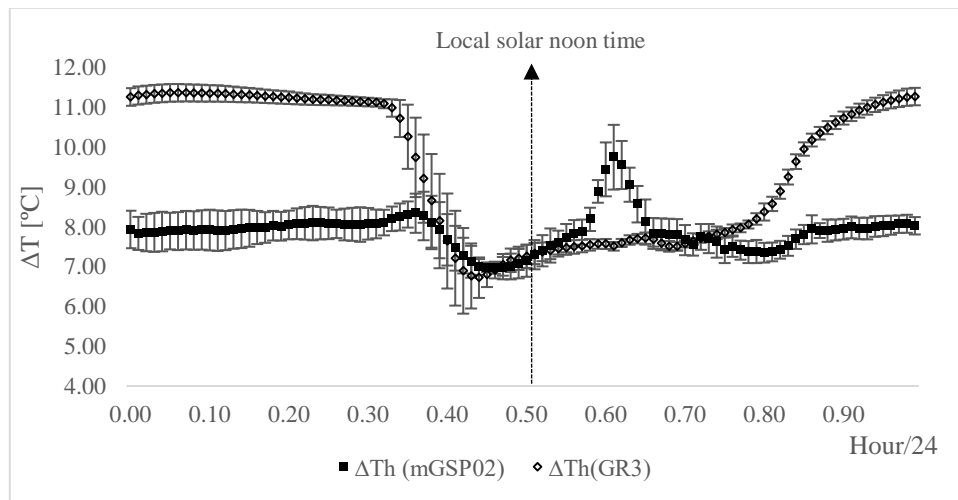
Fig.VI. 13: The temperature differences (ΔT [ºC]) collected from the sap flow sensors in the Adega Catapereiro Vineyard from day 232 to day 240 (2017). The hourly mean (ΔTh [ºC]) with mGSP02 and CGr3 sensors were clustered on an hourly basis (Hour/24). Full square - modified *Granier* data (ΔTh (mGSP02)). Empty square - conventional *Granier* data (ΔTh (CGr3)).

VI.3.   Conclusions

The work presented herein addressed the evaluation and validation of prototypes of a modified *Granier* sensor (mG). The sap flow measurements were implemented using mG sensors including the results obtained with potted olives trees in a greenhouse and in field experiments (kiwi orchard and vineyard).

Concerning the trial in the greenhouse with olive trees, the transpiration measured with mG sensors showed to be in conformity with the measurements observed with the gravimetric approach and based on the *Granier* model. The use of an alternative Biot approach showed to be a significant source of certainty in sap flow estimations. The modified *Granier* sensors associated with *Granier* sap flow index computed based on the Biot approach showed the best conformity with the estimates of sap flow in comparison with the gravimetric test. Future research should focus more strongly on validating of the Biot approach for an extended period.

Regarding the field trials (*i.e.*, kiwi orchard and vineyard), the experimental studies showed the modified sap flow *Granier* sensors provided good accuracy to measure temperatures in trees, estimate the optimal ΔT_{MAX} and allow to adjust NTG automatically. As well, a precision of 0.2 ºC was obtained, what is in agreement with what is required by applications of this nature. Also, preliminary results obtained in the field showed that the FAUSY algorithm could fix the thermistor offset and NTG occurrences. Moreover, the mG sensors demonstrated to be able to measure temperature in trees and elevate the temperature to at least about 6º C when the heater is ON.

Concluding, the sensors described in this chapter were fully developed by the author using easily obtainable parts. Their easy manufacturability makes them prone to be fabricated at low cost and thus widely practical. The same can be said regarding the data acquisition and control hardware, although in this case more electronics specific knowledge is required. This fact, together with the reasonable accuracy of the results that were obtained in the lab and field experiments carried out in two orchards, confirm the validity of the proposed customizable solution as one to obtain cheaper and more flexible devices for the SOIS system under development.

CHAPTER 7

VII. CHAPTER 7: Using SOIS for Orchards and Vineyard

VII.1.   Experimental purpose

The experiments presented in this chapter explores the data acquisition implementation regarding the SOIS system. Also, the purpose of this work consisted on analysing the procedures to combine the data records from SOIS, namely soil evaporation and crop transpiration fluxes and comparing them with measured values obtained with the eddy covariance (ET_{EC}) technique.

SOIS is expected to help a more readily understanding of the ET components in orchards and vineyard and provide insight into the development of ET measurement tools. Thus, the complete system was primarily tried out in a single lemon tree, aiming to assess the interactivity among the sensors and practising the field mounting methodology, and later in a vineyard experiment at the field, being the results herein described.

The assembly for the SOIS system and methodology are described in sections from III.2 and in section III.4.4, respectively. The data acquisition performance and the data records combination were analysed with statistical and graphical techniques

VII.2. Results and discussion

VII.2.1. Single lemon tree

The field mounting configuration is illustrated in Fig.III.24. The weighing device (mLy) data, the modified *Granier* sensor (mG) data and the pair of *Peltier* cells (Pcell$_1$, Pcell$_2$) data were recorded between the days 133 and 135 (2016) deprived of watering, obtained with 15-min measurement intervals and scaled to the hourly mean.

The hourly mean soil moisture (θh [cm^3 cm^{-3}]) data were related to the *Granier* sap flow index (k_{Conv}) estimates from the modified *Granier* sensor (mG). Also, the soil heat flux measurements buried in the depths: 0.1 cm (G$_0$ [W m^{-2}]) and 15 cm (G$_{15}$[W m^{-2}]), were compared to the k_{Conv} curve.

In a qualitative analysis, the soil moisture showed to vary inversely with the index of transpiration configured for k_{Conv} since the transpiration presented the lowest values and the water redistribution into the soil reaches a maximum in simultaneous at night, while the inverse occurs during the day (Fig.VII.1(a)). Indeed, it can be observed that k_{Conv} and soil moisture showed to have an inverse correlation (Fig.VII.1(b)).

a)

b)
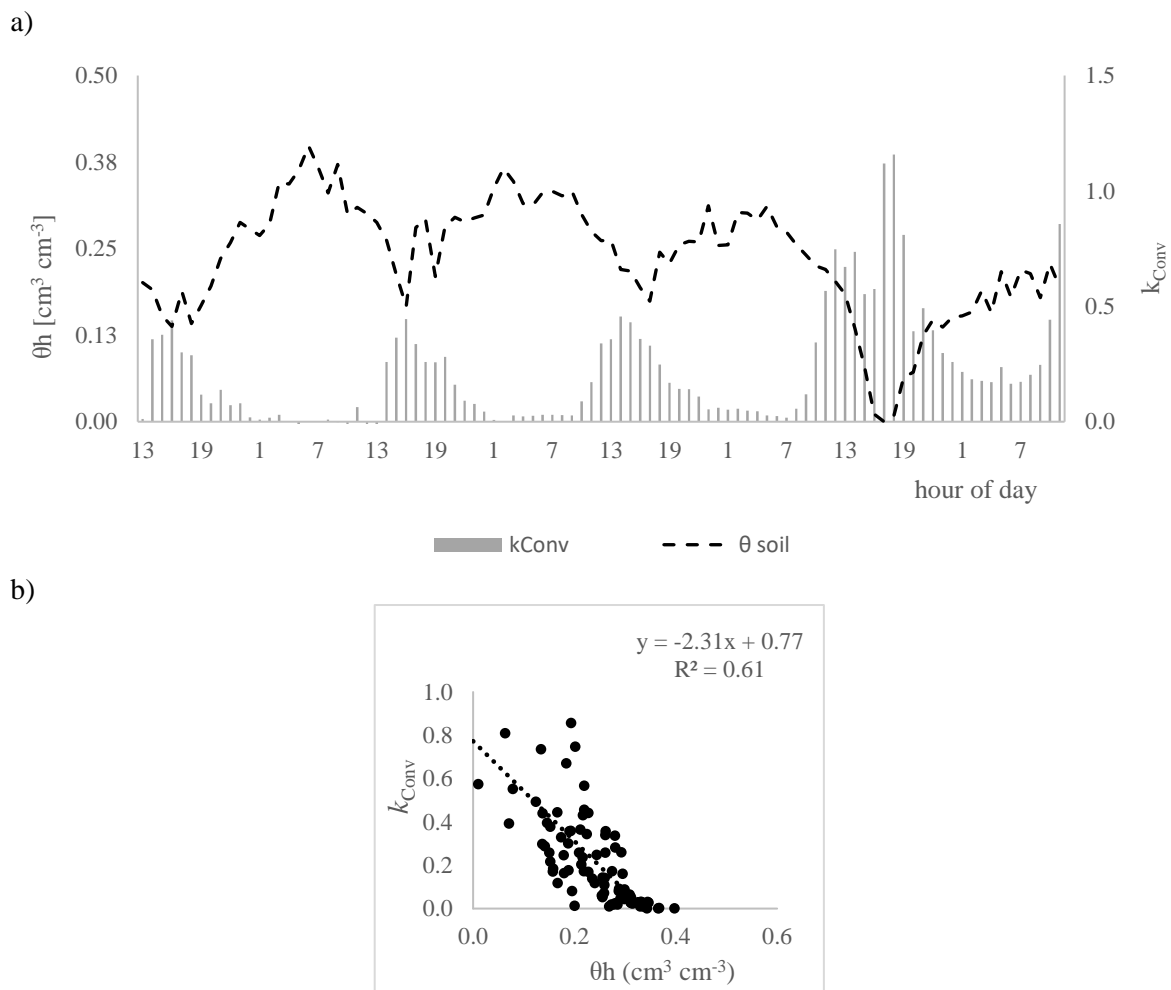
Fig.VII. 1: a) Soil moisture (θh [cm^3 cm^{-3}]) related to the *Granier* sap flow index k_{Conv} observed on single lemon tree experiment from day 133 to day 135 (2016); b) Linear regression to model the relationship between *Granier* sap flow index (k_{Conv}) and soil moisture (θh [cm^3 cm^{-3}]).

Fig.VII.2 shows the soil heat flux curves at two depths, respectively, G$_0$ [W m^{-2}] and G$_{15}$[W m^{-2}]. The same circadian curve behaviour can be observed when compared to the k_{Conv} curve. It can be

understood that the proxy of transpiration (k_{Conv}) and soil heat flux are dependent on solar radiation, thus related, as observed.

Fig.VII. 2: The *Granier* sap flow index curve and the soil heat flux curves at two depths: G_0, G_{15} observed in the single lemon tree experiment on days 133 to 135 of the year 2016.

The inverse relationship between k_{Conv} and θh is due to the plant and soil-surface being equally exposed to solar radiation, and the transpiration and soil evaporation events have occurred in simultaneous, causing high transpiration values and high soil water depletion. At night, it occurred the soil moisture redistribution from more humid surrounding places to the mLy device site, and as it is predictable, the transpiration rate has reduced. Also, the same comparison between k_{Conv} and G_0, G_{15} was observed, which both are related to the soil-air heat flux. Thus, the higher transpiration rate and higher soil heat flux are driven for the higher soil-air temperature.

The SOIS system with all sensors integrated has functioned as projected since both operating on consecutive 3 days and without presenting the usual worries in field conditions. At least, the SOIS system presents the excellent potential to the trial replication in a commercial orchard.

VII.2.2. Vineyard

The vineyard considered in this study is cultivated under rainfed conditions. It is acceptable to consider the ET_{EC} measurements as referring solely to the transpiration estimates during no rain periods, in summer. The results are sectioned in meteorological variables and EC methodology data, and the SOIS performance as compared to the ET_{EC} measurements.

VII.2.2.1.Meteorological parameters and EC methodology

During this study, the maximum absolute values of solar radiation (Rs, [MJ m^{-2} d^{-1}]), reference evapotranspiration (ETo [MJ m^{-2} d^{-1}]) and rainfall (P [mm d^{-1}]) obtained in the days 251 to 305 (2016) were respectively, 23.44 MJ m^{-2} d^{-1}, 13.41 MJ m^{-2} d^{-1} and 35 mm d^{-1} (Fig.VII.3).
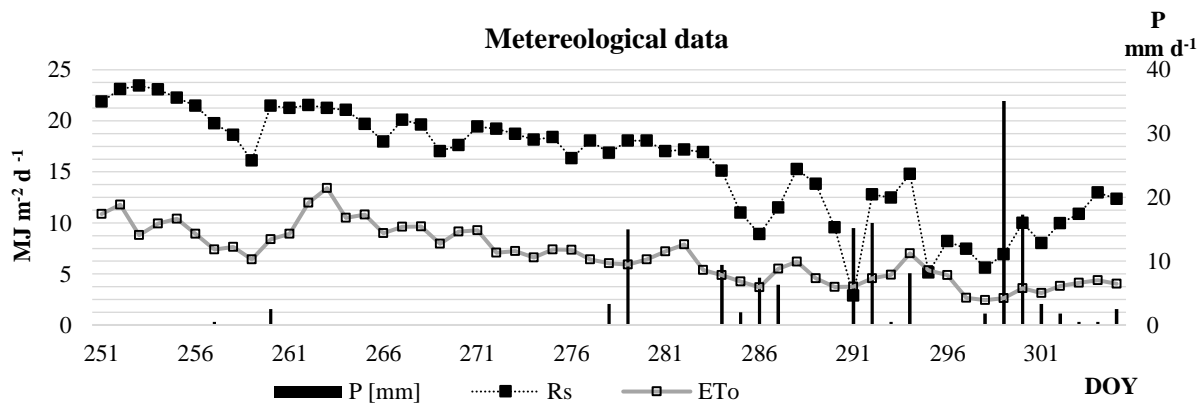
Fig.VII. 3: Solar radiation (Rs [MJ m^{-2} d^{-1}], reference evapotranspiration (ETo [MJ m^{-2} d^{-1}]) and rainfall (P[mm d^{-1}]) over the days 251 to 301 (2016) obtained from Wunderground meteorological station Nova Oeiras1.

The footprint analysis performed for EC data is summarized in Fig.VII.4 (a-b). Fig VII.4 (a) represents the one-dimensional footprint (or footprint function (Qf)). It allows predicting the most representative contributions to the measured flow originate from the area extending from the measuring point to the limit of the plot.

The integration of the footprint function (Qf [m^{-1}]) allows to quantify the cumulative normalised flux (Qc (x_L), which is relative contribution to measured the flux coming from a specific region, at a height z, as a function of the distance to the point (0, z) (Fig VII.4 (b)). The cumulative normalised flux (Qc (x_L) is obtained as a function of x_L, where x_L represents the distance in the wind direction, to the limit of the plot.

The determination of the Qc (x_L) function showed that more than 80 % of the vertical flow measured at the height of 2.5 m comes from points located up to 70 m from the measurement site (Fig.VII.04 (b)). Up to 140 m, this percentage rises to 90% and at 500 m it is around 95%.

a)
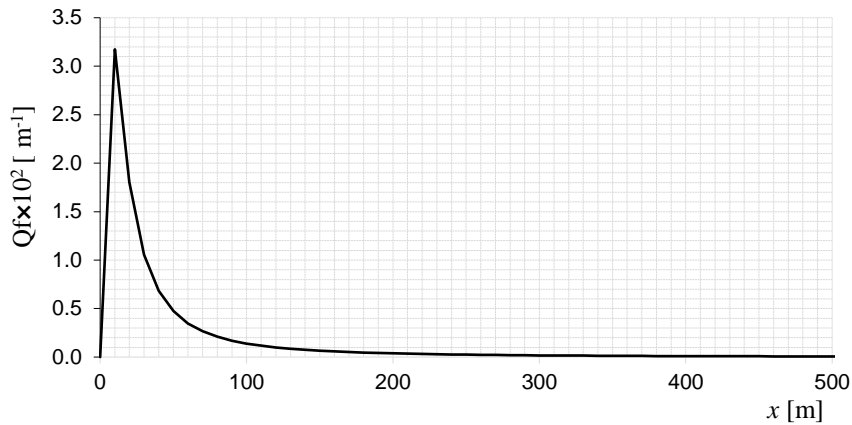
b)
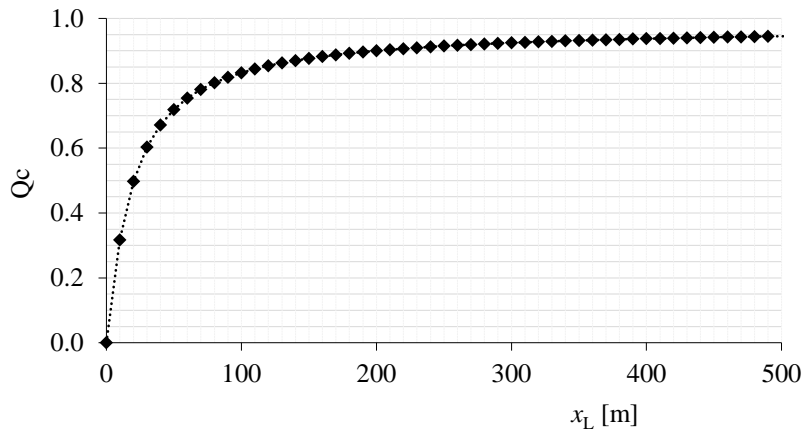
Fig.VII. 4: Footprint analysis of eddy covariance data: a) footprint prediction; Qf [m^{-1}] - footprint function; x [m] – horizontal distance between the measuring point and a point on the region of origin of the flows; b) Cumulative footprint prediction; Qc – Cumulative normalised flux; x_L [m] – distance between the measuring point and the boundary of the source region of the fluxes.

The determination of the maximum footprint function also made possible to predict that measurements made at 2.5 m height were mainly affected by fluxes from an area located at 10 m away from the measuring point in the wind direction (maximum of the relative flux density function).

The fetch was more favourable for the N, NW and W directions (around 124, 210 and 120 m, respectively – Fig.III.27). These directions had a height: fetch ratio lesser than 1: 100. However, according to the footprint analysis, a distance of 120 m in the wind direction (*e.g.*, in the W direction) would mean that it would be expected that almost 87 % of the fluxes, detected by the eddy covariance system, actually come from this area of influence. The same type of analysis for the N and NW direction indicated a percentage of 88 % and 92 %, respectively (Table VII.1).

Thus, the collected data with the EC system in this study was considered on days of prevailing winds blowing from the N, NW and W directions (shaded areas of Table VII.1). The data collected on

days of prevailing winds from other directions were eliminated as the percentage of detected flows coming from the areas of influence located in these directions was estimated to be less than 70%.

Table VII. 1: Selection of the data according to the footprint analysis. Grey-shaded areas indicate the prevailing wind directions on selected data days. Qc - Cumulative normalised flux

Wind Direction	Fetch (m)	Qc	height: fetch ratio
NE	32	0.60	12.8
E	20	0.44	8
SE	10	0.19	4
S	5	0.04	2
SW	15	0.33	6
W	**120**	**0.87**	**48**
NW	**210**	**0.92**	**84**
N	**124**	**0.88**	**49.6**

The eddy covariance measurements (EC) were recorded from day 272 to day 294 (2016) (Fig.VII.5). The maximum fluxes of H and λE were between 403 and 208 W m^{-2}, respectively. The global mean of the ratio between the sensible heat flux and the of latent heat, H / LE (Bowen ratio), during the data collection period was estimated as 2.27 ±0.97. It shows the vineyard as in water-stress condition, given that is a rainfed vineyard in the summer season.

The hourly mean ET_{EC} [mm h^{-1}], the latent heat flux (LE_{EC} [W m^{-2}]) and sensible heat flux (H_{EC} [W m^{-2}]) were computed between the days 272 and 294 and the whole data obtained from EC were clustered on an hourly basis as shown in Fig.VII.6 (a-b).

The maximum ET_{EC} and the maximum sum ($LE_{EC}+H_{EC}$) obtained in the EC were 0.23 mm h^{-1} and 345 W m^{-2} respectively, which are nearby values to those shown by Ferreira *et al*. (2012). These authors have obtained ET_{EC} and (LE_{EC} +H_{EC}) maximum values of 0.35 mm h^{-1} and 500 W m^{-2}, respectively, recorded during afternoon time, with the measurements taken between flowering and maturity in a rainfed vineyard located at Tagus Valley, Santarém. Thus, the ET_{EC} data obtained in this study are close to values obtained in another field experiment.
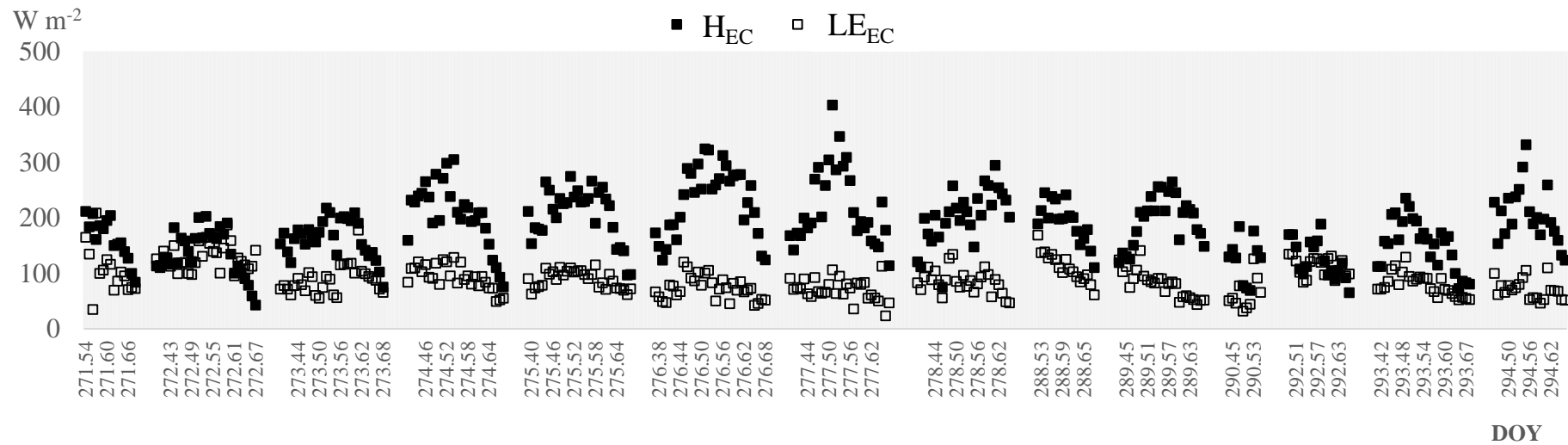
Fig.VII. 5: Sensible heat flux (H_EC [W m^-2]) and latent heat flux (LE_EC [W m^-2]) recorded by eddy covariance methodology in discontinuous time on the days 271 to 294

a)

b)
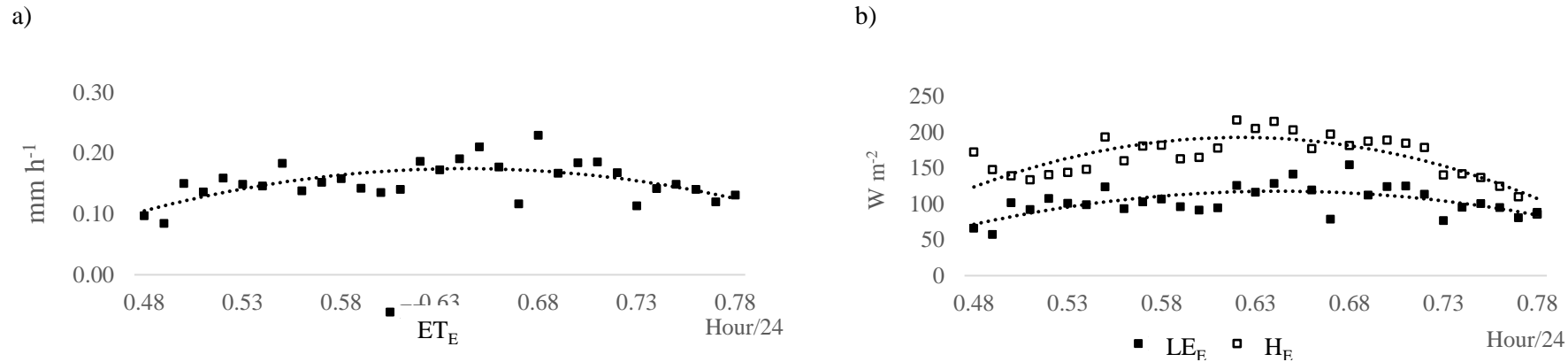
Fig.VII. 6: Hourly mean values obtained from eddy covariance measurements (EC) clustered on an hourly basis. a) evapotranspiration (ET_EC [mm h^-1]); b) latent heat flux (LE_EC, W m^-2) and sensible heat flux (H_EC, W m^-2).

VII.2.2.2.SOIS performance

The raw data from the modified *Granier* sensor (mG$_{SP32L}$) and the mean eddy covariance measurements (ET$_{EC}$ [mm h^{-1}]) obtained in 0.01 hours (14.4 min) intervals, were recorded between the days 288 and 290. The natural thermal gradients occurrences (NTG [ºC]) were recorded from sensor mG$_{SP25L}$ (T$_{heat}$ switch off) positioned 2.20 m from sensor mG$_{SP32L}$ (Fig.III.28).   The transpiration measured by the mG sensor SP32L (F$_{SP32L}$ [mm h^{-1}]) was adjusted to NTG occurrences and related to the actual ET$_{EC}$ measurements (ET$_{actual}$(EC) [mm h^{-1}]).

Fig.VII.7(a) shows the circadian curve comparison from ET$_{actual}$ (EC) with the adjusted sap flow curves in function of conventional *Granier* sap flow index (F(k_{Conv})adj), and Biot *Granier* sap flow index (F(k_{Biot})adj) approaches, respectively. Fig.VII.7 (b) shows the dispersion of the transpiration obtained from mG sensor SP32L data (F(k_{Biot})adj and F(k_{Conv})adj), around the fitted line of the ET$_{actual}$(EC). Albeit, it is not verified satisfactory linear regression to model the relationship between the transpiration obtained from mG sensor SP32L and eddy covariance measurements, both approaches showed similar circadian curves in the days from 288 to 290. The weak correlation could be explained by the fact that the mG sensors have detected the actual sap flow according to the specific conditions where the tree SP32L is positioned, and the eddy covariance has reflected the ET$_{EC}$ encompassing an area with several trees.

Fig.VII.7(a) is sectioned in three intervals ([288.5-288.8], [288.8-289.3], [289.4-289.8]), aiming to analyse in detail the behaviour of the fluxes. The shaded interval [288.8-289.3] shows a consistent performance when compared the low sap flow values in function of k_{Biot}, given to be night-time. Conversely, the sap flow from k_{Conv} computes high values. The high values with F(k_{Conv})adj) are probably due to the zero flow is not reached because of night-time water uptake for vegetative or reproductive growth and replenishment of internal storage (Vandegehuchte & Steppe, 2013). The k_{Biot} approach showed to be useful to overcome the night-time sap flow, adjusting T$_{heat}$ and T$_{no\_heat}$ values to T$_{MAX}$ and T∞ as described in the section III.4.3.1.

The observations referent to the time interval [288.5-288.8] concerns about the (F(k_{Biot})adj values decreasing, ranging initially from 0,135 to 0.042 mm h^{-1}, and at that point, increased up from 0.042 to 0.099 mm h^{-1}. Similarly to the time interval [289.4-289.8], occurred a slight sap flow decreasing from 0.100 to 0.090 mm h^{-1}, and at that point, increased up from 0.090 to 0.158 mm h^{-1}. It could be explained as commented in another vineyard trial (section VI.2.2.2), where it is suggested that the tree uses water-saving strategy assured by stomatal closure under drought stress in that day hour.

a)

b)
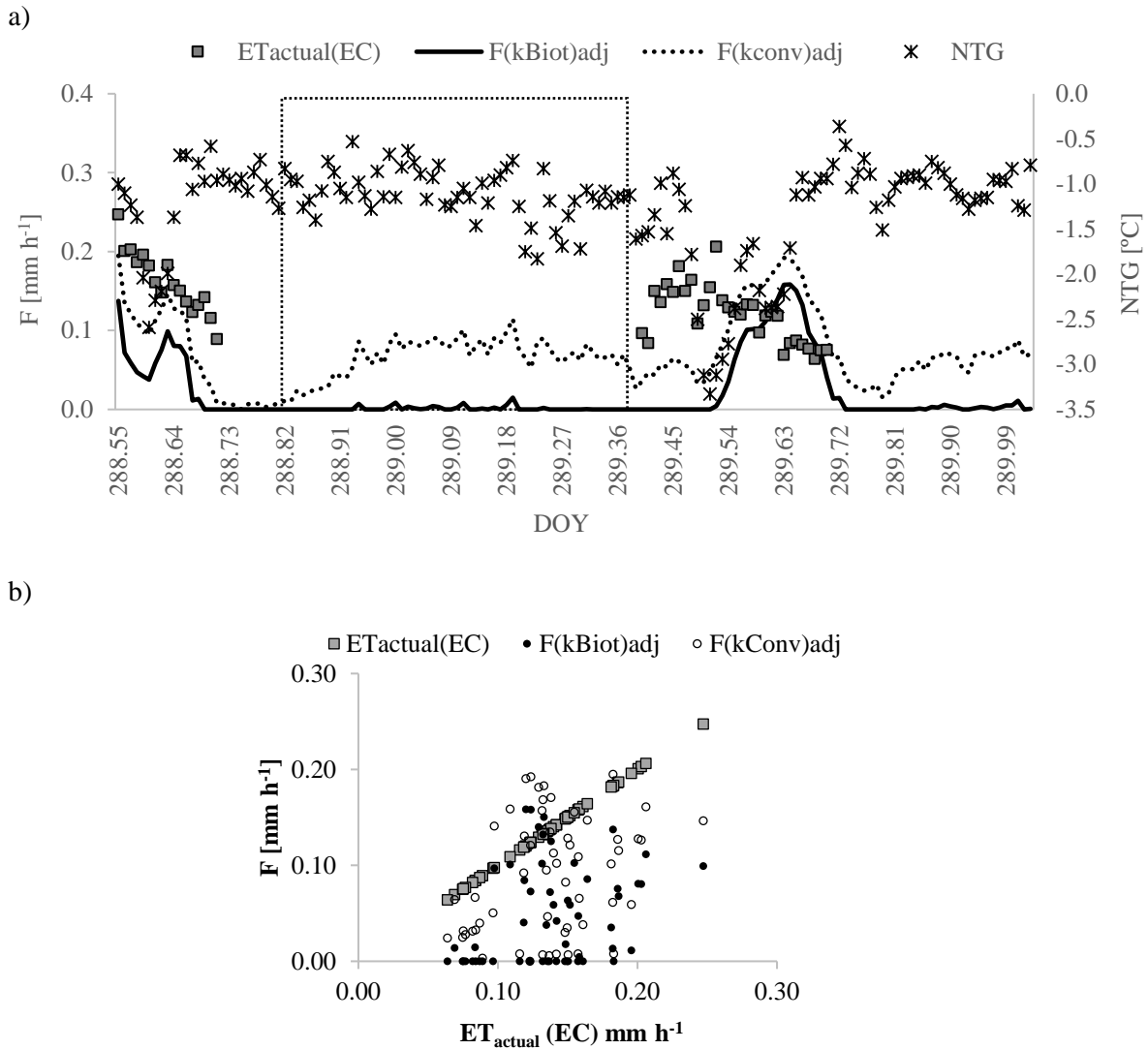
Fig.VII. 7: Comparative diagram of raw data obtained between the days 288 and 290 with an eddy covariance instrument (EC) and a modified *Granier* sensor (SP32L): a) circadian curve of the evapotranspiration measurements (ET$_{actual}$(EC) [mm h^{-1}]) and the adjusted sap flow rate measured in function of conventional *Granier* sap flow index (k$_{Conv\_Adj}$) and Biot number *Granier* sap flow index (k$_{Biot\_Adj}$) approaches; b) dispersion of the transpiration data (F(kBiot)adj and F(kConv)adj) around the fitted line of the ET$_{actual}$(EC).

Fig.VII.8 illustrates the circadian curves for the sap flow measurements with sensor SP32L (F(k_{Biot})adj [mm h^{-1}]) and the soil moisture obtained with the mLy4 (θ_{mLy4} [cm^3 cm^{-3}]) sensor in the days 288 and 289 (2016). The soil moisture measures with mLy4 device showed to vary similarly with the transpiration, given that the transpiration showed the highest values simultaneously with the water redistribution into the soil, while the inverse occurs during the night, contrasting with mLy data from the single lemon tree trial (section VII.2.1). The explanation could be in the different localizations of mLy devices. The mLy4 device was situated under-canopy, and the mLy (single lemon tree trial) was situated in soil exposed to the solar radiation (bare soil). The exposed soil has reached as a significant source and sink of radiation and sensible heat, which could have affected the energy and water balances

of the shaded soil. Heilman *et al.* (1994) suggested that the under-canopy shading, the wind speed and the temperature variations within-canopy can affect energy and water balances since the canopy absorbs sensible heat from the soil, causing air temperature decreasing and humid air accumulation. The humid air would be sourced from the high soil evaporation rate from the bare soil in days after rainfall events, verified in the day 287 (6.3 mm) (Fig.VII.3).
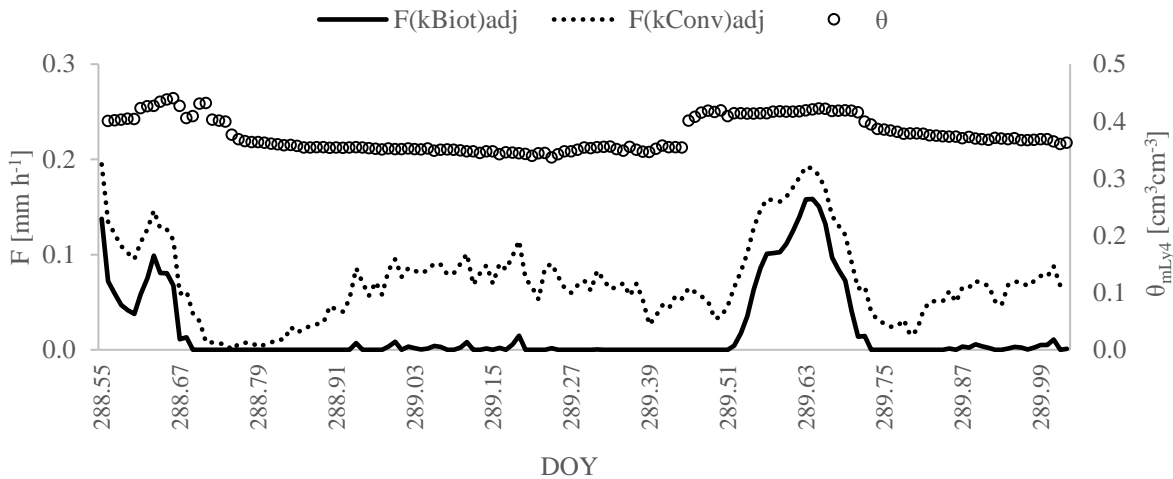
Fig.VII. 8: Comparison of the circadian curve from day 288 to day 290 (2016) between soil moisture estimated with the mLy4 (θ_{mLy4} [cm^{3}cm^{-3}] – empty circle - right vertical axis) sensor and the transpiration (F [mm h^{-1}] – left vertical axis) estimates based on the sap flow approaches: conventional *Granier* sap flow index (k$_{Conv}$) (dash line) and Biot number *Granier* sap flow index (k$_{Biot}$)(full line).

Fig.VII.9 shows the circadian curves for the soil heat storage (ΔG [W m^{-2}]) measured with the pair of *Peltier* cells (ΔG_{Pcell4} [W m^{-2}] and the soil water content estimated with the mLy4 (θ_{mLy4} [m^3 m^{-3}]) sensor, with a significant relationship (R^2=0.80) (Fig.VII.10) from day 253 to day 290 (2016). This shows increasing soil moisture at daytime, which is followed by an increasing soil heat storage. It can be inferred that the higher soil moisture implicates substantial soil heat storage since water has a very high volumetric heat capacity (4.18 MJ m^{-3}K^{-1}).
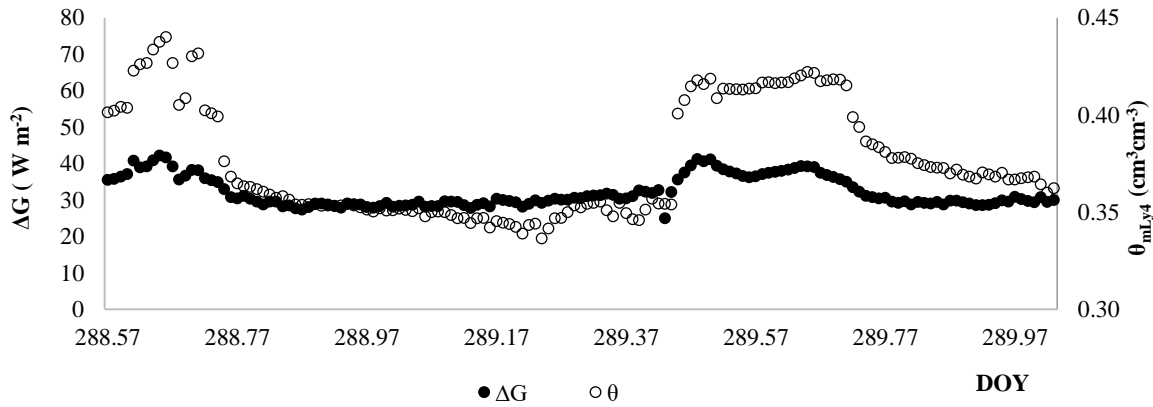
Fig.VII. 9: Comparison of the circadian curve from day 288 to day 290 (2016) between soil moisture estimated with the mLy4 sensor (θ_{mLy4} [cm^{3}cm^{-3}] (empty circle - right vertical axis) and soil heat storage measured with the pair of *Peltier* cells (ΔG_{Pcell4} [W m^{-2}] (full circle – left vertical axis).
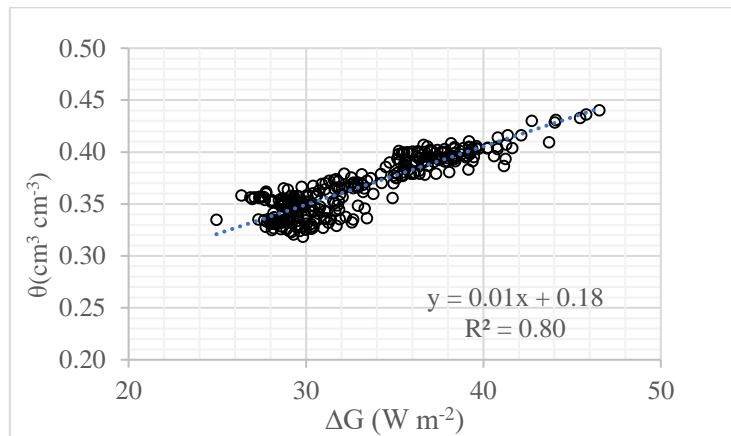
Fig.VII. 10: Comparative linear regression between the soil heat storage measured with the pair of *Peltier* cells (ΔG_{Pcell4} [W m^{-2}]) and the volumetric soil moisture estimated with the weighing device (θ_{mLy4} [cm^3 cm^{-3}]). The data were collected between the day 253 to day 290 (2016).

Correspondingly, Fig.VII.11 illustrates the circadian curves for soil heat storage (ΔG [W m^{-2}]) and sap flow approaches (F(k_{Conv})adj) and F(k_{Biot})adj) in the days 288 and 289 (2016). It can be inferred that the variation of the temperature differences measured into the trunk is related to the soil heat storage in a similar way for (F(k_{Conv})adj) and F(k_{Biot})adj) estimates.
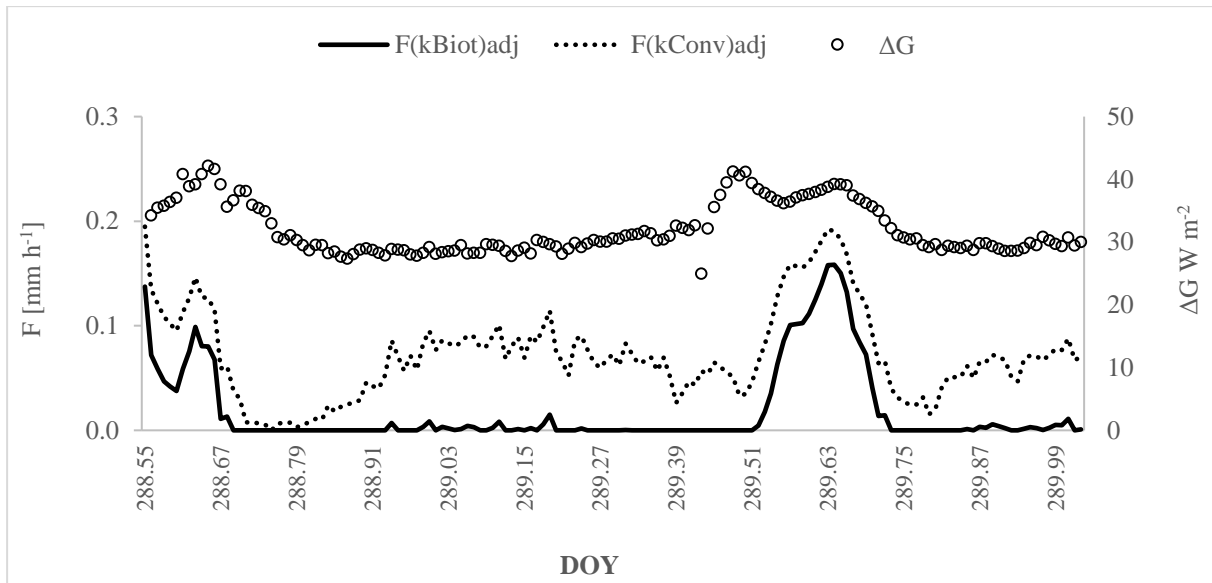
Fig.VII. 11: Comparison of the circadian curves for the soil heat storage measured with the pair of *Peltier* cells (ΔG_{Pcell4} [W m⁻²] empty circle - right vertical axis) and the sap flow rate measurement (F [mm h⁻¹] - left vertical axis) with the modified *Granier* sensor (SP32L) in function of conventional *Granier* sap flow index (k_{Conv}) (dash line) and Biot *Granier* sap flow index (k_{Biot}) (full line).

The soil heat flux estimated from the near soil surface (0.1 cm) (G_0 [W m⁻²]) and at 10 cm depth (G_{10} [W m⁻²]) in the pair of *Peltier* cells Pcell4 were related in the days between 287 and 296 (2016) (Fig VII.13). G_0 showed a significant relationship when compared to G_{10} (R^2=0.99). As expected, the values of G_0 from Pcell4 were 23 % higher than G_{10}, *i.e.*, on the 10 cm layer of soil has been storage 23% of the total solar radiation received. It means that the pair Pcells have related each other and it can benefit in the soil heat storage estimates.
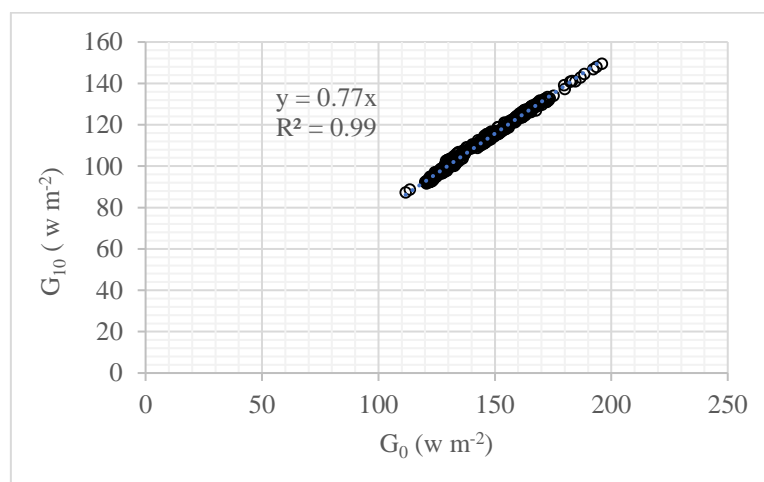
Fig.VII. 12: Comparative linear regression between the soil heat flux near the soil surface (G_0 [W m⁻²]) and the soil heat flux at 10 cm depth (G_{10} [W m⁻²]) measured with the pair of Peltier cells. The data were collected between the day 287 to day 296 (2016).

The pair of *Peltier* cells showed to be useful to fine-tune the soil evaporation and the sap flow estimates, given that the soil heat storage, soil water content and transpiration are intercorrelated. Thus, transpiration and soil water estimations can be checked for a low-cost and straightforward soil heat flux transductor.

VII.3. Conclusions

In the experiments carried out in the field, the data from modified *Granier* sensors demonstrated comparable with ET_{EC} measurements. Similarly, a consistent relation was observed between the data obtained with other SOIS components, *i.e.* the pair of *Peltier* cells (Pcells) and the weighing devices (mLy). It was possible to estimate the soil water content and the soil heat storage from mLy and Pcells devices, respectively. The soil water balance with mLy devices presented suitable to delineate the spatial and temporal soil water distribution and canopy shading effects, as well, showed potential to fine-tune the soil evaporation and the sap flow estimates by means of an efficient data processing tool (*e.g.*, FAUSY algorithm), given the soil heat storage, soil water content and transpiration are related.

The Biot approach showed to be useful to adjust the *Granier* sap flow index, a drawback of that methodology. Also, the sensitivity of the sensors reflected a satisfactory accuracy, and the ability to detect the sudden sap flow reduction in the water stress conditions.

The vineyard and single lemon tree trials allowed to verify the viability of SOIS system and to correct and improve technical features. It could be concluded that the SOIS system could be useful for the efficient use of water with transpiration and soil evaporation measurements in loco and real-time.

CONCLUSIONS

CHAPTER 8

VIII. CHAPTER 8: Conclusions

The present study addressed the development and evaluation of a low-cost open system (SOIS) for the efficient use of water in orchards and vineyards. The hardware and software features developed, such as low acquisition cost and easy customization, combined with unrestricted and transparent access to alternative designs, have overcome the obstacles imposed by the trade market solutions, while still ensuring reliable results.

The SOIS system showed to be reliable and robust, inexpensive, and easy to install, operating and maintaining. It was fully developed by the author using easily obtainable parts. Its simple manufacturability makes it prone to be fabricated at low cost and thus attractive to be adopted in the agricultural environment. The same can be said regarding the data acquisition and control hardware, although in this case more electronics specific knowledge is required. The system comprises: 1) an improved *Granier* sensor, along with an algorithm to enhance data treatment, that provides transpiration estimates, 2) an automated weighing device (mLy) that provides information assort soil water status, 3) *Peltier* cells that help estimate soil evaporation along with mLy and 4) data logging devices and data treatment software.

The FAUSY algorithm, developed in the frame of this study, showed to be an innovative approach for data treatment when using the *Granier* method for sap flow measurement and allowed to overcome the significant restrictions of substantial data processing related to natural temperature gradients and null sap flow detection, especially when practical applications in irrigation management are intended.

The prototypes of the modified *Granier* sensors were evaluated and validated. The results showed that the procedure for *Granier* sap flow index determination has a significant influence on *Granier*-based sap flux density estimations. It is concluded that the alternative Biot method may be a significant source to increase certainty in sap flow measurements. The results suggested that applying the physically-based Biot number approach improved the estimates, since this procedure showed the best conformity with the estimates of sap flow in comparison with the gravimetric test.

Concerning the weighing device (mLy), it is concluded that the mLy developed and tested in this study provided relatively accurate and reliable soil water status changes measurements. The statistical comparisons indicated that the mLy devices were compatibles with the reflectometer sensors. Even better, the mLy devices showed to integrate the effect of the whole substrate layer instead of measuring in the central point of the same layer, given can mirror the under-canopy periodic shading, wind speed and temperature variations effects. Also, the pair of *Peltier* cells could be used to fine-tune the soil evaporation and the sap flow estimates by means of an efficient data processing tool (*e.g.*, FAUSY algorithm), given that the soil heat storage, transpiration and soil water content are intercorrelated. Thus, transpiration and soil water estimations can be checked for a low-cost and straightforward soil heat flux transductor.

The whole SOIS system (using all sensors in simultaneous) demonstrated to help with more readily understanding of the ET components in orchards and vineyard and provided insight into the development of ET measurement tools, being compatible with the eddy covariance approach and providing a pertinent relationship between all output of sensors. Future work is needed to overcome the technical obstacles occurred in the trial but, once these are further corrected and validated, the SOIS system could be useful for the efficient use of water with transpiration and soil evaporation measurements in loco and real-time.

In conclusion, the improvement of the efficient use of water continues to be an actual topic, given the water scarcity conditions in many points of the globe and drought events being essential factors limiting crop production worldwide. Advances in electronic technologies, microcontrollers, and sensors provide researchers with a variety of new and inexpensive sensing, monitoring, and control capabilities. Therefore, the adoption of the low-cost open system concept, including hardware designs, specific algorithms and non-recurring engineering cost that are freely available to all, will facilitate and will expand the adoption of these capabilities. The proposed system presents an excellent potential for implementation in scientific research applications in the field context and can empower researchers, technicians and farmers with flexible, inexpensive tools for expanding data-collection, automation, and control capacities.

BIBLIOGRAPHY

Aboukhaled, A., Alfaro, A. & Smith, M. (1982). *Lysimeters*.(FAO, Ed.) FAO Irriga. Rome.

Ali, A. S., Zanzinger, Z., Debose, D. & Stephens, B. (2016). Open Source Building Science Sensors (OSBSS): A low-cost Arduino-based platform for long-term indoor environmental data collection. *Building and Environment*, 100, pp. 114–126.

Allen, R. G. & Pereira, L. S. (2009). Estimating crop coefficients from fraction of ground cover and height. *Irrigation Science*, 28(1), pp. 17–34.

Allen, R. G., Pereira, L. S., Howell, T. A. & Jensen, M. E. (2011). Evapotranspiration information reporting: I. Factors governing measurement accuracy. *Agricultural Water Management*, 98(6), pp. 899–920 Elsevier B.V.

Allen, R. G., Pereira, L. S., Raes, D. & Smith, M. (1998). *Crop evapotranspiration: Guidelines for computing crop water requirements*. *FAO* FAO, Rome.

Allen, R. G., Pruitt, W. O., Raes, D., Smith, M. & Pereira, L. S. (2005). Estimating Evaporation from Bare Soil and the Crop Coefficient for the Initial Period Using Common Soils Information. *Journal of Irrigation and Drainage Engineering*, 131(1), pp. 14–23.

Allen, R. G., Tasumi, M. & Trezza, R. (2007a). Satellite-Based Energy Balance for Mapping Evapotranspiration with Internalized Calibration (METRIC)—Model. *Journal of Irrigation and Drainage Engineering*, 133(4), pp. 380–394.

Allen, R., Wright, J., Pruitt, W., Pereira, L. & Jensen, M. (2007b). Water requirements. *Design and Operation of Farm Irrigation Systems*. pp. 208–288. St. Joseph, Mich.: ASABE.

Babu, S. (2013). A software model for precision agriculture for small and marginal farmers., August 2013. pp. 352–355. IEEE. ISBN 978-1-4799-1095-3.

Blazy, J.-M., Ozier-Lafontaine, H., Doré, T., Thomas, A. & Wery, J. (2009). A methodological framework that accounts for farm diversity in the prototyping of crop management systems. Application to banana-based systems in Guadeloupe. *Agricultural Systems*, 101(1–2), pp. 30–41 Elsevier Ltd.

Boast, C. W. & Robertson, T. M. (1982). A "Micro-Lysimeter" Method for Determining Evaporation

from Bare Soil: Description and Laboratory Evaluation. *Soil Science Society of America Journal*, 46(4), p. 689.

Bowen, I. S. (1926). The ratio of heat losses by conduction and by evaporation from any water surface. *Physical Review*.

Bristow, K., Kluitenberg, G. & Horton, R. (1994). Measurement of soil thermal properties with a dual-probe heat-pulse technique. *Soil Science Society of America Journal*, (58), pp. 1288–1294.

Bush, S. E., Hultine, K. R., Sperry, J. S. & Ehleringer, J. R. (2010). Calibration of thermal dissipation sap flow probes for ring- and diffuse-porous trees. *Tree Physiology*, 30(12), pp. 1545–1554.

Cammalleri, C., Rallo, G., Agnese, C., Ciraolo, G., Minacapilli, M. & Provenzano, G. (2013). Combined use of eddy covariance and sap flow techniques for partition of ET fluxes and water stress assessment in an irrigated olive orchard. *Agricultural Water Management*, 120(1), pp. 89–97 Elsevier B.V.

Campbell, G. S., Calissendorff, C. & Williams, J. H. (1991). Probe for Measuring Soil Specific Heat Using A Heat-Pulse Method.

Cancela, J. J., Fandiño, M., Rey, B. J. & Martínez, E. M. (2015). Automatic irrigation system based on dual crop coefficient, soil and plant water status for Vitis vinifera (cv Godello and cv Mencía). *Agricultural Water Management*, 151, pp. 52–63.

Cardoso, J. V. J. C. (1965). *Os solos de Portugal: sua classificação, caracterização e génese*.(Secr. Est. da Agric., Ed.) *IA sul do rio Tejo* Lisboa.

Clearwater, M. J., Meinzer, F. C., Andrade, J. L., Goldstein, G. & Holbrook, N. M. (1999). Potential errors in measurement of nonuniform sap flow using heat dissipation probes. *Tree physiology*, 19(10), pp. 681–687.

Daamen, C. C. & Simmonds, L. P. (1996). Measurement of evaporation from bare soil and its estimation using surface resistance. *Water Resources Research*, 32(5), pp. 1393–1402.

Daamen, C., Simmonds, L., Wallace, J., Laryea, K. & Sivakumar, M. (1993). Use of microlysimeters to measure evaporation from sandy soils. *Agricultural and Forest Meteorology*, 65(3–4), pp. 159–173.

Dane, J. H. & Topp, C. G. (2002). Water Content. *Methods of Soil Analysis: Part 4 Physical Methods*. pp. 417–545. SSSA Book Series.

Deol, P., Heitman, J., Amoozegar, A., Ren, T. & Horton, R. (2012). Quantifying nonisothermal

subsurface soil water evaporation. *Water Resources Research*, 48(11), pp. 1–11.

Dias, N. S. N., Lima, F. A., Silva, C. R., Neto, S., Nogueira, O. & Gheyi, H. R. (2010). Use of reject brine from desalination on different development stages of hydroponic lettuce. *Revista Caatinga*, 24(1), pp. 76–81.

Do, F. & Rocheteau, A. (2002a). Influence of natural temperature gradients on measurements of xylem sap flow with thermal dissipation probes. 1. Field observations and possible remedies. *Tree Physiology*, 22(9), pp. 641–648.

Do, F. & Rocheteau, A. (2002b). Influence of natural temperature gradients on measurements of xylem sap flow with thermal dissipation probes.2. Advantages and calibration of a noncontinuous heating system. *Tree Physiology*, 22(9), pp. 649–654.

Er-Raki, S., Chehbouni, A., Guemouria, N., Ezzahar, J., Khabba, S., Boulet, G. & Hanich, L. (2009). Citrus orchard evapotranspiration: Comparison between eddy covariance measurements and the FAO-56 approach estimates. *Plant Biosystems - An International Journal Dealing with all Aspects of Plant Biology*, 143(1), pp. 201–208.

Evett, S. R., Mazahrih, N. T., Jitan, M. A., Sawalha, M. H., Colaizzi, P. D. & Ayars, J. E. (2009). A Weighing Lysimeter for Crop Water Use Determination in the Jordan Valley, Jordan. *Transactions of the Asabe*, 52(1), pp. 155–169.

Evett, S. R., Schwartz, R. C., Casanova, J. J. & Heng, L. K. (2012). Soil water sensing for water balance, ET and WUE. *Agricultural Water Management*, 104(January), pp. 1–9.

Evett, S. R., Warrick, a. W. & Matthias, a. D. (1995). Wall Material and Capping Effects on Microlysimeter Temperatures and Evaporation. *Soil Science Society of America Journal*, 59(2), p. 329.

Fandiño, M., Cancela, J. J., Rey, B. J., Martínez, E. M., Rosa, R. G. & Pereira, L. S. (2012). Using the dual-K c approach to model evapotranspiration of Albariño vineyards (Vitis vinifera L. cv. Albariño) with consideration of active ground cover. *Agricultural Water Management*, 112, pp. 75–87.

Fandiño, M., Olmedo, J. L., Martínez, E. M., Valladares, J., Paredes, P., Rey, B. J., Mota, M., Cancela, J. J. & Pereira, L. S. (2015). Assessing and modelling water use and the partition of evapotranspiration of irrigated hop (Humulus Lupulus), and relations of transpiration with hops yield and alpha-acids. *Industrial Crops and Products*, 77, pp. 204–217.

Farahani, H. J., Howell, T. A., Shuttleworth, W. J. & Bausch, W. C. (2007). Evapotranspiration:

Progress in Measurement and Modeling in Agriculture. *Transactions of the ASABE*, 50(5), pp. 1627–1638.

Fernández, E., Cohen, Y., Ferreira, I., Nadezhdina, N., Testi, L. & Steppe, K. (2017). *Methods to Estimate Sap Flow*. ISHS Working Group on Sap Flow. Updated: February 2017.

Fernández, J. (2017). Plant-Based Methods for Irrigation Scheduling of Woody Crops. *Horticulturae*, 3(2), p. 35.

Fernández, J. E. (2014). Plant-based sensing to monitor water stress: Applicability to commercial orchards. *Agricultural Water Management*, 142, pp. 99–109 Elsevier B.V.

Fernandez, J. E., Duran, P. J., Palomo, M. J., Diaz-Espejo, A., Chamorro, V. & Giron, I. F. (2006). Calibration of sap flow estimated by the compensation heat pulse method in olive, plum and orange trees: relationships with xylem anatomy. *Tree Physiology*, 26(6), pp. 719–728.

Fernández, J. E., Green, S. R., Caspari, H. W., Diaz-Espejo, A. & Cuevas, M. V. (2008). The use of sap flow measurements for scheduling irrigation in olive, apple and Asian pear trees and in grapevines. *Plant and Soil*, 305(1–2), pp. 91–104.

Ferreira, M. I. & Katerji, N. (1992). Is stomatal conductance in a tomato crop controlled by soil or atmosphere? *Oecologia*, 92(1), pp. 104–107.

Ferreira, M. I., Paço, T. A., Silvestre, J. & Silva, R. M. (2008). Evapotranspiration estimates and water stress indicators for irrigation scheduling in woody plants. *Agricultural Water Management Research Trends*. pp. 129–170. ISBN 9781604565799.

Ferreira, M. I., Silvestre, J., Conceição, N. & Malheiro, A. C. (2012). Crop and stress coefficients in rainfed and deficit irrigation vineyards using sap flow techniques. *Irrigation Science*, 30(5), pp. 433–447.

Fisher, D. K. & Gould, P. J. (2012). Open-Source Hardware Is a Low-Cost Alternative for Scientific Instrumentation and Research. *Modern Instrumentation*, 01(02), pp. 8–20.

Flumignan, D. L., Faria, R. T. De & Lena, B. P. (2012). Test of a microlysimeter for measurement of soil evaporation. *Engenharia Agrícola*, 32(1), pp. 80–90.

Flumignan, D. L., Faria, R. T. & Prete, C. (2011). Evapotranspiration components and dual crop coefficients of coffee trees during crop production. *Agricultural Water Management*, 98(5), pp. 791–800 Elsevier B.V.

Forster, M. (2017). How Reliable Are Heat Pulse Velocity Methods for Estimating Tree Transpiration?

Forests, 8(9), p. 350.

Forsythe, W. E. (1964). *Smithsonian physical tables. Smithsonian*.(4169, I. P., Ed.) Washington, DC.

Fuchs, M. (1986). Heat Flux. *Methods of Soil Analysis: Part 1—Physical and Mineralogical Methods*. pp. 957–968. Madison, WI: Soil Science Society of America, American Society of Agronomy. ISBN 978-0-89118-864-3.

Fuchs, M. & Hadas, A. (1973). Analysis of Performance of an Improved Soil Heat-Flux Transducer. *Soil Science Society Of America Journal*, 37(2), pp. 173–175.

Fuchs, M. & Tanner, C. B. (1968). Calibration and Field Test of Soil Heat Flux Plates. *Soil Science Society of America Journal*, 32(3), pp. 326–328.

Fuchs, S., Leuschner, C., Link, R., Coners, H. & Schuldt, B. (2017). Calibration and comparison of thermal dissipation, heat ratio and heat field deformation sap flow probes for diffuse-porous trees. *Agricultural and Forest Meteorology*, 244–245(March), pp. 151–161.

Gaddam, A. & Esmael, W. F. (2014). Designing a Wireless Sensors Network for Monitoring and Predicting Droughts. *Proceedings of the 8th International Conference on Sensing Technology*, pp. 2–4.

Gardner, H. R. & Hanks, R. J. (1966). Evaluation of the Evaporation Zone in Soil by Measurement of Heat Flux. *Soil Science Society of America Journal*, 30(4), p. 425.

Glenn, E. P., Huete, A. R., Nagler, P. L., Hirschboeck, K. K. & Brown, P. (2007). Integrating remote sensing and ground methods to estimate evapotranspiration. *Critical Reviews in Plant Sciences*, 26(3), pp. 139–168.

Granier, A. (1985). Une nouvelle methode pour la measure du flux de seve brute dans le tronc des arbres. *Annales des Sciences Forestieres*, 42(2), pp. 193–200.

Granier, A. (1987). Evaluation of transpiration in a Douglas-fir stand by means of sap flow measurements. *Tree Physiology*, 3(4), pp. 309–320.

Granier, A., Biron, P., Bréda, N., Pontailler, J. Y. & Saugier, B. (1996). Transpiration of trees and forest stands: short and long-term monitoring using sapflow methods. *Global Change Biology*, 2(3), pp. 265–274.

Green, S., Clothier, B. & Jardine, B. (2003). Theory and Practical Application of Heat Pulse to Measure Sap Flow. *Agronomy Journal*, 95(6), p. 1371.

Grimmond, C. S. B., Isard, S. A. & Belding, M. J. (1992). Development and evaluation of continuously weighing mini-lysimeters. *Agricultural and Forest Meteorology*, 62(3–4), pp. 205–218.

Groener, B., Knopp, N., Korgan, K., Perry, R., Romero, J., Smith, K., Stainback, A., Strzelczyk, A. & Henriques, J. (2015). Preliminary Design of a Low-cost Greenhouse with Open Source Control Systems. *Procedia Engineering*, 107, pp. 470–479 Elsevier B.V.

Grové, B. (2011). Review of whole-farm economic modelling for irrigation farming. *Water SA*, 37(5), pp. 789–796.

Ham, J. M. & Benson, E. J. (2004). On the Construction and Calibration of Dual-Probe Heat Capacity Sensors. *Soil Science Society of America Journal*, 68(4), pp. 1185–1190.

Hamdy, A. (2007). Water use efficiency in irrigated agriculture: an analytical review. *In: Water Use Efficiency and water productivity*. pp. 9–19. WASAMED project. (Options Méditerranéennes : Série B.).

Heilman, J. L., McInnes, K. J., Savage, M. J., Gesch, R. W. & Lascano, R. J. (1994). Soil and canopy energy balances in a west Texas vineyard. *Agricultural and Forest Meteorology*, 71(1–2), pp. 99–114.

Heitman, J. L., Horton, R., Ren, T., Nassar, I. N. & Davis, D. D. (2008a). A Test of Coupled Soil Heat and Water Transfer Prediction under Transient Boundary Temperatures. *Soil Science Society of America Journal*, 72(5), pp. 1197–1207.

Heitman, J. L., Horton, R., Sauer, T. J. & DeSutter, T. M. (2008b). Sensible Heat Observations Reveal Soil-Water Evaporation Dynamics. *Journal of Hydrometeorology*, 9(1), pp. 165–171.

Heitman, J. L., Horton, R., Sauer, T. J., Ren, T. S. & Xiao, X. (2010). Latent heat in soil heat flux measurements. *Agricultural and Forest Meteorology*, 150(7–8), pp. 1147–1153.

Heitman, J. L., Xiao, X., Horton, R. & Sauer, T. J. (2008c). Sensible heat measurements indicating depth and magnitude of subsurface soil water evaporation. *Water Resources Research*, 44(4), pp. 1–7.

Hillel, D. (1998). *Environmental soil physics: Fundamentals, applications, and environmental considerations*. Academic press. ISBN 0080544150.

Holland, S., Heitman, J. L., Howard, A., Sauer, T. J., Giese, W., Ben-Gal, A., Agam, N., Kool, D. & Havlin, J. (2013). Micro-Bowen ratio system for measuring evapotranspiration in a vineyard interrow. *Agricultural and Forest Meteorology*, 177, pp. 93–100 Elsevier B.V.

Huang, Y., Lan, Y., Thomson, S. J., Fang, A., Hoffmann, W. C. & Lacey, R. E. (2010). Development

of soft computing and applications in agricultural and biological engineering. *Computers and Electronics in Agriculture*, 71(2), pp. 107–127.

Hurk, van den B. (1996). *Sparse canopy parameterizations for meteorological models.* Diss. *Department of Meteorology* Wageningen Agricultural University, 271 pp.

Incropera, F. P., DeWitt, D. P., Bergman, T. L. & Lavine, A. S. (2007). *Fundamentals of Heat and Mass Transfer*. 6th. ed. John Wiley & Sons, Limited. ISBN 9780471457282.

Jensen, M. & Allen, R. (2016). *Evaporation, Evapotranspiration, and Irrigation Water Requirements*. Reston, VA: American Society of Civil Engineers.

Kamble, B., Kilic, A. & Hubbard, K. (2013). Estimating Crop Coefficients Using Remote Sensing-Based Vegetation Index. *Remote Sensing*, 5(4), pp. 1588–1602.

Khan, A., Singh, S., Shukla, S. & Pandey, A. (2017). Automatic Irrigation System Using internet Of Things. *International Journal Of Advance Research, Ideas And Innovations In Technology*, 3, pp. 526–529.

Knight, J. & Kluitenberg, G. (2004). Simplified computational approach for dual-probe heat-pulse method. *Soil Science Society of America Journal*, 68, pp. 447–449.

Knight, J. & Kluitenberg, G. (2013). Correcting for finite probe diameter in the dual probe heat pulse method of measuring soil water content., 2013. pp. 127–133.

Kool, D., Agam, N., Lazarovitch, N., Heitman, J., Sauer, T. & Ben-Gal, A. (2014). A review of approaches for evapotranspiration partitioning. *Agricultural and Forest Meteorology*, 184, pp. 56–70.

Kool, D., Kustas, W., Ben-Gal, A., Lazarovitch, N., Heitman, J., Sauer, T. & Agam, N. (2016). Energy and evapotranspiration partitioning in a desert vineyard. *Agricultural and Forest Meteorology*, 218–219(January), pp. 277–287.

Kume, T., Tsuruta, K., Komatsu, H., Kumagai, T., Higashi, N., Shinohara, Y. & Otsuki, K. (2010). Effects of sample size on sap flux-based stand-scale transpiration estimates. *Tree Physiology*, 30(1), pp. 129–138.

Kustas, W. P. (2014). Soil: Evaporation. *Encyclopedia of Natural Resources: Land*. pp. 444–453. CRC Press. ISBN 9781439858259.

Lascano, R. J. & van Bavel, C. H. M. (1986). Simulation and Measurement of Evaporation from a Bare Soil. *Soil Science Society of America Journal*, 50(5), pp. 1127–1133.

Lascano, R. J., Goebel, T. ., Booker, J., Baker, J. T. & Gitz III, D. C. (2016). The Stem Heat Balance Method to Measure Transpiration: Evaluation of a New Sensor. *Agricultural Sciences*, 07(09), pp. 604–620.

Li, X., Yang, P., Ren, S., Li, Y., Liu, H., Du, J., Li, P., Wang, C. & Ren, L. (2010). Modeling cherry orchard evapotranspiration based on an improved dual-source model. *Agricultural Water Management*, 98(1), pp. 12–18 Elsevier B.V.

Li, Z.-L., Tang, R., Wan, Z., Bi, Y., Zhou, C., Tang, B., Yan, G. & Zhang, X. (2009). A Review of Current Methodologies for Regional Evapotranspiration Estimation from Remotely Sensed Data. *Sensors*, 9(5), pp. 3801–3853.

Lian, J. & Huang, M. (2016). Comparison of three remote sensing based models to estimate evapotranspiration in an oasis-desert region. *Agricultural Water Management*, 165, pp. 153–162.

Liu, Y., Pereira, L. S. & Fernando, R. M. (2006). Fluxes through the bottom boundary of the root zone in silty soils: Parametric approaches to estimate groundwater contribution and percolation. *Agricultural Water Management*, 84(1–2), pp. 27–40.

Lu, P., Urban, L. & Zhao, P. (2004). Granier's thermal dissipation probe (TDP) method for measuring sap flow in trees: theory and practice. *Acta Botanica Sinica*, 46(6), pp. 631–646.

Lubczynski, M. W., Chavarro-Rincon, D. & Roy, J. (2012). Novel, cyclic heat dissipation method for the correction of natural temperature gradients in sap flow measurements. Part 1. Theory and application. *Tree Physiology*, 32(7), pp. 894–912.

Mackay, D. S., Samanta, S., Nemani, R. R. & Band, L. E. (2003). Multi-objective parameter estimation for simulating canopy transpiration in forested watersheds. *Journal of Hydrology*, 277(3–4), pp. 230–247.

Masmoudi, C., Masmoudi, M., Abid-Karray, J. & Mechlia, N. Ben (2011). Sap flow measurements in young olive trees (Olea europaea L.) cv. Chétoui under Tunisian conditions. *Scientia Horticulturae*, 129(4), pp. 520–527 Elsevier B.V.

MEGA 2560 Arduino. [online] (2014) (arduino.cc). Available from: http://arduino.cc/en/Main/arduinoBoardMega2560.

Mesas-Carrascosa, F. J., Verdú Santano, D., Meroño, J. E., Sánchez de la Orden, M. & García-Ferrer, A. (2015). Open source hardware to monitor environmental parameters in precision agriculture. *Biosystems Engineering*, 137, pp. 73–83.

Miner, G. L., Ham, J. M. & Kluitenberg, G. J. (2017). A heat-pulse method for measuring sap flow in

corn and sunflower using 3D-printed sensor bodies and low-cost electronics. *Agricultural and Forest Meteorology*, 246(May), pp. 86–97 Elsevier.

Misra, R. K., Padhi, J. & Payero, J. O. (2011). A calibration procedure for load cells to improve accuracy of mini-lysimeters in monitoring evapotranspiration. *Journal of Hydrology*, 406(1–2), pp. 113–118 Elsevier B.V.

Monteith, J. L. (1965). Evaporation and environment. *Symposia of the Society for Experimental Biology*, 19, pp. 205–234.

Mori, Y., Hopmans, J. W., Mortensen, A. P. & Kluitenberg, G. J. (2003). Multi-Functional Heat Pulse Probe for the Simultaneous Measurement of Soil Water Content, Solute Concentration, and Heat Transport Parameters. *Vadose Zone Journal*, 2(4), pp. 561–571.

Nair, S., Johnson, J. & Wang, C. (2013). Efficiency of irrigation water use: A review from the perspectives of multiple disciplines. *Agronomy Journal*, 105(2), pp. 351–363.

Nicolas, E., Torrecillas, A., Ortuño, M. F., Domingo, R. & Alarcón, J. J. (2005). Evaluation of transpiration in adult apricot trees from sap flow measurements. *Agricultural Water Management*, 72(2), pp. 131–145.

Odhiambo, L. & Irmak, S. (2011). Performance of Extended Shuttleworth-Wallace Model for Estimating and Partitioning of Evapotranspiration in a Partial Residue-Covered Subsurface Drip-Irrigated Soybean Field. *Transactions of the Asabe*, 54(3), pp. 915–930.

Paço, T. A. (2003). *Modelação da Evapotranspiração em Cobertos Descontínuos Programação da Rega em Pomar de Pessegueiro*. Diss. Tese (Doutorado). Instituto Superior de Agronomia. Universidade de Lisboa.

Paço, T. A., Cameira, M. R., Branquinho, C., Carvalho, R. C. De, Luís, L., Espírito-santo, D., Valente, F., Brandão, C., Soares, A. L., Anico, A., Abreu, F. & Pereira, L. S. (2014a). Innvative Green Roofs for Southern Europe: Biocrusts and Native Species with Low Water Use., 2014. pp. 1–10.

Paço, T. A., David, T. S., Henriques, M. O., Pereira, J. S., Valente, F., Banza, J., Pereira, F. L., Pinto, C. & David, J. S. (2009). Evapotranspiration from a Mediterranean evergreen oak savannah: The role of trees and pasture. *Journal of Hydrology*, 369(1–2), pp. 98–106.

Paço, T. A., Ferreira, M. I., Rosa, R. D., Paredes, P., Rodrigues, G. C., Conceição, N., Pacheco, C. A. & Pereira, L. S. (2012). The dual crop coefficient approach using a density factor to simulate the evapotranspiration of a peach orchard: SIMDualKc model versus eddy covariance measurements. *Irrigation Science*, 30(2), pp. 115–126.

Paço, T. A., Pôças, I., Cunha, M., Silvestre, J. C., Santos, F. L., Paredes, P. & Pereira, L. S. (2014b). Evapotranspiration and crop coefficients for a super intensive olive orchard. An application of SIMDualKc and METRIC models using ground and satellite observations. *Journal of Hydrology*, 519, pp. 2067–2080.

Parisi, S., Mariani, L., Cola, G. & Maggiore, T. (2009). Mini-Lysimeters evapotranspiration measurements on suburban environment. *Italian Journal of Agrometeorology*, 3(3), pp. 13–16.

Penman, H. L. (1948). Natural Evaporation from Open Water, Bare Soil and Grass. *Proceedings of the Royal Society A: Mathematical, Physical and Engineering Sciences*, 193(1032), pp. 120–145.

Pereira, L. (2007). Relating water productivity and crop evapotranspiration. *IN: Water use efficiency and water productivity*. pp. 31–49. WASAMED project. (Options Méditerranéennes : Série B.).

Pereira, L. S., Allen, R. G., Smith, M. & Raes, D. (2015). Crop evapotranspiration estimation with FAO56: Past and future. *Agricultural Water Management*, 147, pp. 4–20.

Pereira, L. S., Cordery, I. & Iacovides, I. (2009). *Coping with Water Scarcity. Addressing the Challenges. cdc.gov* Dordrecht: Springer.

Pereira, L. S., Cordery, I. & Iacovides, I. (2012). Improved indicators of water use performance and productivity for sustainable water conservation and saving. *Agricultural Water Management*, 108, pp. 39–51 Elsevier B.V.

Pereira, L. S., Oweis, T. & Zairi, A. (2002). Irrigation management under water scarcity. *Agricultural Water Management*, 57(3), pp. 175–206.

Persson, M., Berndtsson, R., Nasri, S., Albergel, J., Zante, P. & Yumegaki, Y. (2000). Solute transport and water content measurements in clay soils using time domain reflectometry. *Hydrological Sciences Journal*, 45(6), pp. 833–847.

Plauborg, F. (1995). Evaporation from bare soil in a temperate humid climate—measurement using micro-lysimeters and time domain reflectometry. *Agricultural and Forest Meteorology*, 76(1), pp. 1–17.

Poblete-Echeverría, C., Ortega-Farias, S., Zuñiga, M. & Fuentes, S. (2012). Evaluation of compensated heat-pulse velocity method to determine vine transpiration using combined measurements of eddy covariance system and microlysimeters. *Agricultural Water Management*, 109, pp. 11–19.

Pôças, I., Paço, T. A., Cunha, M., Andrade, J. A., Silvestre, J., Sousa, A., Santos, F. L., Pereira, L. S. & Allen, R. G. (2014). Satellite-based evapotranspiration of a super-intensive olive orchard: Application of METRIC algorithms. *Biosystems Engineering*, 128, pp. 69–81.

Pôças, I., Paço, T., Paredes, P., Cunha, M. & Pereira, L. (2015). Estimation of Actual Crop Coefficients Using Remotely Sensed Vegetation Indices and Soil Water Balance Modelled Data. *Remote Sensing*, 7(3), pp. 2373–2400.

Rabbel, I., Diekkrüger, B., Voigt, H. & Neuwirth, B. (2016). Comparing ΔTmax Determination Approaches for Granier-Based Sapflow Estimations. *Sensors*, 16(12), p. 2042.

Ren, T., Ju, Z., Gong, Y. & Horton, R. (2005). Comparing Heat-Pulse and Time Domain Reflectometry Soil Water Contents from Thermo-Time Domain Reflectometry Probes. *Vadose Zone Journal*, 4(4), p. 1080.

Ren, T., Noborio, K. & Horton, R. (1999). Measuring Soil Water Content, Electrical Conductivity, and Thermal Properties with a Thermo-Time Domain Reflectometry Probe. *Soil Science Society of America Journal*, 63(3), pp. 450–457.

Reyes-Acosta, J. L., Vandegehuchte, M. W., Steppe, K. & Lubczynski, M. W. (2012). Novel, cyclic heat dissipation method for the correction of natural temperature gradients in sap flow measurements. Part 2. Laboratory validation. *Tree Physiology*, 32(7), pp. 913–929.

Romero, R., Muriel, J. L., García, I. & Muñoz de la Peña, D. (2012). Research on automatic irrigation control: State of the art and recent results. *Agricultural Water Management*, 114, pp. 59–66.

Rosa, R. D., Paredes, P., Rodrigues, G. C., Alves, I., Fernando, R. M., Pereira, L. S. & Allen, R. G. (2012a). Implementing the dual crop coefficient approach in interactive software. 1. Background and computational strategy. *Agricultural Water Management*, 103, pp. 8–24.

Rosa, R. D., Paredes, P., Rodrigues, G. C., Fernando, R. M., Alves, I., Pereira, L. S. & Allen, R. G. (2012b). Implementing the dual crop coefficient approach in interactive software: 2. Model testing. *Agricultural Water Management*, 103, pp. 62–77.

Rousseaux, M. C., Figuerola, P. I., Correa-Tedesco, G. & Searles, P. S. (2009). Seasonal variations in sap flow and soil evaporation in an olive (Olea europaea L.) grove under two irrigation regimes in an arid region of Argentina. *Agricultural Water Management*, 96(6), pp. 1037–1044.

Sakai, M., Jones, S. B. & Tuller, M. (2011). Numerical evaluation of subsurface soil water evaporation derived from sensible heat balance. *Water Resources Research*, 47(W02547).

Santos, C., Lorite, I. J., Allen, R. G. & Tasumi, M. (2012). Aerodynamic Parameterization of the Satellite-Based Energy Balance (METRIC) Model for ET Estimation in Rainfed Olive Orchards of Andalusia, Spain. *Water Resources Management*, 26(11), pp. 3267–3283.

Schuepp, P. H., Leclerc, M. Y., MacPherson, J. I. & Desjardins, R. L. (1990). Footprint prediction of

scalar fluxes from analytical solutions of the diffusion equation. *Boundary-Layer Meteorology*, 50(1–4), pp. 355–373.

Silvestre, J. (2003). *Evapotranspiração e funcionamento hídrico em Vitis vinifera L.* Diss. Universidade Técnica de Lisboa.

Siqueira, J. M., Paço, T. A., Silvestre, J. C., Santos, F. L., Falcão, A. O. & Pereira, L. S. (2014). Generating fuzzy rules by learning from olive tree transpiration measurement – An algorithm to automatize Granier sap flow data analysis. *Computers and Electronics in Agriculture*, 101, pp. 1–10.

Siqueira, J., Silva, J. & Paço, T. (2015). Smart Orchard Irrigation System., November 2015. pp. 1–6. IEEE.

Smith, D. M. & Allen, S. J. (1996). Measurement of sap flow in plant stems. *Journal of Experimental Botany*, 47(12), pp. 1833–1844.

Smith, M., Pereira, L., Berengena, J., Itier, B., Goussard, J., Ragab, R., Tollefson, L. & Hoffwegen, P. Van (1996). *Irrigation Scheduling: From Theory to Practice.* Water Report 8, FAO, Rome, 384 p.

Smith, R., Baillie, J., McCarthy, A., Raine, S. R. & Baillie, C. P. (2010). *Review of precision irrigation technologies and their application. National Centre for Engineering in Agriculture.* Technologies and their Application. National Centre for Engineering in Agriculture Publication Publication 1003017/1, USQ, Toowoomba.

Smith, R. J. & Baillie, J. N. (2009). Defining precision irrigation: A new approach to irrigation management. *Irrigation and Drainage Conference*, pp. 1–6.

Smith, S. (2013). *Digital Signal Processing: A Practical Guide for Engineers and Scientists: A Practical Guide for Engineers and Scientists*. Newnes. ISBN 0080477321.

Sperling, O., Shapira, O., Cohen, S., Tripler, E., Schwartz, A. & Lazarovitch, N. (2012). Estimating sap flux densities in date palm trees using the heat dissipation method and weighing lysimeters. *Tree Physiology*, 32(9), pp. 1171–1178.

Stankovic, J. A., Lee, I., Mok, A. & Rajkumar, R. (2005). Opportunities and obligations for physical computing systems. *Computer*, 38(11), pp. 23–31.

Steinhart, J. S. & Hart, S. R. (1968). Calibration curves for thermistors. *Deep Sea Research and Oceanographic Abstracts*, 15(4), pp. 497–503.

Todd, R. W., Evett, S. R., Howell, T. A. & Klocke, N. L. (2000). Soil Temperature And Water

Evaporation Of Small Steel And Plastic Lysimeters Replaced Daily. *Soil Science*, 165(11), pp. 890–895.

Trambouze, W., Bertuzzi, P. & Voltz, M. (1998). Comparison of methods for estimating actual evapotranspiration in a row-cropped vineyard. *Agricultural and Forest Meteorology*, 91(3–4), pp. 193–208.

Vandegehuchte, M. W., Burgess, S. S. O., Downey, A. & Steppe, K. (2015). Influence of stem temperature changes on heat pulse sap flux density measurements. *Tree Physiology*, 35(4), pp. 346–353.

Vandegehuchte, M. W. & Steppe, K. (2013). Sap-flux density measurement methods: working principles and applicability. *Functional Plant Biology*, 40(3), pp. 213–223.

Vellidis, G., Tucker, M., Perry, C., Kvien, C. & Bednarz, C. (2008). A real-time wireless smart sensor array for scheduling irrigation. *Computers and Electronics in Agriculture*, 61(1), pp. 44–50.

Vojtã, P. (2001). Fuzzy logic programming. *Fuzzy Sets and Systems*, 124, pp. 361–370.

Walker, G. K. (1983). Measurement Of Evaporation From Soil Beneath Crop Canopies. *Canadian Journal of Soil Science*, 63(1), pp. 137–141.

Wang, L. X. & Mendel, J. M. (1992). Generating fuzzy rules by learning from examples. *IEEE Transactions on Systems, Man, and Cybernetics*, 22(6), pp. 1414–1427.

Weaver, H. L. & Campbell, G. S. (1985). Use of peltier coolers as soil heat flux transducers. *Soil Science Society of America Journal*, 49, pp. 1065–1067.

Wilson, K. B., Hanson, P. J., Mulholland, P. J., Baldocchi, D. D. & Wullschleger, S. D. (2001). A comparison of methods for determining forest evapotranspiration and its components: sap-flow, soil water budget, eddy covariance and catchment water balance. *Agricultural and Forest Meteorology*, 106(2), pp. 153–168.

Xiao, X., Horton, R., Sauer, T. J., Heitman, J. L. & Ren, T. (2011). Cumulative Soil Water Evaporation as a Function of Depth and Time. *Vadose Zone Journal*, 10(3), p. 1016.

Xiao, Z., Lu, S., Heitman, J., Horton, R. & Ren, T. (2012). Measuring Subsurface Soil-Water Evaporation with an Improved Heat-Pulse Probe. *Soil Science Society of America Journal*, 76(3), p. 876.

Xu, L., Chen, L., Chen, T. & Gao, Y. (2011). SOA-based precision irrigation decision support system. *Mathematical and Computer Modelling*, 54(3–4), pp. 944–949.

Yunusa, I. A. M., Walker, R. R. & Lu, P. (2004). Evapotranspiration components from energy balance, sapflow and microlysimetry techniques for an irrigated vineyard in inland Australia. *Agricultural and Forest Meteorology*, 127(1–2), pp. 93–107.

Zhang, Y., Kang, S., Ward, E. J., Ding, R., Zhang, X. & Zheng, R. (2011). Evapotranspiration components determined by sap flow and microlysimetry techniques of a vineyard in northwest China: Dynamics and influential factors. *Agricultural Water Management*, 98(8), pp. 1207–1214.